Quasiparticle energies from second-order perturbation theory

INAUGURAL DISSERTATION

to obtain the academic degree
Doctor rerum naturalium (Dr. rer. nat.)

submitted to

The Department of Biology, Chemistry, Pharmacy

of Freie Universität Berlin

by

Maria Dragoumi

Berlin, 2022

This work was prepared under supervision of

Prof. Dr. Matthias Scheffler
at
Fritz Haber Institute Berlin

from

June 2016 until June 2022

1st Reviewer: Prof. Dr. Matthias Scheffler

2nd Reviewer: Prof. Dr. Beate Paulus

Date of the defense: 31.10.2022

Declaration of independence:

I hereby declare that this dissertation was written and prepared by me independently. Furthermore, no sources and aids other than those indicated have been used. Intellectual property of other authors has been marked accordingly. I also declare that I have not applied for an examination procedure at any other institution and that I have not submitted the dissertation in this or any other form to any other faculty as a dissertation.

To my grandfather, Ilias Voyatzoglou...

Acknowledgments

The accomplishment of this dissertation would not have been possible without the help and support of my supervisors. I want to express my deepest gratitude to Sergey Levchenko for his support, motivation, and, mostly, for believing in this project. I want to thank Igor Ying Zhang and Matthias for giving me the opportunity to work at Fritz-Haber Institute in Berlin and for their support during this period. Furthermore, I would like to thank Beathe Paulus for her comments which improved my thesis.

Finally, I would like to thank my family, friends, and my partner for lifting my spirit and standing by me through good and bad times. I feel very lucky to have many people in my life that helped me through this challenging period of my life.

Abstract

In this dissertation, we apply second-order many-body perturbation theory (MBPT) to calculate the single-particle (charged) excitations of solids using localized atom-centered orbital basis set.

The single-particle excitation energies that shape the band structure of the solid are defined as the differences of total energies of the neutral and charged systems. It was shown (J.-Q. Sun and R. J. Bartlett: J. Chem. Phys. 107, 5058 (1997)) that a practical approximation can be obtained by applying MBPT to the energy differences. This method can be used for the calculation of the correction to the charged excitation energies with a possibility to systematically improve accuracy by including higher orders of perturbation, without calculating neutral and charged systems separately. We implement and apply this method for corrections up to second order for the calculation of the band gaps and band structure of three-dimensional solids. We find that the second-order correction is not sufficient, and there is the need to include higher-order terms. For this reason, we employ the Dyson equation, which provides an explicit summation of classes of perturbation terms (described by certain diagrams) up to infinite order. We use the Dyson equation with the self-energy that is produced by the second-order MBPT to calculate band gaps of a series of prototypical semiconductors. We find a significant improvement of the calculated band gaps, compared to the second-order correction, which is just the first iteration of the Dyson equation.

A significant difficulty for the application of MBPT to solids is the slow convergence of the reciprocal-space integrals, caused by the singularity of the Coulomb potential. The main approach used until now to overcome the slow convergence is by extrapolation to an infinitely dense k-point grid. We demonstrate that this approach leads to very large errors. The reason is that the converged

single-particle excitation energy value is very sensitive to the extrapolation function that defines the asymptotic behavior of the value as a function of the number of k-points in the first Brillouin zone. To solve this problem, we have examined the singularity and the contribution to the slow convergence of the energies analytically. The analysis is done for a localized basis set, but it can be generalized for any basis set. Due to this analysis, the contribution of the singularity to the slow convergence is now known and can be tackled by either a reliable extrapolation, since the law of extrapolation is now known, or by correcting the value using a generalization of the Gygi-Baldereschi method, as proposed in this thesis. This way, we calculate single-particle energies that are converged in reciprocal space.

Zusammenfassung

In dieser Dissertation wenden wir Vielteilchen-Störungstheorie zweiter Ordnung (MBPT) an, um unter Verwendung eines lokalisierten, atomzentrierten Orbitalbasissatze die (geladenen) Ein-Teilchen-Anregungen von Festkörpern zu berechnen.

Die Ein-Teilchen-Anregungsenergien, die die elektronische Bandstruktur von Festkörpern bestimmen, sind definiert als die Differenz der Gesamtenergien des neutralen und des geladenen Systems. Es ist bekannt, [J.-Q. Sun und R. J. Bartlett: J. Chem. Phys. 107, 5058 (1997)], dass diese näherungsweise bestimmt werden können, indem MBPT bei der Berechnung von Energiedifferenzen eingesetzt wird. Dies ermöglicht es, Korrekturterme für die Berechnung von geladenen Anregungsenergien zu verwenden, deren Genauigkeit durch Einbeziehung von Störungstermen höhere Ordnungen systematisch verbessert werden kann, ohne neutrale und geladene Systeme explizit getrennt berechnen zu müssen. Wir haben diese Methode für die Berechnung der Bandlücken und der Bandstruktur von dreidimensionalen Festkörpern implementiert und verwendet, wobei Korrekturen bis zur zweiten Ordnung berücksichtigt wurden. Damit konnten wir zeigen , dass Korrekturen zweiter Ordnung nicht ausreichend sind und dass es notwendig ist, auch Terme höherer Ordnung zu berücksichtigen. Um dies zu ermöglichen, verwenden wir die Dyson Gleichung, die eine explizite Summierung von Störungstermen einer bestimmten Klasse, die durch spezifische Diagramme beschrieben wird, bis zu einer unendlichen Ordnung ermöglicht. Wir haben die Dyson-Gleichung und MBPT-Eigenenergie zweiter Ordnung verwendet, um die Bandlücken für eine Reihe von prototypischen Halbleitern zu berechnen. Dabei haben wir eine signifikante Verbesserung der berechneten Bandlücken festgestellt, insbesondere im Vergleich mit Korrekturen zweiter Ordnung, die nur der ersten Iteration der Dyson-Gleichung entsprechen.

Eine erhebliche Schwierigkeit bei der Anwendung von MBPT für Festkörper ist die langsame Konvergenz der Integrale im reziproken Raum, die durch die Singularität des Coulomb-Potentials verursacht wird. Bisher ist die Extrapolation auf ein unendlich dichtes k-Punkt-Gitter der weitverbreitetste Ansatz, um diese langsame Konvergenz zu überwinden. Wir konnten zeigen, dass eine solche Extrapolation zu sehr großen Fehlern führen kann. Der Grund dafür ist, dass der konvergierte Wert der Ein-Teilchen-Anregungsenergie sehr empfindlich auf die Extrapolationsfunktion reagiert, die das asymptotische Verhalten dieses Wertes in Abhängigkeit der Anzahl von k-Punkten in der ersten Brillouin-Zone beschreibt. Zur Lösung dieses Problems haben wir die Singularität und den Beitrag, der die langsame Konvergenz der Energien verursacht, analytisch untersucht. Für diese Analyse wurde ein lokalisierter Basissatz verwendet, aber der dargestellte Formalismus kann für jeden Basissatz verallgemeinert werden. Da damit der Beitrag der Singularität zur langsamen Konvergenz analytisch bekannt ist, können zuverlässige Extrapolationsmethoden entworfen werden. Wie in dieser Arbeit vorgeschlagen, lassen sich dadurch nun auch mit Hilfe einer Verallgemeinerung der Gygi-Baldereschi-Methode akkurate Korrekturterme bestimmen. Wir zeigen dies durch die Berechnung von Ein-Teilchen Energien, die bezüglich der Integrale im reziproken Raum konvergiert sind.

Contents

Chapter 1

Introduction

During the first years after the foundation of quantum theory, the difficulties of applying it to real-life problems surfaced, leading Dirac to state:

"The underlying physical laws necessary for the mathematical theory of a large part of physics and the whole of chemistry are thus completely known, and the difficulty is only that the exact application of these laws leads to equations much too complicated to be soluble. It therefore becomes desirable that approximate practical methods of applying quantum mechanics should be developed, which can lead to an explanation of the main features of complex atomic systems without too much computation."[1]

The underlying physical laws that Dirac is referring to are the Schrödinger equation [2] and its solutions that govern the evolution of quantum systems. The non-relativistic Schrödinger equation is a partial differential equation:

$$i\hbar\frac{\partial\left|\psi(t)\right\rangle}{\partial t} = \widehat{H}\left|\psi(t)\right\rangle \tag{1.1}$$

where $|\psi(t)\rangle$ is the time-dependent wavefunction and $\widehat{H}$ is the Hamiltonian operator representing the total energy. The Hamiltonian equation:

$$\widehat{H}\left|\psi\right\rangle = E\left|\psi\right\rangle \tag{1.2}$$

is the time-independent form of the Schrödinger equation, as a result of the variable separation method. The Schrödinger equation can describe any quantum me-

chanical system on a non-relativistic level. Therefore, we can assume[1] that predicting the properties of matter can be reduced to solving the Schrödinger equation or if relativity cannot be ignored, the relativistic analogue, the Dirac equation [4]. Incorporating relativistic effects by solving the Dirac equation, the wavefunction is no longer scalar but a four-component vector. For this reason, solving it is significantly more demanding than the non-relativistic Schrödinger equation. However, the effects of relativity are negligible for light elements [5] and, as a first approximation, are ignored for many applications[2]. Thus, the objective of quantum chemistry and first-principle material science is to solve the Schrödinger equation (or the Dirac equation when relativity is relevant) for systems composed of atoms.

Solving the Schrödinger equation for systems with a few atoms is a demanding task that can turn impossible for systems with a substantial number of atoms. This is because the Coulomb interaction included in the Schrödinger equation couples the degrees of freedom of all the electrons and nuclei of the system, and there is no known general transformation to decouple them. Consequently, as the degrees of freedom of the system increase, so does the complexity of the equation to be solved. Therefore, as Dirac's quote suggests, the need for approximations is inevitable. The Born-Oppenheimer approximation [7] is commonly employed first, decoupling the degrees of freedom of nuclei and electrons. Solving the exact electronic problem requires the diagonalization of the Hamiltonian matrix. Full Configuration Interaction Method (Full CI) [8] is an exact technique that relies on calculating Hartree-Fock (HF) energy and single-particle states [9], [10] and constructing a basis set from a linear combination of Slater determinants of the HF states. Assuming that the system consists of N particles, and we use a basis set with n HF states, the dimension of the matrix to be diagonalized is $\binom{n}{N}$. This number becomes extremely large as the number of electrons of the system increases. Thus, FCI is unfeasible for systems with more than a few electrons due

[1]The properties prediction reduction into the description of the interactions of the building particles of matter assumes that no new properties emerge at higher-level structures. See, for example, this article from P. W. Anderson: [3].

[2]Relativistic effects can be significant for heavy elements and can be approximately accounted for by replacing the Schrödinger equation with a two-component or scalar approximate equation [6].

to limited computational capacity.

Many methods have been developed to approximate the many-body problem and the solution of the time-independent Schrödinger equation. An efficient approximation must balance the desired accuracy and the computational cost. For instance, density-functional theory (DFT) [11], [12] based methods are widely used and are, in general, of relatively low computational cost since they access only the electron density. DFT within the Kohn-Sham (KS) ansatz [13] has been the leading method by virtue of its low computational cost. The Kohn-Sham ansatz gives a practical way to solve the many-body problem by replacing it with fictitious non-interacting particles moving in a potential that depends on the density and counts for all interactions, known as the Hartree plus exchange-correlation (XC) potential. The exact XC potential is unknown, but many approximations have been developed. The most widely used approximations are the local-density approximation (LDA) [13] and generalized gradient approximation (GGA) [14]–[16], which are computationally inexpensive and produce good results in many cases. The limitation of DFT methods comes from the fact that there is no systematic way to approach the exact potential that would lead to the exact density.

Consequently, there are many different XC potential approximations, and each may improve the results for some materials and properties, but not all. This limitation does not help achieving the predictive power that a method requires to discover new materials.

The most acknowledged case of DFT failure is related to the excitation energies, where it significantly underestimates the bandgaps in solids [17]. This thesis aims to explore alternatives to DFT by applying quantum chemistry and wavefunction methods to excitation energies and bandgap prediction. Before we review existing approaches for the excitation energies that go beyond DFT, we will examine the quantum chemistry methods for the ground state energy prediction.

Approaches to the ground state energy

Quantum chemistry methods for the ground state energy include, among others, the coupled-cluster (CC) theory [18], the many-body perturbation theory (MBPT) [19], [20], and the latter's widely used variant Møller–Plesset (MP) perturbation

theory [21]. These methods can achieve high accuracy by approaching the many-body wavefunction directly and constitute a robust alternative, considering they are, in principle, systematically improvable. Nonetheless, they can be computationally high demanding.

In the case of MBPT, the many-body wavefunction and energy are written as an infinite series of ordered terms, with each term improving the accuracy[3] [22]. This way, the exact result can be approximated by the sum of a finite number of terms. The diagrammatic representation of the correction in each order is an essential tool for tracking the complex expressions that must be evaluated to apply MBPT. The drawback of MBPT is its computational demand, which raises in response to the increase of the complexity of higher-order terms.

While MBPT can start from any approximate Hamiltonian, MP perturbation theory, which has HF as a starting point, is a commonly-used variety of MBPT. MP starts with the self-consistent solution to the HF equation and approaches the exact ground state energy with corrections of increasing order n (MPn). The difference between the exact ground state total energy and HF total energy is known as correlation energy. The first-order correction is zero as a result of Brillouin's theorem [23]. Thus second-order MP (MP2) is the first step beyond HF to approach the exact solution. MP2 has been applied to a wide range of molecules, including typically 85% to 95% of the correlation energy[24]. Hence, interest in the application of MP2 to solids has been growing in the last years (see [25] and references within).

However, its application to solids is limited due to computational demand that increases with the size of the system, as $\mathcal{O}(N^5)$ [26]. For this reason, early implementations were applied in one-dimensional systems [27], [28]. One of the most important features of any implementation is the basis set that spans the single-particle orbitals. An effective selection allows accurate calculations by spanning the wavefunction space with fewer functions. For example, the first implementation for general three-dimensional materials, reported in 2005 by Pissani et al. [29], became feasible by introducing non-canonical local functions to span the

[3]MBPT corrections improve the accuracy under the constraint that the Hamiltonian can be properly separated into a solvable part and a perturbation part, where the effect of the perturbation part is such that the corrections form a descending sequence and the series converges.

space. This version of MP2 is known as local-MP2 or LMP2. This local approximation [30] allowed reducing the size scale to $\mathcal{O}(N)$.

Other three-dimensional periodical implementations followed [31], including also canonical implementations, as the one based on VASP code [32] which adopts plane-waves as the basis set and efficiently exploits parallel computing [33]. Plane-waves are advantageous because of their analytical form that allows simplifications for the matrix elements of the Hamiltonian. While they can describe very well the delocalized, almost-free electrons, the description of localized electrons, as is the case of electrons close to the nuclei, is not practical, resulting in the necessity of approximation methods such as the frozen-core method or the introduction of pseudopotentials, such as the Projector-Augmented-Wave (PAW) method [34] also utilized in the VASP code.

On the other hand, numerical atom-centered orbitals (NAOs) [35], [36] can describe localized electrons eliminating the need for approximate potentials. Moreover, some variations can be very efficient for MBPT methods such as MP [37]. A disadvantage is that their form does not allow for an analytical calculation of the products needed for the Coulomb interaction term. For numerical atom-centered orbitals, but also for any general non-analytic basis, the density fitting technique, also known as resolution of identity (RI) [38]–[40], is preferable since it reduces computational cost [41]–[43]. The basic idea of the RI technique is to represent the products of orbitals with an auxiliary basis set, thus, reducing the cost of the integrations needed for the calculation of the Coulomb matrix elements. This calculation is the most time-consuming step of HF, MP2, as well as for other MBPT approximations. The representation is not unique [44], but the choice defines different varieties of RI. For extended systems, a localized version of RI (RI-LVL) [45], [46] is of practical use for MP2 and other methods that depend on the calculation of the Coulomb matrix by reducing the size scale significantly, even down to linear scale. Fritz Haber Institute 'ab initio molecular simulations' (FHI-aims) is an all-electron, full-potential electronic-structure package that uses NAOs and includes a massively parallel, in-memory implementation of periodic MP2, taking advantage of RI-LVL [47], [48].

Approaches to the excitation energies

A valuable concept for the study of excitations in solids is the quasiparticle [49], [50]. It is based on the assumption that the interacting electron system behaves like a normal Fermi liquid [51], in which the interactions do not dramatically change the system's properties. Still, when one electron is excited, the other electrons will react as a result of the interactions. One can imagine an excited electron moving around other electrons. This electron repels those in its neighbourhood, creating a "lack of electrons" around it. It will move together with this "lack of electrons", forming in this way a collective excitation. This combination is called a quasiparticle. Likewise, if a delocalized electron is excited, it will affect other electrons' momentum. In both cases, the quasiparticle can be described as a particle with altered properties. Thus the non-interacting particle picture does not entirely break, and the excitations resemble the excitations of the non-interacting case. However, instead of particle excitations, we consider collective excitations, namely the quasiparticles.

For a non-interacting system, the Hamiltonian reduces into equivalent independent Hamiltonians for each electron. The solutions constitute the states the electrons can occupy, following the Fermi-Dirac distribution. The energy for removing an electron is connected to the energy of the eigenstate that it was occupying and adding an electron to the energy of the previously empty eigenstate that it will occupy, in both cases, without changing the energy of any other electron. When exciting any interacting system instead, by removing or adding an electron, we end up with a linear combination of the many-body eigenstates of the $N-1$ or $N+1$ system. We can define the energy differences of the neutral and the charged system as the single-particle excitation energies, independently of whether the quasiparticle picture holds. If the quasiparticle picture holds, then the resulting state will approximate one of the eigenstates of the charged system.

Single-particle excitations are obtainable through experiment, in which an electron is removed or added to a solid [52]. Additionally, they define properties such as density of states, band structure, and, in the case of insulators and semiconductors, bandgap. Thus, single-particle excitations are essential for describing solids, but as energy differences, they are equally or more complex to calculate than the ground state energy.

A well-known approach for the single-particle excitations is the single-particle Green's function-based methods, where the propagator (or Green's function) is approximated using the time-dependent MBPT, resulting in a sequence of corrections, as in MBPT [53]. Those methods provide direct access to the single-particle excitation energies straight from the Lehmann representation of the propagator [54], without needing to calculate energy differences. Therefore, they are preferred in the case of band-structure calculations. Furthermore, the advantageous Dyson equation formulation [55], [56] offers a summation of infinite order terms that originate from an order by order approximation to the self-energy.

One established approximation to the propagator is the GW approximation [57]–[59], the most known representative of Green's function methods. It introduces the screened Coulomb potential and approximates the Green's function within the Dyson equation formulation, and has been applied on a wide range of materials, most commonly in a non-self-consistent approximation, known as single-shot GW or G^0W^0 [60], [61]. One way to go beyond GW is the inclusion of parts of the vertex correction, for example, the second and higher-order exchange terms as applied by Ren et al. on molecular systems [62]. The same strategy can be used for periodic solids in principle, but the application is restrained due to the considerably higher cost and complexity. Another approach is Green's function approximations based on CC theory [63], [64], which receives growing interest [65], [66].

An alternative practical theory was developed by Sun and Bartlett in 1997 [67], obtaining the single-particle energies directly from MBPT. They generated a diagrammatic theory to express any-order correction to the single-particle energies. When the HF Hamiltonian is used as a starting point, then this approach defines a series of approximations which we will refer to as sp-Møller–Plesset(n) or sp-MP(n). Furthermore, the Dyson equation can be used to go beyond by including infinite ordered terms. While there are a few reported sp-MP2 energies of one-dimensional systems [28], [31], [68], [69], single-particle energies from MBPT have not yet been well researched for three-dimensional materials. One report for single-particle energies comes from Grüneis et al. in 2010 [70], where they applied an approximate form of the Dyson equation for three-dimensional materials.

Convergence of MBPT

One of the most known challenges for calculating the total and single-particle energies from MBPT in periodic systems is the convergence of lattice points summations present in the Coulomb potential matrix elements. The summation can be performed in real, reciprocal or, when using the Ewald method [71], partially in real and partially in reciprocal space. A proof of the convergence of MBPT correction terms in all orders is described by Sun and Bartlett in 1997 [72], with the lattice points summation performed over real space. Although the MBPT corrections are proven to converge, the convergence is very slow and unpractical, requiring computationally expensive summations, especially for three-dimensional cases.

The issue of slow convergence is already known from HF calculations [73]. When the Coulomb potential is represented in reciprocal space, the slow convergence is assigned to the singularity arising when the denominator is zero. Many efforts have been made to improve the convergence in HF, such as the Gygi-Baldereschi method [73], [74] and the truncated Coulomb potential [75], both reducing the grid density needed for a converged result, therefore their computational effort. Both methods have been successfully implemented for HF, and DFT hybrid functionals [47], [76].

In MP2 and other MBPT-based methods, such as for example CC with singles and doubles (CCSD), the dense grid limit is approached by an extrapolation [32], [77]–[79]. Different extrapolation schemes have been proposed for MP2 and CCSD methods. They are easy to define and they depend on the mathematical treatment of the calculation components. For example, in the case of a plane-wave basis, a linear relation between the inverse of the grid size and the finite-size error is proposed to extrapolate to the infinite limit [80]. On the other hand, for a Gaussian basis a linear relation between the inverse of the grid's size third root and the finite-size error [65] is suggested. With careful comparison of the two methods, one can understand that this contradiction derives from a different treatment of different components. Note here that the size dependence of the finite size error requires attentive consideration for each method and its components. Regarding sp-MP2 convergence, there are reports for the one-dimensional case [31], [81]. It is found to be slower than ground-state MP2, but there is a lack of further research

for higher-dimensional cases.

Moreover, a scheme reducing the computational cost of the lattice summations, as exemplified by Gygi-Baldereschi for the HF case, could expand the applicability of MBPT methods.

Thesis overview

This thesis aspires to explore MBPT for the band structure of solids, as established by Sun and Bartlett [67]. More specifically, it focuses on calculating single-particle excitations, particularly the bandgap using the sp-MP2 and the Dyson equation for three-dimensional insulators and semiconductors. Beyond that, we address the convergence issue of sp-MP2 for three-dimensional cases by generating a method that treats the issue with an extrapolation based on the analytical behaviour of the Coulomb matrix. Furthermore, we suggest a technique to reduce the grid density needed, in the spirit of Gygi-Baldereschi's method.

We initiate with a theoretical introduction to MBPT and the single-particle MBPT in chapter two. In the first section, we state the problem mathematically and describe the difficulties of finding the exact solution, even for simple systems. In the second section, we review the single-particle approximations that serve as a starting point for MBPT and are essential for the correction's accuracy. In the third section, we review MBPT and how diagrams can help keeping track of every order's contributions. In the fourth section, we define single-particle excitations as energy differences and how MBPT is applied to these differences. A diagrammatic notation is introduced following Sun and Bartlett's theory. Section five introduces time-dependent perturbation theory and the Dyson equation to go beyond single-particle MBPT. Sections six and seven introduce an efficient basis set based on localized orbitals and describe the Coulomb operator, a crucial ingredient of MBPT.

Chapter three of this thesis presents the outcome of our research. In the first section, we analyze the singularity and its effect on the convergence of the reciprocal-space integrals. We also prove the integrability of the singularity in MP2 and sp-MP2 equations, and we demonstrate that the treatments applied previously to HF are not suitable for MP2. Moreover, we suggest a way to generalize

Gygi-Baldereschi's method to improve accuracy and treat the convergence of sp-MP2. The second section presents our sp-MP2 implementation and the results for a set of selected materials. Additionally, we implement and apply the Dyson equation with the self-energy in a diagonal second-order approximation to calculate band structure and bandgap. We showcase the importance of the Dyson equation by improving the sp-MP2 bandgaps significantly.

Chapter 2

Theoretical background

2.1 The many-body Hamiltonian

We begin by formulating the main purpose of the electronic-structure theory, which is to solve the many-body Schrödinger equation, and we discuss the challenges to fulfilling this task. We see how the electronic and nuclear degrees of freedom can be separated within the Born-Oppenheimer approximation. For now, we ignore relativistic effects.

The non-relativistic Hamiltonian required to solve in order to define the properties of a molecular or solid system with N electrons and M nuclei will be the sum of the operators of the electrons' kinetic energy $\widehat{T}_e$, kinetic energy of nuclei $\widehat{T}_{nuc}$, and interactions between electrons and nuclei $\widehat{V}_{nuc-e}$, between nuclei $\widehat{V}_{nuc-nuc}$ and between electrons $\widehat{V}_{e-e}$:

$$\widehat{H} = \widehat{T}_e + \widehat{T}_{nuc} + \widehat{V}_{nuc-e} + \widehat{V}_{nuc-nuc} + \widehat{V}_{e-e}. \tag{2.1}$$

In Hartree atomic units ($\hbar = m_e = e = 1$), the kinetic energy of electrons and the kinetic energy of the nuclei will be, respectively:

$$\widehat{T}_e = \sum_{i=1}^{N} -\frac{1}{2}\nabla^2_{\mathbf{r}_i} \tag{2.2}$$

$$\widehat{T}_{nuc} = \sum_{n=1}^{M} -\frac{1}{2m_n}\nabla^2_{\mathbf{R}_n}. \tag{2.3}$$

The interaction between nuclei, electrons and electrons-nuclei is:

$$\widehat{V}_{nuc-nuc} = \frac{1}{2}\sum_{n\neq m}\frac{Z_n Z_m}{|\mathbf{R}_n - \mathbf{R}_m|} \tag{2.4}$$

$$\widehat{V}_{e-e} = \frac{1}{2}\sum_{i\neq j}\frac{1}{|\mathbf{r}_i - \mathbf{r}_j|} \tag{2.5}$$

$$\widehat{V}_{nuc-e} = \sum_{i}^{N}\sum_{n}^{M}\frac{Z_n}{|\mathbf{r}_i - \mathbf{R}_n|}. \tag{2.6}$$

The last term is mixing degrees of freedom of electrons and nuclei, increasing the complexity of solving the problem directly.

2.1.1 Born-Oppenheimer approximation

Due to their large mass m_n, the nuclei move much slower than electrons. As a first approximation, it can be assumed that the electrons follow the motion of the nuclei instantaneously, and the nuclei are affected only by the average electron distribution. This is the Born-Oppenheimer approximation[7] , also called adiabatic, which decouples the motion of nuclei and electrons. Since it is assumed that the electrons follow the motion of the nuclei instantaneously, the wavefunction of the electrons is determined by ignoring the motion of the nuclei and treating their positions as parameters. The wavefunction will be the solution of the Hamiltonian [82]:

$$\widehat{H}_N = \widehat{T}_e + \widehat{V}_{ext} + \widehat{V}_{e-e} \tag{2.7}$$

where $\widehat{V}_{ext}$ is the interaction between electrons and nuclei, and between the nuclei, for a defined position of the nuclei. The wavefunctions of the above Hamiltonian depend on the nuclei positions and define the average electron density in which the nuclei moves, under the Born-Oppenheimer approximation. This thesis focuses on solving the Hamiltonian 2.7, the solutions of which are defined by the equation:

$$\widehat{H}_N\Psi_n^N(\mathbf{r}_1\sigma_1, \mathbf{r}_2\sigma_2, ..., \mathbf{r}_N\sigma_N) = E_n^N\Psi_n^N(\mathbf{r}_1\sigma_1, \mathbf{r}_2\sigma_2, ..., \mathbf{r}_N\sigma_N) \tag{2.8}$$

where $\mathbf{r}_i$ and σ_i are the coordinates and spin of the electron i, respectively. E_n^N are the total energies of the system, with E_0^N being the ground-state energy, which we will denote as E^N for simplification.

The wavefunction depends on the degrees of freedom of all particles in the system. The interaction between electrons couples the electron degrees of freedom, making the problem extremely hard to solve, since the computational effort increases exponentially as the number of electrons in the system increases in an arbitrary system. As discussed in the introduction, a systematic way to approach the solution of this equation is MBPT, which to be applied requires a reliable starting point. This is discussed in the next section.

2.2 Single-particle approximations

As stated in the previous section, the electronic part of the Hamiltonian within the Born-Oppenheimer approximation (equation 2.7), ignoring relativistic effects, has three terms. The first two are single-particle operators, thus, by ignoring the third term the equation can be solved separately for each electron by using the separation of variables technique. The many-body solution will be just a linear combination of the products of single-body wavefunctions. The first step one can do to approach the solution of the Hamiltonian 2.7 is to approximate the two-body Coulomb potential with an appropriate single-particle potential, and we can split the Hamiltonian into the single-electron part:

$$\widehat{H}_0 = \sum_{i=1}^{N} \widehat{T}_i + \sum_{i=1}^{N} \widehat{V}_{ext}(\mathbf{r}_i) + \sum_{i=1}^{N} \widehat{V}_{eff}(\mathbf{r}_i) \tag{2.9}$$

and the remaining interactions:

$$\widehat{V}_{int} = \frac{1}{2} \sum_{i \neq j} \frac{1}{|\mathbf{r}_i - \mathbf{r}_j|} - \sum_{i=1}^{N} \widehat{V}_{eff}(\mathbf{r}_i). \tag{2.10}$$

If the choice of the effective potential is adequate, the many-body interaction (eq. 2.10) can be treated as a perturbation, and MBPT can be applied. This way, a part of the complexity of the problem is passed on to finding an adequate effective potential. After that, MBPT can be applied to describe the system within the desired precision.

2.2.1 Many-body states for indistinguishable particles

The electrons are indistinguishable particles and, therefore, the observables should not change under the exchange of two electrons and the exact solution of the electronic problem should obey this symmetry. As a result, the wavefunction should be symmetric or antisymmetric under the exchange of two particles. Based on the Pauli exclusion principle and quantum field theory, the appropriate solution is antisymmetric.

Suppose $\{\phi_n\}$ is the set of orthogonal eigenfunctions of the single-particle Hamiltonian. In that case, a subset of N eigenfunctions $\phi_1, \phi_2, ..., \phi_N$ can be the occupied states for a problem with N electrons. The many-body independent particle solution for this subset will be an antisymmetric wavefunction that can be expanded as a Slater determinant:

$$\Phi_n^N(\mathbf{r}_1\sigma_1, \mathbf{r}_2\sigma_2, ..., \mathbf{r}_N\sigma_N) = \frac{1}{\sqrt{N!}} \begin{vmatrix} \phi_1(\mathbf{r}_1\sigma_1) & \phi_2(\mathbf{r}_1\sigma_1) & \phi_3(\mathbf{r}_1\sigma_1) & \dots & \phi_N(\mathbf{r}_1\sigma_1) \\ \phi_1(\mathbf{r}_2\sigma_2) & \phi_2(\mathbf{r}_2\sigma_2) & \phi_3(\mathbf{r}_2\sigma_2) & \dots & \phi_N(\mathbf{r}_2\sigma_2) \\ \dots & \dots & \dots & \dots & \dots \\ \phi_1(\mathbf{r}_N\sigma_N) & \phi_2(\mathbf{r}_N\sigma_N) & \phi_3(\mathbf{r}_N\sigma_N) & \dots & \phi_N(\mathbf{r}_N\sigma_N) \end{vmatrix} \tag{2.11}$$

Following the Dirac notation, a single-particle state is denoted by a ket $|\phi_n\rangle$. The position and spin representation of the state n for the particle i will be $\phi_n(\mathbf{r}_i\sigma_i) = \langle \mathbf{r}_i\sigma_i|\phi_n\rangle$, that can be separated into a spin part and a position part as $\phi_n(\mathbf{r}_i\sigma_i) = \psi_n(\mathbf{r}_i)\chi_n(\sigma_i)$. The spin part can be projected to two spin functions, for spin up:

$$\chi_\uparrow = \begin{bmatrix} 1 \\ 0 \end{bmatrix} \tag{2.12}$$

and spin down:

$$\chi_\downarrow = \begin{bmatrix} 0 \\ 1 \end{bmatrix} \tag{2.13}$$

We can separate the wavefunction in spin-up part and spin-down part: $\phi_p(\mathbf{r}\sigma) = \psi_{p\sigma}(\mathbf{r})\chi_\sigma$ where $\sigma = \uparrow, \downarrow$. The antisymmetric Slater determinant wavefunction is denoted as: $\left|\Phi_n^N\right\rangle = |\phi_1\phi_2...\phi_N\rangle$.

In the lowest-energy state, the ground state $\left|\Phi_0^N\right\rangle$, N states with the lowest eigenvalues are occupied[1]. Since the set $\{\phi_n\}$ forms a basis for the single particle problem, we can form a basis for the many-particle problem with the set of anti-symmetric many-body wavefunctions, corresponding to all possible combinations of occupied states. Starting from the ground state by replacing one occupied state i with an unoccupied state a, we obtain:

$$\left|\Phi_i^a\right\rangle = \left|\phi_1 ... \phi_{i-1}\phi_{i+1} ... \phi_N, \phi_a\right\rangle \tag{2.14}$$

In the same way, we can replace two occupied with two unoccupied states to form $\left|\Phi_{ij}^{ab}\right\rangle$[2], and so forth. In general, we denote by $i, j, ...$ the states that are occupied in the ground state, and by $a, b, ..$ the ones that are unoccupied. This set can be used as a basis to expand the many-body state solution of the interacting Hamiltonian. Any many-body state can be written as:

$$\left|\Psi_n^N\right\rangle = c_0\left|\Phi_0^N\right\rangle + \sum_{ai} c_{ai}\left|\Phi_i^a\right\rangle + \sum_{abij} c_{abij}\left|\Phi_{ij}^{ab}\right\rangle + ... \tag{2.15}$$

2.2.2 Approximations to the single-particle potential

Hartree-Fock approximation

By approximating the many-body state as a single Slater determinant and minimizing the expectation value of the Hamiltonian [83], we obtain the many-body wavefunctions as solutions of the effective Hamiltonian:

$$\widehat{H}_{HF} = \widehat{T}_e + \widehat{V}_{ext} + \widehat{V}_{Hartree} + \widehat{V}_x \tag{2.16}$$

where the Hartree potential for each electron is:

$$\widehat{V}_{Hartree}(\mathbf{r}) = \sum_{i,\sigma}\int d\mathbf{r}' \frac{|\psi_{i\sigma}(\mathbf{r}')|^2}{|\mathbf{r}-\mathbf{r}'|} \tag{2.17}$$

[1]The case where the way to take the first N eigenvalues that give the lowest energy is not unique (degenerate ground state) needs special care as it is be explained later.

[2]The antisymmetry leads to the relations: $\left|\Phi_{ij}^{ab}\right\rangle = \left|\Phi_{ji}^{ba}\right\rangle = -\left|\Phi_{ij}^{ba}\right\rangle = -\left|\Phi_{ji}^{ab}\right\rangle$

and $\widehat{V}_x$ is the exchange operator defined by the operation:

$$\widehat{V}_x(\mathbf{r})\psi_{j\sigma_j}(\mathbf{r}) = \sum_{i,\sigma_i} \delta_{\sigma_i,\sigma_j} \int d\mathbf{r}' \frac{\psi^*_{i\sigma_i}(\mathbf{r}')\psi_{j\sigma_j}(\mathbf{r}')}{|\mathbf{r}-\mathbf{r}'|}\psi_{i\sigma_i}(\mathbf{r}) \tag{2.18}$$

This is called Hartree-Fock (HF) approximation, and it describes a system where every electron is moving in the mean-field created by the charge density of the rest of electrons and nuclei, obeying Pauli's exclusion principle. In this approximation, the many-body problem is converted to a set of effective single-particle equations, with the Hamiltonian itself depending on all occupied eigenfunctions. This defines a nonlinear problem that needs to be solved self-consistently. The HF eigenfunctions are used to construct the Slater determinant $\left|\Phi_0^{HF}\right\rangle = \left|\phi_1^{HF}\phi_2^{HF}, ..., \phi_N^{HF}\right\rangle$. The energy will be the expectation value of the Hamiltonian:

$$E^{HF} = \left\langle \phi_1^{HF}\phi_2^{HF}, ..., \phi_N^{HF}\middle|\widehat{H}\middle|\phi_1^{HF}\phi_2^{HF}, ..., \phi_N^{HF}\right\rangle \tag{2.19}$$

Note here that the total energy E^{HF} is not in zeroth order, since it is not calculated as the sum of the eigenvalues, but it includes first order contribution as the expectation value of the Hamiltonian. As a virtue of the variational principle, this energy constitutes an upper limit to the exact total energy. The exact wavefunction is a linear combination of all Slater determinants that can be assembled from the HF functions.

Kohn-Sham effective potential

Kohn-Sham approach, based on density-functional theory (DFT), provides another way to approximate the many-body problem by solving a set of independent particle equations. DFT is based on Hohenberg-Kohn theorem[13], which states that all properties of the ground state can be determined from the ground-state density, thus, a single space variable function is required instead of the N variable wavefunction. However, the connection from the density to any property, i.e., the functional, is unknown and there is no trivial way to find it. The Kohn and Sham ansatz states that the density of the interacting system is equal to the density of a different fictitious non-interacting system which obeys to the Hamiltonian [84]:

$$\widehat{H}_{KS} = \widehat{T}_s + \widehat{V}_{ext} + \widehat{V}_{Hartree} + \widehat{V}_{xc} \tag{2.20}$$

While $\widehat{T}_s$ is the kinetic energy operator, its expectation value does not represent the kinetic energy of true interacting system but of the fictitious non-interacting system. The form of $\widehat{V}_{xc}$ is unknown and, thus, many approximations exist, such as local-density approximation (LDA) or generalized gradient approximation (GGA). These approximations, although quite simple, have proven to be efficient in many systems and are widely used.

The eigenfunctions and eigenvalues of the KS Hamiltonian, even though not representing real particle energies, can serve as an approximation or as a starting point for perturbation theory, as we will see in section 2.3, many-body perturbation theory.

Crystalline solids and periodic boundary conditions

Periodic boundary conditions can model crystalline large systems for which the effects of non-periodicity is negligible. In a periodic system, the positions of all atoms can be obtained by translating a small subset of atoms (lattice basis) along the lattice vectors. A unit cell is a volume containing the lattice basis, if it fills the entire space when periodically repeated, but does not overlap with its periodic images.

Even when there is a translational symmetry in atomic positions, the electronic wavefunctions are not necessarily periodic with the same lattice vectors. To make electronic states countable, Born-von-Karman conditions can be used:

$$\psi(\mathbf{r} + N_i\mathbf{a}_i) = \psi(\mathbf{r}) \tag{2.21}$$

where N_i is the number of cells in the box in each direction so that $N_1N_2N_3 = N^3$. This condition results in a discrete set of wavefunctions, and the exact solution can be obtained in the thermodynamic limit ($N_i \to \infty$).

[3] In the case of a many-particle wavefunction the same condition would be implied but this time we should write

$$\psi(\mathbf{r}_1, ..., \mathbf{r}_i + N_i\mathbf{a}_i, ...) = \psi(\mathbf{r}_1, ..., \mathbf{r}_i, ...)$$

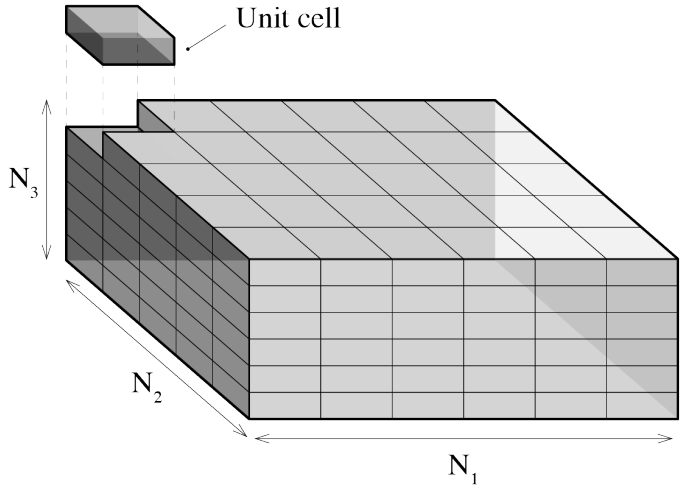

Figure 2.1: A volume $V_N = N_1 N_2 N_3 \Omega$ where Ω is the volume of the unit cell.

Bloch theorem

The wavefunctions of a Hamiltonian with translational symmetry[4] can be written as:

$$\psi_{i\mathbf{k}}(\mathbf{r}) = u_{i\mathbf{k}}(\mathbf{r}) e^{\mathrm{i}\mathbf{k}\mathbf{r}} \tag{2.22}$$

where the function u is satisfying the equation: $u_{i\mathbf{k}}(\mathbf{r}+\mathbf{R}) = u_{i\mathbf{k}}(\mathbf{r})$, following the lattice periodicity. This is the Bloch's theorem. Its proof (See for example: Neil Ashcroft and N. David Mermin, Solid State Physics, 1976 [85]) is based on the translational symmetry of the lattice. Another useful form of Bloch's theorem is $\psi_{i\mathbf{k}}(\mathbf{r}-\mathbf{R}) = \psi_{i\mathbf{k}}(\mathbf{r}) e^{\mathrm{i}\mathbf{k}\mathbf{R}}$, which shows that for a symmetrically equivalent points in space, the wavefunction changes only by a phase. It follows from the Born-von-Karman boundary conditions (equation 2.21), that the crystal momentum quantum number $\mathbf{k}$ should obey the relation:

$$e^{\mathrm{i}\mathbf{k}N_i\mathbf{a}_i} = 1 \tag{2.23}$$

[4]The Hamiltonian is translationally invariant in the case we have a periodic potential $V(\mathbf{r}+\mathbf{R}) = V(\mathbf{r})$

For a set of vectors $\mathbf{g}_1$ such that $\mathbf{g}_1\mathbf{a}_j = 2\pi\delta_{i,j}$, the crystal momentum can be written as:

$$\mathbf{k} = \frac{m_1}{N_1}\mathbf{g}_1 + \frac{m_2}{N_2}\mathbf{g}_2 + \frac{m_3}{N_3}\mathbf{g}_3$$

with $m_1, m_2, m_3 = 0, \pm1, \pm2, ...$ The vectors $\mathbf{g}_1, \mathbf{g}_2, \mathbf{g}_3$ define a lattice in the reciprocal space. In the limit of infinite crystal $N_1, N_2, N_3 \to \infty$, the crystal momentum is continuous. The relation between energy and crystal momentum is called dispersion relation.

2.3 Many body perturbation theory

There are multiple ways to apply MBPT. We start with Rayleigh-Schrödinger perturbation theory, which is widely applied. Applying HF as the unperturbed Hamiltonian (MP perturbation theory) has the advantage of canceling many of the contributions, since they are already included by virtue of the self-consistency of HF wavefunctions. MBPT provides an approximation to the many-body eigenstates and eigenenergies of the interacting system, allowing to obtain the single particle excitation energies, as presented in the next section 2.4.

2.3.1 Rayleigh-Schrödinger perturbation theory

To apply MBPT, we separate the Hamiltonian into two parts: one with a known solution, and the other is the perturbation term that should be small. Therefore, the Hamiltonian is expressed as:

$$\widehat{H} = \widehat{H}_0 + \lambda\widehat{V}_{int} \tag{2.24}$$

where λ is a small constant which ensures that the perturbation term is small [82]. The solutions of the Hamiltonian obey the equation: $\widehat{H}\left|\Psi_n\right\rangle = E_n\left|\Psi_n\right\rangle$. The unperturbed energies and wavefunctions are solutions of the equation: $\widehat{H}_0\left|\Psi_n^{(0)}\right\rangle = E_n^{(0)}\left|\Psi_n^{(0)}\right\rangle$ where the wavefunctions are chosen to be orthonormal, following the relation : $\left\langle\Psi_n^{(0)}\middle|\Psi_m^{(0)}\right\rangle = \delta_{m,n}$. The wavefunctions depend, in general, on the coordinates and spin of all particles in the system. Applying perturbation theory, the exact wavefunction and energy can be written as an expansion:

$$\left|\Psi_n\right\rangle = \left|\Psi_n^{(0)}\right\rangle + \lambda\left|\Psi_n^{(1)}\right\rangle + \lambda^2\left|\Psi_n^{(2)}\right\rangle + ... \tag{2.25}$$

$$E_n = E_n^{(0)} + \lambda E_n^{(1)} + \lambda^2 E_n^{(2)} + ... \tag{2.26}$$

The solutions for the perturbed system can be found on every order from the equations:

$$E_n^{(m)} = \left\langle \Psi_n^{(0)} \middle| \widehat{V}_{int} \middle| \Psi_n^{(m-1)} \right\rangle \tag{2.27}$$

and:

$$\left|\Psi_n^{(m)}\right\rangle = \sum_k \alpha_{kn}^m \left|\Psi_k^{(0)}\right\rangle \tag{2.28}$$

where the coefficients α_{kn}^m should obey the relation:

$$(E_n^0 - E_k^0)\alpha_{kn}^m = \sum_j V_{int}^{kj} \alpha_{jn}^{m-1} - \sum_{l=0}^{m-1} E_n^{m-l} \alpha_{kn}^l \tag{2.29}$$

V_{int}^{kj} are the matrix elements of the perturbation in the basis set of the unperturbed system's eigenvectors. An extra relation for the coefficients arises from normalization, where most commonly the unperturbed wavefunctions are chosen orthogonal to the correction in every order: $\left\langle \Psi_n^{(0)} \middle| \Psi_n^{(m)} \right\rangle = \delta_{m,0}$. From the above equations, it is easy to express the first-order correction in energy:

$$E_n^{(1)} = \left\langle \Psi_n^{(0)} \middle| \widehat{V}_{int} \middle| \Psi_n^{(0)} \right\rangle = V_{int}^{nn} \tag{2.30}$$

and wavefunction:

$$\left|\Psi_n^{(1)}\right\rangle = \sum_{k \neq n} \frac{V_{int}^{kn}}{(E_n^0 - E_k^0)} \left|\Psi_k^{(0)}\right\rangle \tag{2.31}$$

Knowing the first-order correction, we can directly calculate the second-order correction to the energy:

$$E_n^{(2)} = \sum_{k \neq n} \frac{V_{int}^{kn} V_{int}^{nk}}{(E_n^0 - E_k^0)} = \sum_{k \neq n} \frac{|V_{int}^{nk}|^2}{(E_n^0 - E_k^0)} \tag{2.32}$$

In this expression there are two perturbation matrix elements multiplied for $E_n^{(2)}$, while for $E_n^{(1)}$ we have only one. This is true for all orders, i.e., in the third order we have three, and so forth. The same is true for the states. The second-order correction to the state is:

$$\left|\Psi_n^{(2)}\right\rangle = \sum_{k \neq n} \left[\sum_{j \neq n} \frac{V_{int}^{kj} V_{int}^{jn}}{(E_n^0 - E_k^0)(E_n^0 - E_j^0)} - \frac{V_{int}^{kn} V_{int}^{nn}}{(E_n^0 - E_k^0)^2} \right] \left|\Psi_k^{(0)}\right\rangle \tag{2.33}$$

Following the same process higher-order corrections can be calculated, but its expressions become increasingly complex.

Degenerate case

In the degenerate case, applying the theory as described above is problematic because there is no unique way to go from the perturbed system to the unperturbed for $\lambda \to 0$. Since this case is out of the scope of this thesis, it will only be discussed briefly. For the degenerate states, the quantity $(E_n^0 - E_k^0)$ will be zero for some $n \neq k$. This does not provide a unique way to project the perturbed states to the unperturbed, since the eigenstates are not uniquely defined in the degeneracy subspace. We can solve this by choosing the right linear combination of the eigenstates that diagonalize the perturbation directly in the degeneracy subspace, under the condition that the perturbation does not share the same symmetry with the unperturbed Hamiltonian.

2.3.2 Application to many-body problems

As described in section 2.2, the many-body problem can be separated into a single-particle part and an interaction part that can be treated as a perturbation. The solutions to the single-particle part will be the antisymmetrized states (the Slater determinants) described in section 2.2.1. Before we apply perturbation theory to many-body problems, we demonstrate how to calculate the expectation values of single-particle operators and two-particle operators, in particular the Coulomb interaction. For this purpose, it is useful to introduce the second quantization formulation.

Second quantization

We begin by defining the removal and addition operators, $\widehat{\alpha}_p$ and $\widehat{\alpha}_q^\dagger$ as:

$$\widehat{\alpha}_p \left|\phi_1, ..., \phi_p, ..., \phi_N\right\rangle = (-1)^P \left|\phi_1, ..., \phi_N\right\rangle \text{, or zero if } p \text{ not present} \tag{2.34}$$

$$\widehat{\alpha}_p^\dagger \left|\phi_1, ..., \phi_N\right\rangle = (-1)^P \left|\phi_1, ..., \phi_p, ..., \phi_N\right\rangle \text{, or zero if } p \text{ present} \tag{2.35}$$

where P is the number of permutations needed to bring the p function from the most left position to the final one, according to ascending energy. A single-particle operator can be written as:

$$\widehat{O} = \sum_{pq} O_{pq} \widehat{\alpha}_p^\dagger \widehat{\alpha}_q \tag{2.36}$$

where O_{pq} is the matrix element of the operator $O_{pq} =< \phi_p|\widehat{O}|\phi_q >$. For two Slater determinants the matrix element will be:

$$\langle\Psi|\widehat{O}|\Phi\rangle = \langle\psi_1\psi_2...\psi_N|\widehat{O}|\phi_1\phi_2...\phi_N\rangle \tag{2.37}$$

where replacing the second-quantized form we will have:

$$\langle\Psi|\widehat{O}|\Phi\rangle = \sum_{pq} O_{pq} \langle\psi_1\psi_2, ..., \psi_N|\widehat{\alpha}_p^\dagger\widehat{\alpha}_q|\phi_1\phi_2, ..., \phi_N\rangle \tag{2.38}$$

According to the order of the operators, the function ϕ_q should exist in the right state, otherwise the action of the operator will result in zero. Then the addition operator acts, adding a function ϕ_p. In order for this operation to be non-zero, the function ϕ_p should either be identical to ϕ_q (the element will be non-zero for all occupied functions) or it should not be present in the right state in the first place. The matrix element will be non-zero, if the state created coincides with a permutation of the left state. In other words, if there is a permutation in which all orbitals coincide: $|\psi_1\psi_2, ..., \psi_N\rangle = (-1)^P\widehat{P}\,|\phi_1\phi_2, ..., \phi_N\rangle$, then:

$$\langle\Psi|\widehat{O}|\Phi\rangle = \sum_{i=1}^{N}(-1)^P \langle\phi_i|\widehat{O}|\phi_i\rangle \tag{2.39}$$

If there is a permutation in which $|\psi_1, ..., \psi_i, ..., \psi_N\rangle = (-1)^P\widehat{P}\,|\phi_1, ..., \psi_i, ..., \phi_N\rangle$, with $\psi_i \neq \phi_i$, i.e., there is one orbital that does not coincide in the two determinants, then:

$$\langle\Psi|\widehat{O}|\Phi\rangle = (-1)^P \langle\psi_i|\widehat{O}|\phi_i\rangle \tag{2.40}$$

If there are two or more orbitals that do not coincide the expectation value is zero, since we cannot create the same state or a permutation of it while acting with one removal and one addition operator.

For two-particle operators symmetric to the exchange of two particles, as is the Coulomb interaction, we can write in second quantization:

$$\widehat{V} = \frac{1}{4}\sum_{pqrs} V_{pq,rs}\widehat{\alpha}_p^\dagger\widehat{\alpha}_q^\dagger\widehat{\alpha}_s\widehat{\alpha}_r \tag{2.41}$$

where

$$\begin{aligned} &V_{pq,rs} = \langle\phi_p\phi_q|\widehat{V}|\phi_r\phi_s\rangle = \\ &2\left(\frac{1}{2}\langle\phi_p|\langle\phi_q|\widehat{V}\,|\phi_r\rangle\,|\phi_s\rangle - \frac{1}{2}\langle\phi_p|\langle\phi_q|\widehat{V}\,|\phi_s\rangle\,|\phi_r\rangle\right) \equiv \langle\phi_p\phi_q|\,|\phi_r\phi_s\rangle \end{aligned} \tag{2.42}$$

In the second-quantized form:

$$\langle\Psi|\widehat{V}|\Phi\rangle = \frac{1}{2}\sum_{pqrs} V_{pq,rs}\,\langle\psi_1\psi_2,...,\psi_N|\widehat{\alpha}_p^\dagger\widehat{\alpha}_q^\dagger\widehat{\alpha}_s\widehat{\alpha}_r|\phi_1\phi_2,...,\phi_N\rangle \tag{2.43}$$

In this case, both functions ϕ_r and ϕ_s must exist in the right state to yield a non-zero result. Then, if ϕ_p and ϕ_q do not exist in the state created after the operation of both removal operators, the action of the addition operators will give a non-zero result. If the state created after the operation of the addition operators is the left state or a permutation of it, the matrix element will be non-zero. Thus, if all orbitals coincide under some permutation P, we will have:

$$\langle\Psi|\widehat{V}|\Phi\rangle = (-1)^P\frac{1}{2}\sum_{i,j}^{N,N}\langle\phi_i\phi_j|\,|\phi_i\phi_j\rangle \tag{2.44}$$

If there is one non-coincidence $\psi_i \neq \phi_i$:

$$\langle\Psi|\widehat{V}|\Phi\rangle = (-1)^P\sum_{j}^{N}\langle\psi_i\phi_j|\,|\phi_i\phi_j\rangle \tag{2.45}$$

If there are two non-coincidences $\psi_i \neq \phi_i$ and $\psi_j \neq \phi_j$:

$$\langle\Psi|\widehat{V}|\Phi\rangle = \langle\phi_i\phi_j|\,|\phi_i\phi_j\rangle \tag{2.46}$$

For more than two non-coincidences the matrix element is zero.

Zeroth order

In the zeroth order, we arrive at the solutions of the Hamiltonian 2.9, $|\Phi_n\rangle$. We start with $\{\phi_i\}$ that are eigenfunctions of the single-particle Hamiltonian 2.9 solved for each electron separately. For a system with N particles, we can form states where we select N functions $\phi_i\phi_j,...\phi_k$ to be occupied and the rest $\phi_a\phi_b,...$ unoccupied. The antisymmetric Slater determinants: $|\Phi_n\rangle = |\phi_i\phi_j...\phi_k\rangle$ composed of different occupied functions will be the set of zeroth-order wavefunctions. We denote the ground state as $|\Phi\rangle$, composed of the lowest-energy functions as described in section 2.2.1. The highest of the occupied functions' energies is denoted as ϵ_{HO} and the lowest of the unoccupied functions energies as ϵ_{LU}. Excitations

are formed by leaving unoccupied functions with energies smaller than ϵ_{HO} and occupy functions with energies higher than ϵ_{LU}. When one occupied function is replaced with an unoccupied we have the single excited state $|\Phi_i^a\rangle$. For two replacements we have the double excited state $\left|\Phi_{ij}^{ab}\right\rangle$, and so forth. The energy of any state is the sum of the energies of the occupied functions.

First-order correction

While we focus on the correction of the ground state, the same process applies to any state. From the relation 2.30:

$$E^{(1)} = \langle\Phi|\widehat{V}_{int}|\Phi\rangle = \langle\Phi|\widehat{V} - \widehat{V}_{eff}|\Phi\rangle \tag{2.47}$$

Here, $\widehat{V}$ is the Coulomb operator:

$$\langle\Phi|\widehat{V}|\Phi\rangle = \frac{1}{2}\sum_{i,j}^{N,N}\langle\phi_i\phi_j|\,|\phi_i\phi_j\rangle \tag{2.48}$$

and $\widehat{V}_{eff}$ is the effective potential in the Hamiltonian 2.9:

$$\langle\Phi|\widehat{V}_{eff}|\Phi\rangle = \sum_{i=1}^{N}\langle\phi_i|\widehat{V}_{eff}|\phi_i\rangle \tag{2.49}$$

We note that:

$$\langle\Phi|\widehat{H}|\Phi\rangle = E^{(0)} + E^{(1)} \tag{2.50}$$

This is the reference energy. For example, if we use HF as a starting point then: $E_{HF} = \langle\Phi_{HF}|\widehat{H_N}|\Phi_{HF}\rangle$, where H is the full many-body Hamiltonian of the electrons (eq. 2.7).

Second-order correction

The second-order correction to the energy is given in equation 2.32. The summation over the states excludes the state that we want to correct, so only the excited determinants (with at least one orbital different from the reference determinant)

are included in the sum. Since we have only one- and two-body operators in our perturbation, just the single and double excitations will result in a non-zero matrix element. For single excitations, the matrix element is:

$$\langle \Phi_i^a | \widehat{V}_{int} | \Phi \rangle = \langle \Phi_i^a | \widehat{V} - \widehat{V}_{eff} | \Phi \rangle \tag{2.51}$$

and for double excitations, the single-particle part will be zero:

$$\left\langle \Phi_{ij}^{ab} \middle| \widehat{V}_{int} \middle| \Phi \right\rangle = \left\langle \Phi_{ij}^{ab} \middle| \widehat{V} \middle| \Phi \right\rangle \tag{2.52}$$

We can write the correction in two parts, the part that comes from double excitations:

$$E_d^{(2)} = \frac{1}{4} \sum_{ijab} \frac{|\langle \phi_i \phi_j | \, | \phi_a \phi_b \rangle|^2}{\epsilon_i + \epsilon_j - \epsilon_a - \epsilon_b} \tag{2.53}$$

and the part coming from singly excited states:

$$E_s^{(2)} = \sum_{ia} \frac{|\frac{1}{2} \sum_j \langle \phi_i \phi_j | \, | \phi_a \phi_j \rangle - \langle \phi_i | \widehat{V}_{eff} | \phi_a \rangle|^2}{\epsilon_i - \epsilon_a} \tag{2.54}$$

We express the effective potential as the difference of two operators: one defined as an operator $\widehat{U}$ that when projected to a basis set for a system with N occupied single-particle states results in:

$$U_{pq} = \sum_j \langle \phi_q \phi_j | \, | \phi_q \phi_j \rangle \tag{2.55}$$

and the other, defined as:

$$\widehat{F}_{eff} = \widehat{U} - \widehat{V}_{eff}. \tag{2.56}$$

Then we can rewrite this term as:

$$E_s^{(2)} = \sum_{ia} \frac{|\langle \phi_i | \widehat{F}_{eff} | \phi_a \rangle|^2}{\epsilon_i - \epsilon_a}. \tag{2.57}$$

When Hartree-Fock orbitals are used, the contribution of this term is zero since $\widehat{V}_{eff(HF)} = \widehat{U}$.

In general, the interaction can be written as:

$$\widehat{V}_{int} = \widehat{W} + \widehat{F}_{eff} \tag{2.58}$$

with $\widehat{W} = \widehat{V} - \widehat{U}$. Consequently, some parts of the Coulomb matrix elements cancel. For example, in the matrix element:

$$\begin{aligned}&\left\langle \Phi_i^a \middle| \widehat{W} \middle| \Phi_{ij}^{ab} \right\rangle = \\ &\sum_k \langle \phi_b \phi_k | \, | \phi_j \phi_k \rangle + \langle \phi_b \phi_a | \, | \phi_j \phi_a \rangle - \langle \phi_b \phi_i | \, | \phi_j \phi_i \rangle \\ &- \sum_k \langle \phi_b \phi_k | \, | \phi_j \phi_k \rangle\end{aligned} \tag{2.59}$$

the last term comes from $\widehat{U}$ and cancels the first term coming from $\widehat{V}$.

2.3.3 Elements of diagrammatic notation

Writing and keeping track of the corrections becomes challenging as we increase in order. A convenient way to overcome this is the diagrammatic notation combined with the necessary rules that describe the connection of a diagram to an equation. There are many diagrammatic notations including Feynman, Goldstone, Hugenholtz diagrams, besides others. In many cases there is a connection between representations. For example, the connection between Feynman and Goldstone diagrams is described in literature by Fetter and Walecha in Quantum Theory of Many-Particle Systems [86], and the connection between Goldstone and Hugenholtz diagramms by Shavitt and Bartlett on Many-body methods in chemistry and physics [22]. Here we review some basics principles of Goldstone diagrams [19] and how to read them. Goldstone showed that the energy difference between the ground states of the interacting and non-interacting Hamiltonians can be written as:

$$E - E^{(0)} = \langle \Phi | \widehat{V}_{int} \sum_n \left(\frac{1}{E^{(0)} - \widehat{H}_0} \widehat{V}_{int} \right)^n |\Phi\rangle_{connected} \tag{2.60}$$

where "$connected$" means we should keep only the connected diagrams, as will be explained as soon as we review how to represent the above expression diagrammatically. In order to understand this expression we expand the summation:

$$\begin{aligned}&\widehat{V}_{int} \left(\sum_n \frac{1}{E^{(0)} - \widehat{H}_0} \widehat{V}_{int} \right)^n = \\ &\widehat{V}_{int} + \widehat{V}_{int} \frac{1}{E^{(0)} - \widehat{H}_0} \widehat{V}_{int} + \widehat{V}_{int} \frac{1}{E^{(0)} - \widehat{H}_0} \widehat{V}_{int} \frac{1}{E^{(0)} - \widehat{H}_0} \widehat{V}_{int} + ...\end{aligned} \tag{2.61}$$

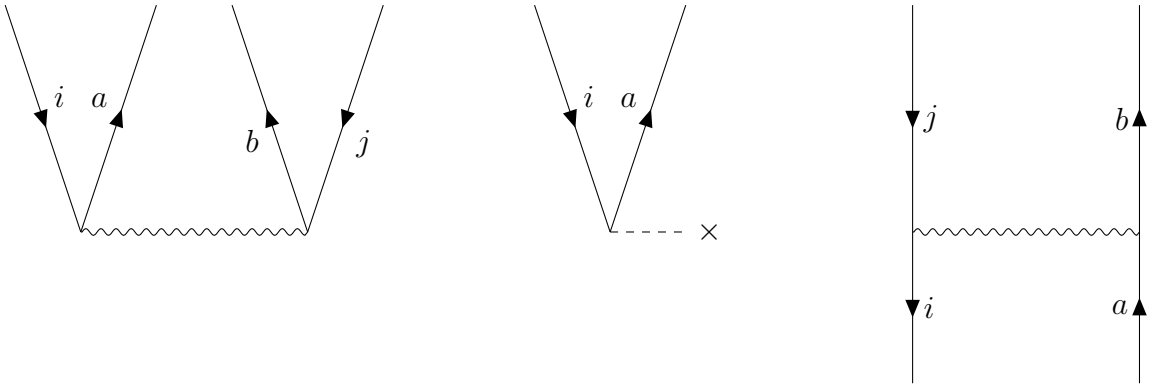

Figure 2.2: Examples of diagram parts. The first of the above diagrams represents the term $\langle\phi_i|\,\langle\phi_j|\,\widehat{V}\,|\phi_a\rangle\,|\phi_b\rangle$, the second represents single-body interaction $\langle\phi_i|\widehat{f}_{eff}|\phi_a\rangle$, and the third represents the interaction between a particle and a hole $\langle\phi_i|\,\langle\phi_a|\,\widehat{V}\,|\phi_j\rangle\,|\phi_b\rangle$. In general, the rule $\langle$left-out right-out$|\widehat{V}|$left-in right-in$\rangle$ holds.

We can now insert the projection operator: $\sum_k |\Phi_k\rangle\,\langle\Phi_k|$ between the operators:

$$\langle\Phi|\widehat{V}_{int}|\Phi\rangle + \sum_k \frac{\langle\Phi|\widehat{V}_{int}|\Phi_k\rangle\ \langle\Phi_k|\widehat{V}_{int}|\Phi\rangle}{E^{(0)} - E_k^{(0)}} + ... \tag{2.62}$$

The interaction creates excited states where the excited orbitals can be interpreted as particles, and the orbitals that were occupied in $|\Phi\rangle$ but unoccupied in the excited state as holes. A particle-hole pair propagates until the next interaction operator scatters them or creates new particles and holes, and so forth. This can be depicted by representing a particle (hole) a (i) by a line with an arrow going up (down), the two-body interaction $\widehat{V}$ as a wavy line, and the single-body interaction $\widehat{F}_{eff}$ as a dashed line.

We may create diagrams representing the expectation value of the sequence of operators by starting at the bottom, where the ground state is represented by nothing, i.e., no particle or hole lines, then adding all interaction lines as they appear in the sequence, and finally connecting with the hole and particle lines that end on the top of the diagram with the ground state again. The order of the diagram is the number of two-particle interaction lines that it has, e.g., a diagram with five

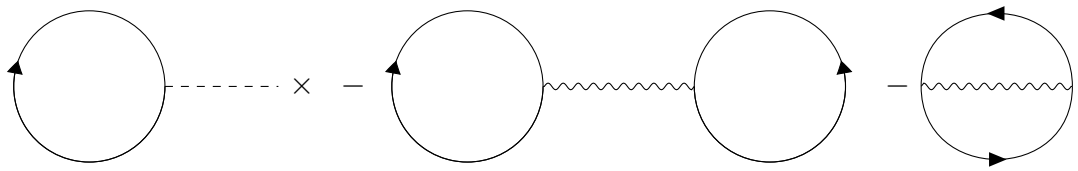

Figure 2.3: First order diagrams.

wavy lines will be of fifth order. From all possible diagrams, Goldstone's theorem states to choose only the connected ones. Connected diagrams are the ones that cannot be separated into two or more diagrams, i.e., all parts of the diagram are connected with an interaction line.

First-order diagrams

The first order correction is the interaction's expectation value:

$$E^{(1)} = \langle \Phi | \widehat{V}_{int} | \Phi \rangle \,,$$

so that no holes or particles are created, and only the interaction between the occupied orbitals is present. By rewriting the first-order correction using the definition 2.56, we get:

$$E^{(1)} = \sum_i \langle \phi_i | \widehat{F}_{eff} | \phi_i \rangle - \frac{1}{2} \sum_{ij} \langle \phi_i \phi_j | \, | \phi_i \phi_j \rangle \,. \tag{2.63}$$

This corresponds to the diagrams of figure 2.3.

Second-order diagrams

In the second order particle-hole pairs are created and propagate until they interact again to recombine. The first two diagrams of figure 2.4 represent the direct and exchange parts of the two-body term shown in the equation 2.53, and the third diagram represents the single-body part 2.57. This thesis we focuses on theories based on second-order perturbation correction so, even though the diagrammatic representation is a very useful tool to keep track of higher-order corrections, we

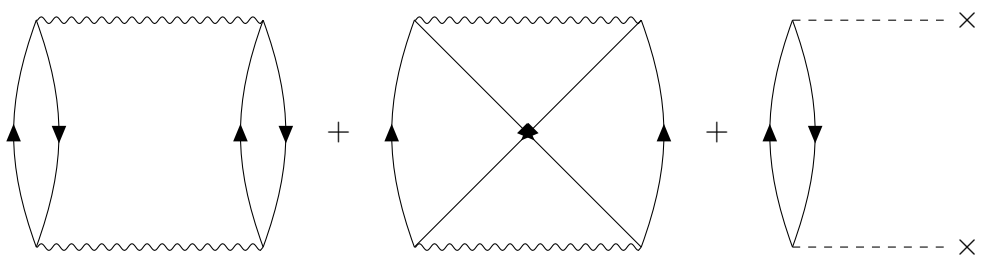

Figure 2.4: Second-order diagrams.

will not need them here. Instead, we will show how we can use second-order diagrams can be applied to go beyond second order by using summation techniques. Such techniques are beneficial when it is not sufficient to end the expansion in a finite order.

Antisymmetrized Goldstone diagrams

The diagrammatic representation can be simplified by taking advantage of the symmetries. In this case, we can represent the antisymmetrized Coulomb matrix element:

$$\langle \phi_i \phi_j | \, | \phi_a \phi_b \rangle$$

with one interaction line instead of having both:

$$\langle \phi_i | \, \langle \phi_j | \, \widehat{V} \, | \phi_a \rangle \, | \phi_b \rangle$$

and:

$$\langle \phi_i | \, \langle \phi_j | \, \widehat{V} \, | \phi_b \rangle \, | \phi_a \rangle$$

The direct and exchange diagrams will be equivalent, but we need to assign a factor of $1/2$ for each equivalent pair, since the summation over all states will include each pair twice. With the antisymmetric diagrammatic notation, the first- and second-order diagrams are found in figures 2.5 and 2.6.

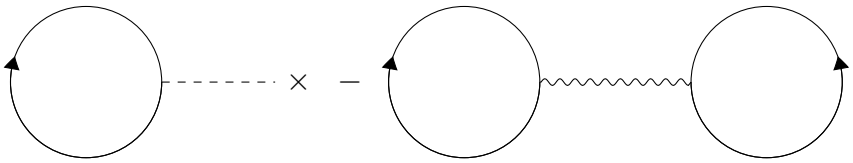

Figure 2.5: Antisymmetrized Goldstone diagrams representing the first-order corrections to the total energy.

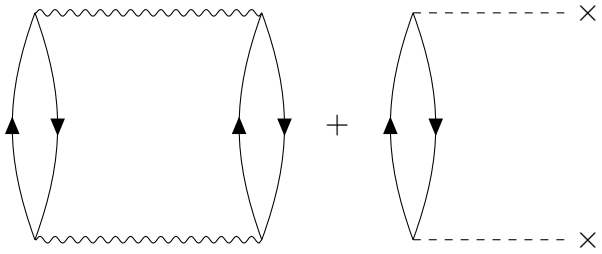

Figure 2.6: Antisymmetrized Goldstone diagrams representing the second-order corrections to the total energy.

2.4 MBPT for the band structure of solids

The main goal of this thesis is the application of second-order based theories for the calculation of the bandgap and band structure of semiconductors and insulators. For this reason, we start by exploring how to apply Rayleigh-Schrödinger MBPT, based on the theory developed by J.Q. Sun and R.J. Bartlet in 1997 [67] for the calculation of the bandgap and band structure of solids. More specifically, we focus on single-particle excitations, known also as charged excitations, since they describe the addition or removal of an electron to/from the ground state. These excitations are relevant for the band structure and gap. Single-particle excitation energies are accessible experimentally. In the case of solids, direct and inverse photoelectron spectroscopy can give important information about the band structure and the bandgap of solids [59].

The energy of a single-particle excitation[5] is defined as the energy difference between the ground state of N electrons and a state with one less or extra electron:

$$\begin{aligned} \epsilon_p^- &= E(N) - E_p(N-1) \\ \epsilon_p^+ &= E_p(N+1) - E(N) \end{aligned} \tag{2.64}$$

The bandgap is then the minimum of the difference $G = \epsilon_p^+ - \epsilon_p^- = [E_p(N+1) - E(N)] - [E(N) - E_p(N-1)]$.

2.4.1 Single-particle excitations in single-particle approximations

Within the independent-particle picture, removing one electron will leave a previously occupied state unoccupied, whereas adding an electron will occupy one extra state.

Since the total energy is the sum of the energies of the occupied states, the bandgap is $\epsilon_{LU} - \epsilon_{HO}$[6].

2.4.2 MBPT for single-particle excitations

To calculate the single-particle (charged) excitation energies we should solve the Hamiltonian not only for the neutral system but also for the charged systems with $N-1$ and $N+1$ electrons:

$$\widehat{H}^{N-1} \left|\Psi_p^{N-1}\right\rangle = E_p^{N-1} \left|\Psi_p^{N-1}\right\rangle$$

$$\widehat{H}^{N+1} \left|\Psi_p^{N+1}\right\rangle = E_p^{N+1} \left|\Psi_p^{N+1}\right\rangle$$

[5]We note here that the single particle excitations that are charged excitations, as the two-particle, three-particle, etc. excitations, that describe the removal or addition of two, three, etc, electrons, there are also the neutral excitations that are the excited states of the Hamiltonian H_N of eq. 2.7. These excitations can be found, for example, from the theory of the previous section applying MBPT for the excited states.

[6]This is not so when the potential in the single-particle Hamiltonian depends on the states or the density of other electrons, as in HF, LDA, or GGA, because removing or adding an electron affects in general the wavefunctions of the other electrons. What happens is that the effective potential can be different for different number of electrons.

The exact solution of the many-body Hamiltonian cannot be obtained for most systems of practical interest. Instead, we apply MBPT and the excitation energy can be evaluated in each order of perturbation as follows:

$$\begin{aligned}\pm\epsilon_p^{\mp} =& E(N) - E_p(N\mp 1) = \\ & [E^{(0)}(N) - E_p^{(0)}(N\mp 1)] + [E^{(1)}(N) - E_p^{(1)}(N\mp 1)] \\ & + [E^{(2)}(N) - E_p^{(2)}(N\mp 1)] + ... = \\ & \pm\epsilon_p^{\mp(0)} + \pm\epsilon_p^{\mp(1)} + \pm\epsilon_p^{\mp(2)} + ...\end{aligned} \tag{2.65}$$

We start with an approximate single particle Hamiltonian with the form of eq. 2.9, assuming an appropriate effective potential V_{eff} that is a good approximation for the charged and the neutral system. For the charged system, the summation will be for $N \pm 1$ electrons instead of N. Let us denote as $|\Phi_{p^{\pm}}\rangle$ a Slater determinant of the charged system where an electron has been removed from or added to the state p. Then:

$$E_p^{(0)}(N\pm 1) = E^{(0)}(N) \pm \epsilon_p^{\pm}$$

For the addition of an electron, p must be an unoccupied orbital, whereas for the removal it should be an occupied orbital of the ground state $|\Phi\rangle$. For the neutral system, we have defined an operator $\widehat{U}$ (see section **??**) in such a way that it cancels a part of the Coulomb operator. Then the interaction can be expressed as:

$$\widehat{V}_{int} = (\widehat{V} - \widehat{U}) + \widehat{F}_{eff} \tag{2.66}$$

with $\widehat{F}_{eff} = \widehat{U} - \widehat{V}_{eff}$. The operator $\widehat{U}$ is defined by its matrix elements:

$$U_{qr} = \sum_j^N \langle\phi_q\phi_j|\,|\phi_r\phi_j\rangle \tag{2.67}$$

Denoting $\widehat{W} = \widehat{V} - \widehat{U}$, we can write:

$$\widehat{V}_{int}^N = \widehat{W} + \widehat{F}_{eff} \tag{2.68}$$

For the charged system, the interaction can be written as

$$\widehat{V}_{int}^p = \widehat{W} + \widehat{F}_{eff}^p \tag{2.69}$$

The operator in the equation 2.67 does not include the effect of the addition or removal of an electron. To include the effect we need to add:

$$U^p_{qr} = \pm \langle \phi_q \phi_p | \, | \phi_r \phi_p \rangle \tag{2.70}$$

where the $+/-$ sign is for addition/removal of an electron. By comparing, we can observe that $\widehat{F}^p_{eff} = \widehat{F}_{eff} + \widehat{U}^p$.

The neutral system's energy is:

$$E = \langle \Phi | \widehat{H} | \Phi \rangle + \langle \Phi | \widehat{V}_{int} \left(\sum_{n=1}^{\infty} \frac{1}{E^{(0)} - \widehat{H}_0} \widehat{V}_{int} \right)^n | \Phi \rangle_{connected} \tag{2.71}$$

The charged system's energy is:

$$\begin{aligned} E_p(N \pm 1) = \langle \Phi_p | \widehat{H}^{N \pm 1} | \Phi_p \rangle + \\ \langle \Phi_p | \widehat{V}^p_{int} \left(\sum_{n=2}^{\infty} \frac{1}{E^{(0)} - \widehat{H}_0} \widehat{V}^p_{int} \right)^n | \Phi_p \rangle_{connected} \end{aligned} \tag{2.72}$$

The single-electron excitation energies are the differences between the above total energies. To calculate the excitation energies in different orders of perturbation, we derive the first- and second-order differences and then generalize the derivation to higher-order terms.

First order

In the first order we have:

$$\begin{aligned} \mp \epsilon^{(1)}_p &= \langle \Phi_p | \widehat{V}^p_{int} | \Phi_p \rangle - \langle \Phi | \widehat{V}_{int} | \Phi \rangle = \\ &= \mp \langle \phi_p | \widehat{F}_{eff} | \phi_p \rangle = \mp \sum_j^N \langle \phi_p \phi_j | \, | \phi_p \phi_j \rangle \mp \langle \phi_p | \widehat{V}_{eff} | \phi_p \rangle \end{aligned} \tag{2.73}$$

Following the diagrammatic notation as defined for the ground state, we can write the diagrams for $\epsilon^{(1)}_p$ in the same way, only that now we must represent also the selected state p. This is done with a thicker line, following J.-Q. Sun and R. J. Bartlett [67]. The first-order diagram is represented in figure 2.7.

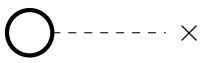

Figure 2.7: First order diagram for the quasiparticle energies.

Second order

The second-order correction is:

$$\begin{aligned}\mp\epsilon_p^{(2)} = \ & \langle\Phi_p|\widehat{V}_{int}^p\frac{1}{E^{(0)}-\widehat{H}_0}\widehat{V}_{int}^p|\Phi_p\rangle_{connected} - \\ & \langle\Phi|\widehat{V}_{int}\frac{1}{E^{(0)}-\widehat{H}_0}\widehat{V}_{int}|\Phi\rangle_{connected}\end{aligned} \tag{2.74}$$

Inserting the projection operator between the interaction operator $\widehat{V}_{int}^p$ and the fraction $\frac{1}{E^{(0)}-\widehat{H}_0}$ of the equation 2.74, we obtain the matrix elements to be calculated: $\left\langle\Phi_p\middle|\widehat{V}_{int}^p\middle|\Phi_{p_i}^{\ a}\right\rangle$, and $\left\langle\Phi_p\middle|\widehat{V}_{int}^p\middle|\Phi_{p_{ij}}^{\ ab}\right\rangle$. For electron addition, the states a, b cannot be p. Instead, p should be treated as an occupied state. Similarly, for electron removal, the states i, j cannot be p because it should be treated as be unoccupied. Remembering that $\widehat{V}_{int}^p = \widehat{W} + \widehat{F}_{eff} + \widehat{U}^p$ and $\left\langle\Phi_p\middle|\widehat{W}\middle|\Phi_{p_i}^{\ a}\right\rangle = 0$, we obtain:

$$\begin{aligned}\left\langle\Phi_p\middle|\widehat{V}_{int}^p\middle|\Phi_{p_i}^{\ a}\right\rangle = \left\langle\Phi_p\middle|\left(\widehat{F}^{eff}+\widehat{U}^p\right)\middle|\Phi_{p_i}^{\ a}\right\rangle = \\ \langle\phi_i|(\widehat{F}_{eff}+\widehat{U}^p)|\phi_a\rangle\end{aligned} \tag{2.75}$$

and

$$\left\langle\Phi_p\middle|\widehat{V}_{int}^p\middle|\Phi_{p_{ij}}^{\ ab}\right\rangle = \left\langle\Phi_p\middle|\widehat{W}\middle|\Phi_{p_{ij}}^{\ ab}\right\rangle = \langle\phi_i\phi_j|\,|\phi_a\phi_b\rangle \tag{2.76}$$

The second-order correction can then be written as:

$$\begin{aligned}\mp\epsilon_p^{(2)} = & \sum_{ia\pm\{p\}}\left\langle\Phi_p\middle|\widehat{V}_{int}^p\frac{1}{E^{(0)}-\widehat{H}_0}\middle|\Phi_{i\,p}^{\ a}\right\rangle\left\langle\Phi_{i\,p}^{\ a}\middle|\widehat{V}_{int}^p\middle|\Phi_p\right\rangle \\ & -\sum_{ia}\langle\Phi|\widehat{V}_{int}\frac{1}{E^{(0)}-\widehat{H}_0}|\Phi_i^a\rangle\,\langle\Phi_i^a|\widehat{V}_{int}|\Phi\rangle \\ & +\sum_{ijab\pm\{p\}}\left\langle\Phi_p\middle|\widehat{V}_{int}^p\frac{1}{E^{(0)}-\widehat{H}_0}\middle|\Phi_{ij\,p}^{\ ab}\right\rangle\left\langle\Phi_{ij\,p}^{\ ab}\middle|\widehat{V}_{int}^p\middle|\Phi_p\right\rangle \\ & -\sum_{ijab}\left\langle\Phi\middle|\widehat{V}_{int}\frac{1}{E^{(0)}-\widehat{H}_0}\middle|\Phi_{ij}^{ab}\right\rangle\left\langle\Phi_{ij}^{ab}\middle|\widehat{V}_{int}\middle|\Phi\right\rangle\end{aligned} \tag{2.77}$$

For the singles part we have:

$$\begin{aligned} S = & \sum_{ia\pm\{p\}} \left\langle \Phi_p \middle| \widehat{V}_{int}^p \frac{1}{E^{(0)} - \widehat{H}_0} \middle| \Phi_{i\,p}^{a} \right\rangle \left\langle \Phi_{i\,p}^{a} \middle| \widehat{V}_{int}^p \middle| \Phi_p \right\rangle \\ & - \sum_{ia} \langle \Phi | \widehat{V}_{int} \frac{1}{E^{(0)} - \widehat{H}_0} | \Phi_i^a \rangle \ \langle \Phi_i^a | \widehat{V}_{int} | \Phi \rangle = \\ & \sum_{ia} \frac{1}{\epsilon_i - \epsilon_a} | \langle \phi_i | (\widehat{F}_{eff} + \widehat{U}^p) | \phi_a \rangle |^2 - \sum_{ia} \frac{1}{\epsilon_i - \epsilon_a} | \langle \phi_i | \widehat{F}_{eff} | \phi_a \rangle |^2 \\ & \pm \sum_{a \neq p} \frac{1}{\epsilon_i - \epsilon_a} | \langle \phi_p | \widehat{F}_{eff} | \phi_a \rangle |^2 \mp \sum_{i \neq p} \frac{1}{\epsilon_i - \epsilon_a} | \langle \phi_i | \widehat{F}_{eff} | \phi_p \rangle^2 \end{aligned} \tag{2.78}$$

For the doubles part we have:

$$\begin{aligned} D = & \sum_{ijab\pm\{p\}} \left\langle \Phi_p \middle| \widehat{V}_{int}^p \frac{1}{E^{(0)} - \widehat{H}_0} \middle| \Phi_{ij\,p}^{ab} \right\rangle \left\langle \Phi_{ij\,p}^{ab} \middle| \widehat{V}_{int}^p \middle| \Phi_p \right\rangle \\ & - \sum_{ijab} \left\langle \Phi \middle| \widehat{V}_{int} \frac{1}{E^{(0)} - \widehat{H}_0} \middle| \Phi_{ij}^{ab} \right\rangle \left\langle \Phi_{ij}^{ab} \middle| \widehat{V}_{int} \middle| \Phi \right\rangle \end{aligned} \tag{2.79}$$

All terms coming from the first row of equation 2.79, that do not have a p orbital, will cancel with the terms of the second row. Only the terms that have p orbitals, either as occupied or unoccupied, will remain. The denominator will give us the energies of the single-particle wavefunctions. Replacing the second-quantized form of the Coulomb operator, the expression 2.79 can be written as:

$$\begin{aligned} D = & \mp \frac{1}{2} \sum_{iab} \frac{| \langle \phi_p \phi_i | \, | \phi_a \phi_b \rangle |^2}{(\epsilon_p + \epsilon_i - \epsilon_a - \epsilon_b)} \pm \frac{1}{2} \sum_{iab} \frac{| \langle \phi_i \phi_j | \, | \phi_p \phi_a \rangle |^2}{(\epsilon_i + \epsilon_j - \epsilon_p - \epsilon_a)} \\ & - \sum_{ia} \frac{| \langle \phi_i \phi_p | \, | \phi_a \phi_p \rangle |^2}{(\epsilon_i - \epsilon_a)} \end{aligned} \tag{2.80}$$

The correction will be the sum of singles and doubles, $S + D$. The last term of the doubles will cancel with the $\widehat{U}^p$ term in singles, resulting in the expression:

$$\begin{aligned} \epsilon_p^{(2)} = & \frac{1}{2} \sum_{iab} \frac{| \langle \phi_p \phi_i | \, | \phi_a \phi_b \rangle |^2}{(\epsilon_p + \epsilon_i - \epsilon_a - \epsilon_b)} + \frac{1}{2} \sum_{iab} \frac{| \langle \phi_i \phi_j | \, | \phi_p \phi_a \rangle |^2}{(\epsilon_i + \epsilon_j - \epsilon_p - \epsilon_a)} + \\ & \sum_{a \neq p} \frac{1}{\epsilon_i - \epsilon_a} | \langle \phi_p | \widehat{F}_{eff} | \phi_a \rangle |^2 - \sum_{i \neq p} \frac{1}{\epsilon_i - \epsilon_a} | \langle \phi_i | \widehat{F}_{eff} | \phi_p \rangle |^2 + \\ & \sum_{ia} \frac{1}{\epsilon_i - \epsilon_a} \Big[\langle \phi_i | \widehat{F}_{eff} | \phi_a \rangle \ \langle \phi_a \phi_p | \widehat{V} | \phi_i \phi_p \rangle_A + c.c. \Big] \end{aligned} \tag{2.81}$$

The corresponding second-order diagrams are shown in figure 2.8.

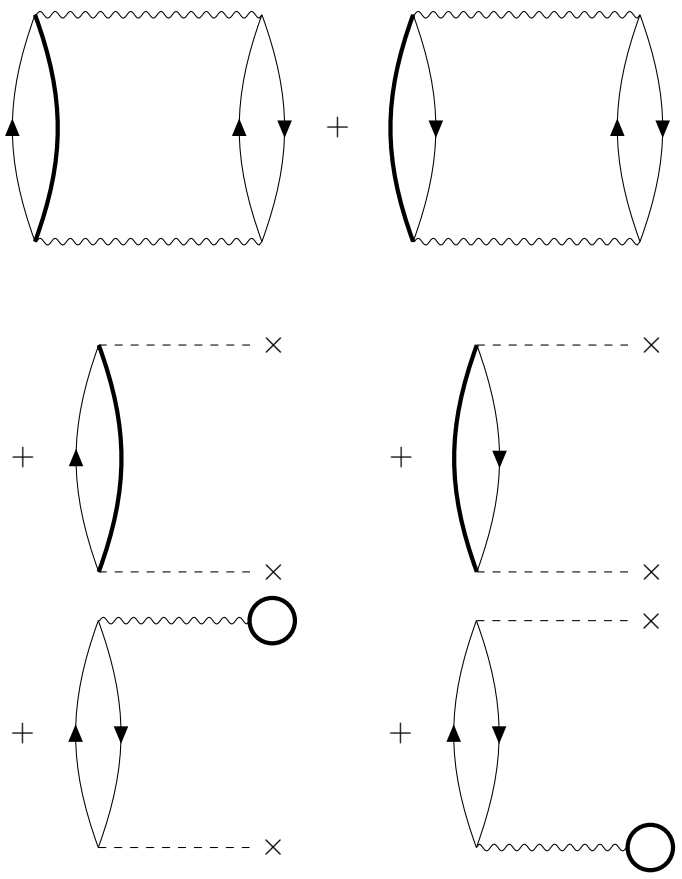

Figure 2.8: Second-order diagrams for the quasiparticle energies.

Higher orders

For any order n, the correction can be evaluated as follows:

$$\begin{aligned} \mp\epsilon_p^{(n)} = \langle\Phi_p|\widehat{V}_{int}^p\left(\frac{1}{E^{(0)}-\widehat{H}_0}\widehat{V}_{int}^p\right)^n|\Phi_p\rangle_{connected} - \\ \langle\Phi|\widehat{V}_{int}\left(\frac{1}{E^{(0)}-\widehat{H}_0}\widehat{V}_{int}\right)^n|\Phi\rangle_{connected} \end{aligned} \tag{2.82}$$

Diagrammatically, the non-zero terms are the total-energy diagrams that have at least one wavefunction p, and the diagrams that have at least one bubble coming from the extra term $\widehat{U}^p$. There is cancellation of some terms. For example, the diagrams:

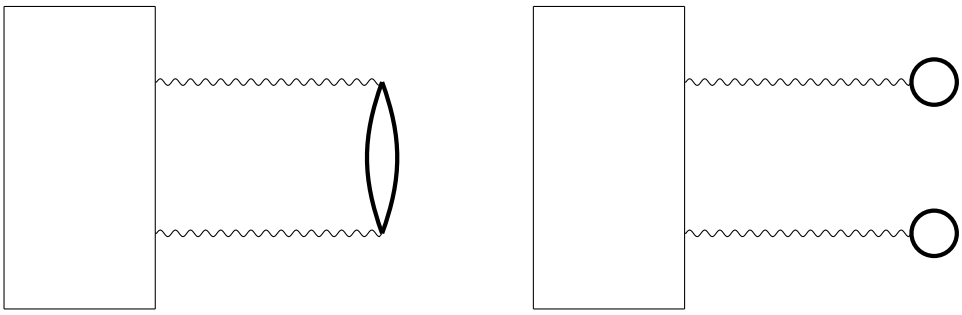

where the box represents any equivalent structure common in both diagrams, which will cancel each other, as we saw in the case of second-order correction, when adding singles and doubles in the equation 2.81. Despite this cancellation, the diagrams become quite complicated compared to total-energy diagrams. For example, in the third order, for single-particle excitations there are 60 diagrams, 12 of which are non-zero when HF is used as a reference, while for total energy there are 14 diagrams, 3 of which are non-zero for HF reference. Another important difference is that every diagram in $\epsilon_p^{(n)}$ has at least one less summation index, since at least one index is fixed. For example, in the second-order there are summations over one or three indices, while for total energy there are summations over two or four indices.

2.5 Single-particle propagator and the Dyson equation

This section presents how to go beyond second-order perturbation theory for solids using the Dyson equation.

2.5.1 Single-particle propagator

Another way to assess the single-particle energies is through the single-particle propagator or Green's function. The single-particle propagator is really useful, since it can provide the expectation value of any single-particle operator in the ground state, the ground state energy, and the single-particle excitation energies.

The propagator definition is:

$$G(p,q;t,t') = -\mathrm{i}\langle\Psi^N|\mathcal{T}\left[\widehat{\alpha}_{pH}(t)\widehat{\alpha}^\dagger_{qH}(t')\right]|\Psi^N\rangle \tag{2.83}$$

where $\widehat{\alpha}_p$ and $\widehat{\alpha}^\dagger_q$ are the removal and addition operators in the Heisenberg picture, defined as:

$$\widehat{\alpha}_{pH}(t) = e^{\mathrm{i}\widehat{H}t}\widehat{\alpha}_p e^{-\mathrm{i}\widehat{H}t}$$

$$\widehat{\alpha}^\dagger_{pH}(t) = e^{\mathrm{i}\widehat{H}t}\widehat{\alpha}^\dagger_p e^{-\mathrm{i}\widehat{H}t}$$

and $\mathcal{T}$ is the time ordering operator. The single-particle propagator within the Lehmann representation, which is relevant for the single-particle excitations, can be written as:

$$\begin{aligned} G(p,q;\epsilon) = \lim_{\eta\to 0}\Bigg[\sum_n \frac{\langle\Psi^N|\widehat{\alpha}^\dagger_p|\Psi^{N-1}_n\rangle\langle\Psi^{N-1}_n|\widehat{\alpha}_q|\Psi^N\rangle}{\epsilon - [E(N) - E_n(N-1)] - \mathrm{i}\eta} + \\ \sum_m \frac{\langle\Psi^N|\widehat{\alpha}_p|\Psi^{N+1}_m\rangle\langle\Psi^{N+1}_m|\widehat{\alpha}^\dagger_q|\Psi^N\rangle}{\epsilon - [E_m(N+1) - E(N)] + \mathrm{i}\eta}\Bigg] \end{aligned} \tag{2.84}$$

where p, q denote the orthogonal basis functions on which we project our propagator. The above equation is the Fourier transform of the propagator in eq. 2.83 from time to energy domain. This form of the propagator shows that the single-particle excitation energies, as defined in equation 2.64, are the poles of the propagator.

For the propagator of the non-interacting system, it is beneficial to use the eigenfunctions of a single-particle Hamiltonian as defined in eq. 2.9. As we have seen, this is usually the Kohn-Sham or HF wavefunctions. The non-interacting propagator takes the following form:

$$G^0(p,q;\epsilon) = \delta_{p,q}\lim_{\eta\to 0}\left[\frac{\theta(n_{ho}-p)}{\epsilon - \epsilon_p - \mathrm{i}\eta} + \frac{\theta(p-n_{lu})}{\epsilon - \epsilon_p + \mathrm{i}\eta}\right] \tag{2.85}$$

where n_{ho} is the index of the highest occupied state, n_{lu} the index of the lowest unoccupied state, and $\theta(n) = 1$ for $n \geq 0$, $\theta(n) = 0$ for $n < 0$. In other words, when p is an occupied state, the first term will be non-zero, whereas the second term will be zero, and the other way around when p is an unoccupied state.

2.5.2 Time-depended perturbation theory for the propagator

To find the propagator of the interacting system, we apply the time-dependent perturbation theory, which is based on the time-evolution operator defined as:

$$|\Psi_I(t)\rangle = \widehat{U}(t,t_0)|\Psi_I(t_0)\rangle \tag{2.86}$$

The notation I denotes the interaction picture defined as:

$$|\Psi_I(t)\rangle = e^{\mathrm{i}\widehat{H}_0 t}|\Psi(t)\rangle \tag{2.87}$$

where $|\Psi(t)\rangle$ is the solution of the time-dependent Schrödinger equation $\mathrm{i}\frac{\partial}{\partial t}|\Psi(t)\rangle = \widehat{H}|\Psi(t)\rangle$, and $\widehat{H}_0$ is the single-particle Hamiltonian 2.9. The Schrödinger equation can be rewritten as:

$$\mathrm{i}\frac{\partial}{\partial t}\widehat{U}(t,t_0)|\Psi_I(t_0)\rangle = \widehat{V}_{int}(t)\widehat{U}(t,t_0)|\Psi_I(t_0)\rangle \tag{2.88}$$

where $\widehat{V}_{int}(t) = e^{\mathrm{i}\widehat{H}_0 t}\widehat{V}_{int}e^{-\mathrm{i}\widehat{H}_0 t}$. Then the time evolution operator can be written as:

$$\widehat{U}(t,t_0) = \mathcal{T}\left[exp\left[-\mathrm{i}\int_{t_0}^{t} dt'\widehat{V}_{int}(t')\right]\right] \tag{2.89}$$

Expanding the exponential gives the perturbation expansion. To find a connection between the ground states of the unperturbed and perturbed systems, we use the adiabatic switching method for the perturbation $\widehat{V}_{int}e^{-\epsilon|t|}$. Then:

$$|\Psi\rangle = \widehat{U}_\epsilon(0,-\infty)\,|\Phi\rangle \tag{2.90}$$

where $|\Phi\rangle$ is the non-interacting system's ground state. The Gell-Mann and Low theorem then states that if the quantity:

$$\lim_{\epsilon\to 0}\frac{\widehat{U}_\epsilon(0,-\infty)|\Phi\rangle}{\langle\Phi|\widehat{U}_\epsilon(0,-\infty)|\Phi\rangle} \equiv \frac{|\Psi\rangle}{\langle\Phi|\Psi\rangle}$$

exists in all orders of the perturbation expansion, then:

$$\frac{\widehat{H}|\Psi\rangle}{\langle\Phi|\Psi\rangle} = \frac{E|\Psi\rangle}{\langle\Phi|\Psi\rangle} \tag{2.91}$$

and:

$$E - E_0 = \frac{\langle\Phi|\widehat{V}_{int}|\Psi\rangle}{\langle\Phi|\Psi\rangle} \tag{2.92}$$

From the property of the evolution operator, $\widehat{U}(t,t_0) = e^{\mathrm{i}\widehat{H}_0 t}e^{-\mathrm{i}\widehat{H}(t-t_0)}e^{-\mathrm{i}\widehat{H}_0 t}$ (which can be proven from the definitions in eq. 2.86 and eq. 2.87) for an arbitrary operator in Heisenberg picture, we can write:

$$\frac{\langle\Psi|\widehat{O}_H(t)|\Psi\rangle}{\langle\Psi|\Psi\rangle} = \lim_{\epsilon\to 0}\frac{\langle\Phi|\widehat{U}_\epsilon(+\infty,t)\widehat{O}_I(t)\widehat{U}_\epsilon(t,-\infty)|\Phi\rangle}{\langle\Phi|\widehat{U}_\epsilon(+\infty,-\infty)|\Phi\rangle} \tag{2.93}$$

By inserting here $\widehat{U}_\epsilon$ from eq. 2.89, expanding the exponential and rearranging terms we obtain:

$$\frac{\langle\Psi|\widehat{O}_H(t)|\Psi\rangle}{\langle\Psi|\Psi\rangle} = \frac{1}{\langle\Phi|\widehat{U}(+\infty,-\infty)|\Phi\rangle}\langle\Phi|\sum_{n=0}^{\infty}\frac{(-\mathrm{i})^n}{n!}\int_{\infty}^{\infty}dt_1...\int_{\infty}^{\infty}dt_n\times \tag{2.94}$$
$$\mathcal{T}\left[\widehat{V}_{int}(t_1)...\widehat{V}_{int}(t_n)\widehat{O}_I(t)\right]|\Phi\rangle$$

In particular, for the single-particle propagator this yields:

$$G(p,q;t,t') = -\mathrm{i}\frac{1}{\langle\Phi|\widehat{U}(+\infty,-\infty)|\Phi\rangle}\sum_{n=0}^{\infty}\frac{(-\mathrm{i})^n}{n!}\int_{\infty}^{\infty}dt_1...\int_{\infty}^{\infty}dt_n\times \tag{2.95}$$
$$\langle\Phi|\mathcal{T}\left[\widehat{V}_{int}(t_1)...\widehat{V}_{int}(t_n)\widehat{\alpha}_p(t)\widehat{\alpha}_q^\dagger(t')\right]|\Phi\rangle$$

where the removal and addition operators are in the interaction picture.

The disconnected parts factor out and cancel with the denominator (see, for example: Quantum theory of many-particle systems, A. Fetter and J. Walecka), resulting in:

$$G(p,q;t,t') = -\mathrm{i}\sum_{n=0}^{\infty}\frac{(-i)^n}{n!}\int_{\infty}^{\infty}dt_1...\int_{\infty}^{\infty}dt_n\times \tag{2.96}$$
$$\langle\Phi|\,\mathcal{T}\left[\widehat{V}_{int}(t_1)...\widehat{V}_{int}(t_n)\widehat{\alpha}_p(t)\widehat{\alpha}_q^\dagger(t')\right]|\Phi\rangle_{connected}$$

2.5.3 Feynman Diagrams

As in the case of MBPT, there is a convenient way to illustrate with diagrams the expressions of the corrections for the propagator at each order. Starting with

zero order, $G^0(p,q;t,t') = -\mathrm{i}\,\langle\Phi|\,\mathcal{T}\left[\widehat{\alpha}_p(t)\widehat{\alpha}_q^\dagger(t')\right]|\Phi\rangle$ (see eq. 2.96). This is the propagator of the non-interacting system:

$$\begin{aligned} G^0(p,q;t,t') = -\mathrm{i}\delta_{p,q}\Big[&\theta(t-t')\theta(n_{ho}-p)e^{-\mathrm{i}\epsilon_p(t-t')} \\ &-\theta(t'-t)\theta(q-n_{lu})e^{\mathrm{i}\epsilon_p(t'-t)}\Big] \end{aligned} \tag{2.97}$$

The Fourier transform of the above expression will give eq. 2.85.

Diagrammatically, the non-interacting propagator G^0 is represented as a line:

Replacing the operators with their second-quantization form of the interaction operator 2.41 and taking into account the definition of the interaction picture, we can write:

$$\widehat{V}_{int}(t) = \frac{1}{4}\sum_{pqrs} V_{pq,rs}\widehat{\alpha}_p^\dagger(t)\widehat{\alpha}_q^\dagger(t)\widehat{\alpha}_s(t)\widehat{\alpha}_r(t) - \sum_{pq} V_{eff}^{pq}\widehat{\alpha}_p^\dagger(t)\widehat{\alpha}_q(t) \tag{2.98}$$

To evaluate the expression for the propagator in any order, we need to evaluate the expectation value of time-ordered addition and removal operators. To do this, we will use Wick's theorem:

$$\begin{aligned} &\mathcal{T}\left[\widehat{\alpha}_p(t_1)\widehat{\alpha}_q^\dagger(t_1)\widehat{\alpha}_r(t_3)\widehat{\alpha}_s^\dagger(t_4)...\widehat{\alpha}_y(t_{n-1})\widehat{\alpha}_z^\dagger(t_n)\right] = \\ &\mathcal{N}\left[\widehat{\alpha}_p(t_1)\widehat{\alpha}_q^\dagger(t_1)\widehat{\alpha}_r(t_3)\widehat{\alpha}_s^\dagger(t_4)...\widehat{\alpha}_y(t_{n-1})\widehat{\alpha}_z^\dagger(t_n)\right] + \\ &\mathcal{N}\left[\text{sum over all possible pairs of contractions}\right] = \\ &\mathcal{N}\left[\widehat{\alpha}_p(t_1)\widehat{\alpha}_q^\dagger(t_1)\widehat{\alpha}_r(t_3)\widehat{\alpha}_s^\dagger(t_4)...\widehat{\alpha}_y(t_{n-1})\widehat{\alpha}_z^\dagger(t_n)\right] + \\ &\mathcal{N}\left[\overbrace{\widehat{\alpha}_p(t_1)\widehat{\alpha}_q^\dagger}(t_2)\widehat{\alpha}_r(t_3)\widehat{\alpha}_s^\dagger(t_4)...\widehat{\alpha}_y(t_{n-1})\widehat{\alpha}_z^\dagger(t_n)\right] + \\ &\mathcal{N}\left[\overbrace{\widehat{\alpha}_p(t_1)\widehat{\alpha}_q^\dagger(t_2)\widehat{\alpha}_r(t_3)\widehat{\alpha}_s^\dagger}(t_4)...\widehat{\alpha}_y(t_{n-1})\widehat{\alpha}_z^\dagger(t_n)\right] + ... \\ &\mathcal{N}\left[\overbrace{\widehat{\alpha}_p(t_1)\widehat{\alpha}_q^\dagger}(t_2)\overbrace{\widehat{\alpha}_r(t_3)\widehat{\alpha}_s^\dagger}(t_4)...\widehat{\alpha}_y(t_{n-1})\widehat{\alpha}_z^\dagger(t_n)\right] + ... \end{aligned} \tag{2.99}$$

where $\mathcal{N}$ is the normal ordering, defined by rearranging an operator to the right, if that operator results in zero when acting on the ground state. This way, if not

all operators are contracted the expectation value of a normal order will always be zero. The expectation value of the time-ordered product at any order of correction for the propagator will be the product of all possible contraction pairs.

A contraction is defined as the difference between the time ordering of the two operators minus the normal ordering. It is denoted by a line that connects the operators in the previous equation. For a pair of removal and addition operators, the normal order will be:

$$\mathcal{N}\left[\widehat{\alpha}_p(t)\widehat{\alpha}_q^\dagger(t')\right] = \begin{cases} -\widehat{\alpha}_q^\dagger(t')\widehat{\alpha}_p(t), & \text{if } p \text{ and } q \text{ are unoccupied} \\ \widehat{\alpha}_p(t)\widehat{\alpha}_q^\dagger(t'), & \text{otherwise} \end{cases} \tag{2.100}$$

Then a contraction will be equal to the propagator:

$$\overbrace{\widehat{\alpha}_p(t)\widehat{\alpha}_q^\dagger}(t) = -\overbrace{\widehat{\alpha}_q^\dagger(t)\widehat{\alpha}_p}(t) = \mathrm{i}G^{(0)}(p,q;t,t') \tag{2.101}$$

First order

In first order we have:

$$G^{(1)}(p,q;t,t') = -\mathrm{i}\int_{\infty}^{\infty} dt_1 \left\langle\Phi\right| \mathcal{T}\left[\widehat{V}_{int}(t_1)\widehat{\alpha}_p(t)\widehat{\alpha}_q^\dagger(t')\right] \left|\Phi\right\rangle_{connected} \tag{2.102}$$

Replacing the interaction in second-quantization form, eq. 2.98, the propagator will be the summation of a term coming from the two-particle part and a term from the single-particle part. For the single-particle part, we need to contract the operators:

$$\widehat{\alpha}_r^\dagger(t_1)\widehat{\alpha}_s(t_1)\widehat{\alpha}_p(t)\widehat{\alpha}_q^\dagger(t') \tag{2.103}$$

From all possible contractions, we must choose the connected ones. Each contraction will result in a propagator according to equation 2.101. The propagator is then represented by a steady line. For example, the contraction:

$$\overbrace{\widehat{\alpha}_r^\dagger(t_1)\widehat{\alpha}_s}(t_1)\overbrace{\widehat{\alpha}_p(t)\widehat{\alpha}_q^\dagger}(t') \tag{2.104}$$

generates a disconnected diagram:

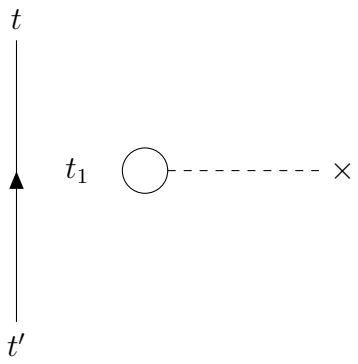

The dashed line represents the matrix element of the single-particle part of the interaction V_{eff}^{rs}.

The other possible set of contracted pairs is:

$$\widehat{\alpha}_r^\dagger(t_1)\widehat{\alpha}_s(t_1)\widehat{\alpha}_p(t)\widehat{\alpha}_q^\dagger(t') \tag{2.105}$$

This generates the connected diagram:

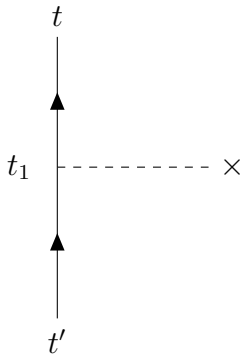

Since we have to integrate over all time, only the topology is important in Feynman's diagrams and not the time order. For example, the previous diagram is topologically equivalent to:

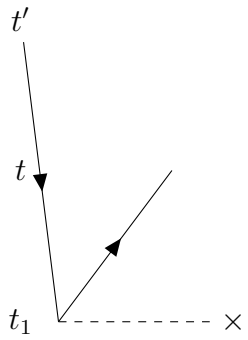

The corresponding contribution to the $G^{(1)}$ propagator will be:

$$-\,\mathrm{i}\int_{\infty}^{\infty} dt_1 \sum_{rs} V_{eff}^{rs} G^0(p,r;t_1,t')(-1)G^0(s,q;t,t_1) \tag{2.106}$$

For the two-particle part we must contract the operators:

$$\widehat{\alpha}_r^\dagger(t_1)\widehat{\alpha}_s^\dagger(t_1)\widehat{\alpha}_t(t_1)\widehat{\alpha}_w(t_1)\widehat{\alpha}_p(t)\widehat{\alpha}_q^\dagger(t') \tag{2.107}$$

Note that interchanging r with s and t with w will give the same result since we sum over all possible values the indices can take. Then all distinct connected diagrams will come from the contractions:

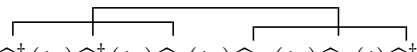

(2.108)

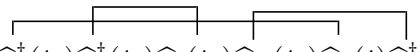

(2.109)

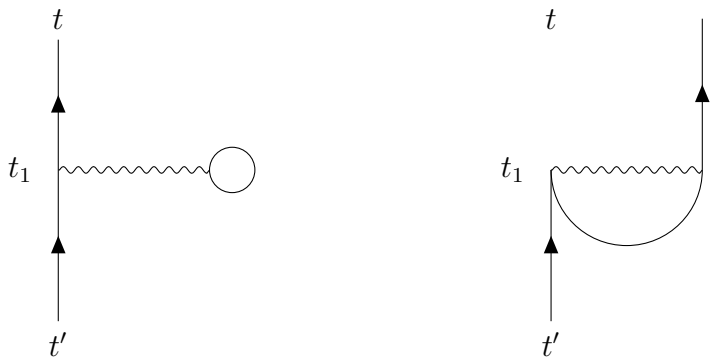

The two-particle part of the interaction is represented with a wavy line. Due to their shapes, the first diagram is called "bubble" and the second "oyster". For finding the single-particle excitation spectrum, only the Fourier-transformed propagator is relevant. Therefore, we use the inverse Fourier transform of the time-dependent non-interacting propagator:

$$G^0(p,q;t,t') = \frac{1}{2\pi}\int_{\infty}^{\infty} d\epsilon G^0(p,q;\epsilon)e^{-\mathrm{i}\epsilon(t-t')} \tag{2.110}$$

to replace the contractions. Then, time integrations in equation 2.96 can be explicitly done for any order. Each integration will give δ-functions that preserve the energy of each interaction line. Each propagator line should then be labeled with an energy variable taking into account the energy conservation and thus, time becomes irrelevant.

Second order

In the second-order, we have diagrams that derive from the two-particle part of the interaction – the Coulomb operator – and the ones that include the single-particle effective potential. The second-order diagrams will be:

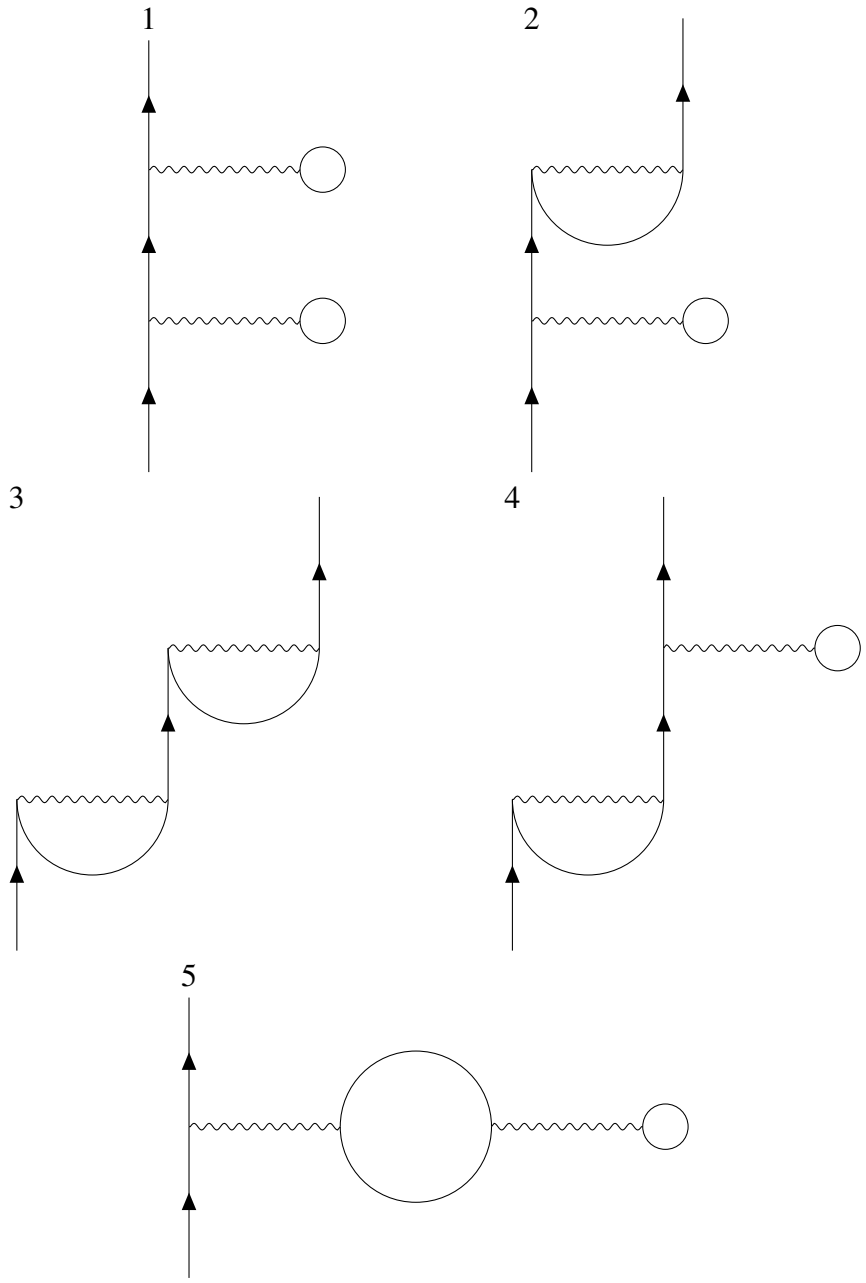
1
2
3
4
5

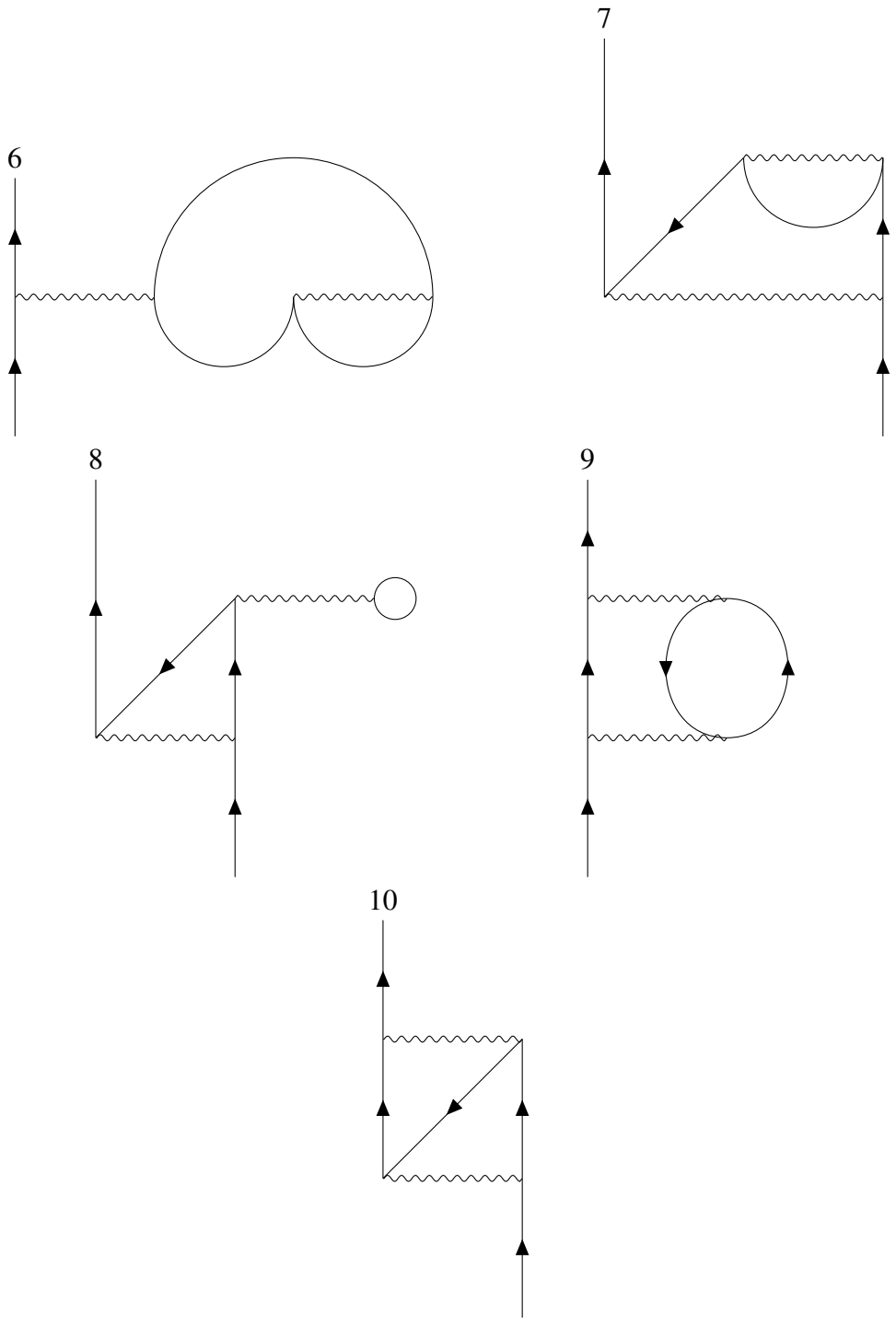

As one can see, diagrams 1-4 include parts that are connected only with a non-interacting propagator. Such diagrams are called reducible diagrams. The rest of

the diagrams are not reducible, but diagrams 5-8 can be produced by first-order diagrams if we replace a non-interacting propagator line $G^{(0)}$ with the propagator line $G^{(1)}$. For example, diagram 5 can be generated by replacing the non-interacting propagator circle line of the bubble diagram with the bubble diagram itself. If instead we replace the oyster diagram, we end up with diagram 6. Similarly, we can produce diagrams 7 and 8 starting from the oyster diagram. Diagrams 9 and 10 cannot be produced from first-order diagrams.

As in Goldstone diagrams, we can define an antisymmetric version. In this case, we require only the first diagram in first order, the bubble diagram. In the second order, we can skip diagrams 2, 3, and 4, keeping only 1, and skip 6, 7, 8 by keeping only 5. For the last two diagrams, 9 is antisymmetric with 10, so we can retain only 9. Finally, we include the second-order diagrams that have at least one effective potential line:

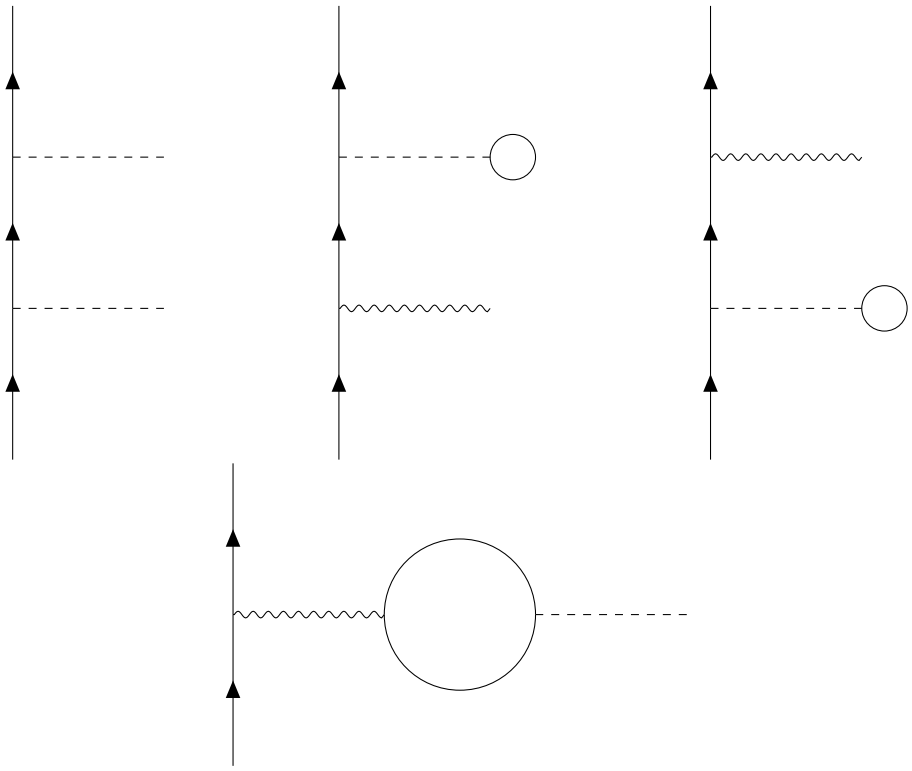

2.5.4 Dyson equation

The Dyson equation for the single-particle propagator is:

$$G(p,q;\epsilon) = G^0(p,q;\epsilon) + \sum_{rs} G^0(p,r;\epsilon)\Sigma(r,s;\epsilon)G(s,q;\epsilon) \tag{2.111}$$

where Σ is the self-energy defined by this equation. This equation is represented diagrammatically as:

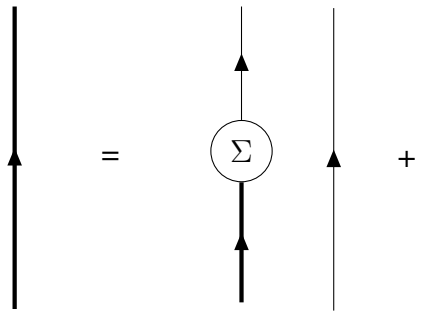

where the thick line represents the propagator of the interacting system G. Self-energy will include all irreducible parts of the diagrams of all orders. By approximating the self-energy to include, for example, only all first-order contributions, we include in the propagator reducible diagrams of all orders that are assembled from the first-order diagrams. This becomes clear if we rewrite the equation as a series:

$$\begin{aligned} G(p,q;\epsilon) &= G^0(p,q;\epsilon) + \sum_{rs} G^0(p,r;\epsilon)\Sigma(r,s;\epsilon)G^0(s,q;\epsilon) + \\ &\sum_{rs}\sum_{tu} G^0(p,r;\epsilon)\Sigma(r,s;\epsilon)G^0(s,t;\epsilon)\Sigma(t,u;\epsilon)G^0(u,q;\epsilon) + ... \end{aligned} \tag{2.112}$$

The Dyson equation provides a non-pertubative propagator since it includes corrections of all orders. As an example, the diagrams that are included in the propagator if we approximate self-energy by the first-order diagrams are:

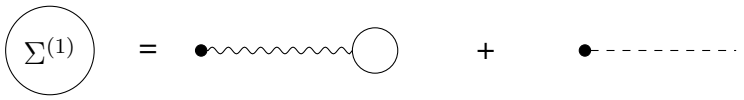

where the dots represent the connection point of the two propagators (see eq. 2.111). Remember that this is the antisymmetrized version of diagrams, so the

bubble diagram includes in fact two diagrams. The propagator is represented as follows:

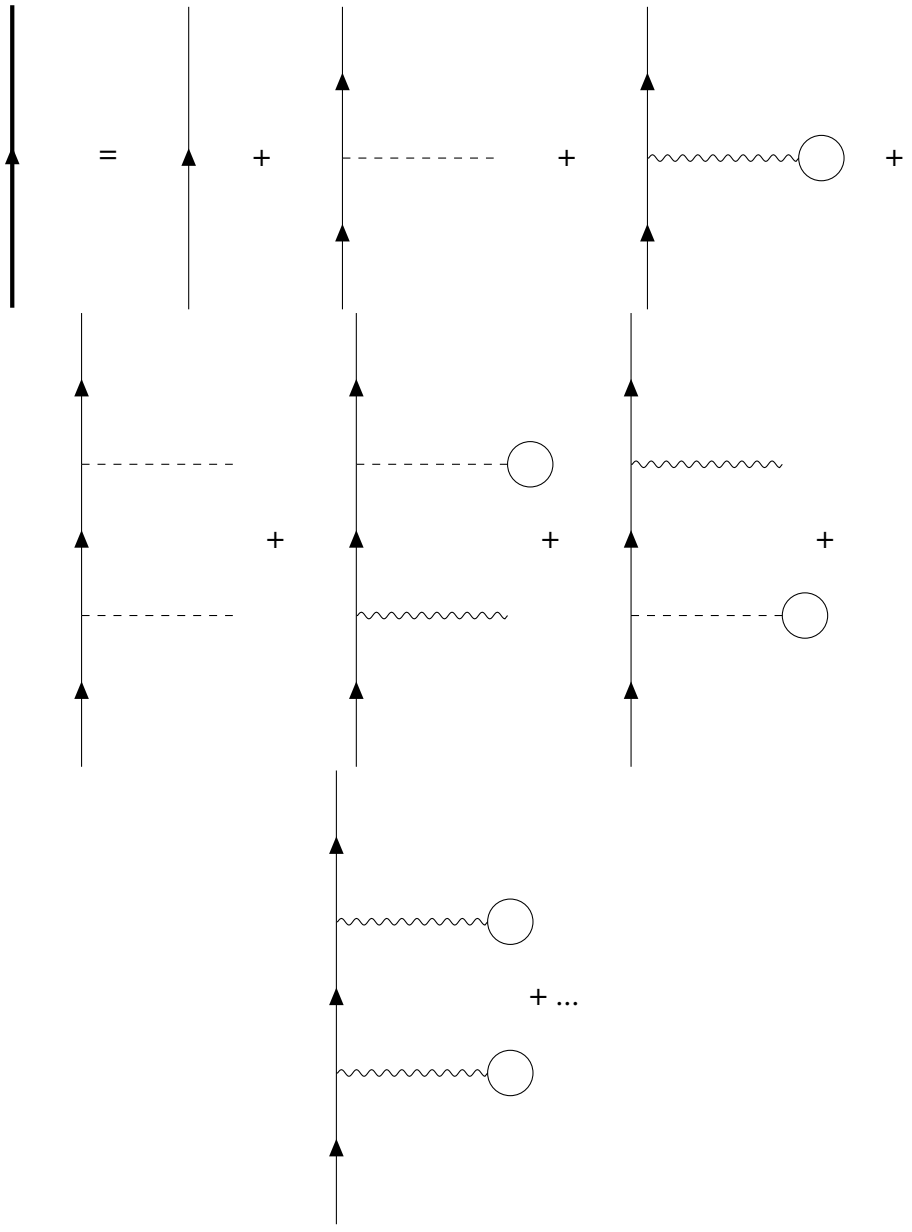

We see that the reducible diagrams of second and higher orders are included, although we have considered the self-energy only up to first-order approximation.

The next step is to include the diagrams as diagram 5 of second order, which can also be produced by first-order diagrams, as explained in section 2.5.3. Since

we use antisymmetrized diagrams, exchange diagrams are included as well (diagrams 6, 7, and 8 in this case). We achieve that by replacing the non-interacting propagators G^0 with the interacting propagators G in the self-energy.

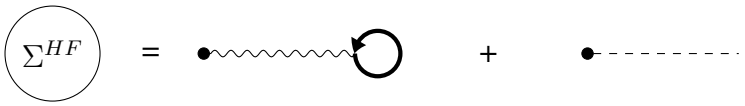

The above approximation of the self-energy gives the HF approximation. To go beyond HF and include second-order diagrams that cannot be produced by first order, the only extra diagram we need is diagram 9, since we use antisymmetrized diagrams. To include all diagrams that can be produced by second-order, in the same way we did with Σ^1 to produce Σ^{HF}, the non-interacting propagator is replaced with the interacting one:

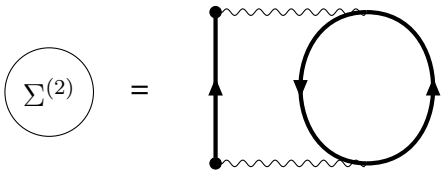

The complete self-consistent self-energy up to second order is[7]:

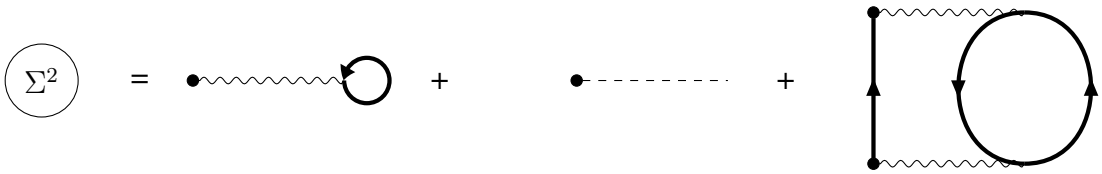

[7]It can be shown that the exact self-energy can be written as

$$\Sigma(p,q;\epsilon) = -\langle\phi_p|\widehat{V}_{eff}|\phi_q\rangle - \mathrm{i}\int\limits_{C\uparrow}\frac{d\epsilon'}{2\pi}\sum_{rs}G(p,r;\epsilon)\,\langle\phi_p\phi_p|\widehat{V}|\phi_q\phi_p\rangle +$$

$$+\frac{1}{2}\int\frac{d\epsilon'}{2\pi}\int\frac{d\epsilon''}{2\pi}\sum_{rs}\sum_{tu}\sum_{vw}\langle\phi_p\phi_p|\widehat{V}|\phi_q\phi_p\rangle\times$$

$$\times G(p,r;\epsilon')G(s,t;\epsilon'')G(u,q;\epsilon'+\epsilon''-\epsilon)\,\langle\phi_p\phi_p|\widehat{\Gamma}(\epsilon',\epsilon'';\epsilon,\epsilon'+\epsilon''-\epsilon)|\phi_q\phi_p\rangle$$

where Γ is the vertex correction. Approximating Σ with self-consistent Σ^2 is equivalent to approximating the "dressed" interaction Γ, with the bare interaction V [87].

2.6 Localized basis set

In practical calculations, single-particle states are expanded in a basis set. In principle, the basis set should be complete. However, in practice this is not possible, since we would need an infinite set of functions. For this reason, a finite set of functions must be chosen. This selection is essential for a particular numerical implementation: If the number of functions needed is large, then the computational efficiency of the code is decreasing, and the time needed for a computation can become impractical.

An orbital can be written as:

$$\phi_p(\mathbf{r}\sigma) = \psi_{p\sigma}(\mathbf{r})\chi_\sigma$$

where $\sigma = \uparrow, \downarrow$ and χ_σ are the basis functions for spin space. To expand the spatial part we need a basis set in real space that can express any state $\psi_{p\sigma}(\mathbf{r})$ as a linear combination of the basis functions:

$$\psi_{p\sigma}(\mathbf{r}) = \sum_{i=1}^{N_b} c^i_{p\sigma}\varphi_i(\mathbf{r}) \tag{2.113}$$

Plane waves, localized functions, or a combination of the two can be used as a basis set.

2.6.1 Atom-centered orbitals

A basis set that has proven efficacy, by virtue of its flexibility, is the NAO's basis set [35]. The general form of the orbitals is:

$$\varphi_i(\mathbf{r}) = \frac{u_i(r)}{r} Y_{lm}(\Omega_r)$$

where Y_{lm} are the spherical harmonics. The radial part $u_i(r)$ can be defined analytically, e.g. Gaussian, or numerically as a solution to the radial part of a Schrödinger equation with a spherically symmetric potential:

$$\left[-\frac{1}{2}\frac{d^2}{dr^2} + \frac{l(l+1)}{r^2} + V_i(r) + V_{cut}(r)\right] u_i(r) = \epsilon_i u_i(r) \tag{2.114}$$

where V_{cut} is a function that allows the smooth decay to zero after a certain radius, and V_i can be any numerically defined potential, for example, the free-atom

potential from a single-particle approximation such as HF or LDA. The success of NAO's comes from the flexibility of defining V_i that allows an optimization of the basis sets for every element.

2.6.2 Bloch functions from atom-centered orbitals

In the case of periodic systems, a set of Bloch functions are defined from NAO's as follows:

$$\varphi_{i\mathbf{k}}(\mathbf{r}) = \sum_{\mathbf{R}} e^{\mathrm{i}\mathbf{k}\mathbf{R}} \varphi_i(\mathbf{r} - \mathbf{R} - \mathbf{R}_{at}) \tag{2.115}$$

where $\mathbf{R}_{at}$ refers to the position of the atom where the orbital is centered, and $\mathbf{R}$ is a lattice vector. This indeed defines a Bloch function:
1) for any lattice vector $\mathbf{R}$:

$$\varphi_{i\mathbf{k}}(\mathbf{r} + \mathbf{R}) = e^{\mathrm{i}\mathbf{k}\mathbf{R}} \varphi_{i\mathbf{k}}(\mathbf{r}); \tag{2.116}$$

2) we can rewrite the wavefunction as a product of a lattice-periodic part and a phase factor:

$$\varphi_{i\mathbf{k}}(\mathbf{r}) = e^{\mathrm{i}\mathbf{k}\mathbf{r}} \left[e^{-\mathrm{i}\mathbf{k}\mathbf{r}} \sum_{\mathbf{R}} e^{\mathrm{i}\mathbf{k}\mathbf{R}} \varphi_i(\mathbf{r} - \mathbf{R} - \mathbf{R}_{at}) \right] = e^{\mathrm{i}\mathbf{k}\mathbf{R}} u_{i\mathbf{k}}(\mathbf{r}) \tag{2.117}$$

where it is easy to conclude that the expression in the bracket:

$$u_{i\mathbf{k}}(\mathbf{r}) = \sum_{\mathbf{R}} e^{\mathrm{i}\mathbf{k}(\mathbf{R}-\mathbf{r})} \varphi_i(\mathbf{r} - \mathbf{R} - \mathbf{R}_{at}) \tag{2.118}$$

is lattice-periodic:

$$u_{i\mathbf{k}}(\mathbf{r} + \mathbf{R}) = u_{i\mathbf{k}}(\mathbf{r}) \tag{2.119}$$

With the above Bloch functions, the spatial part of single-particle states with spin σ can be written as:

$$\psi_{p\mathbf{k}\sigma}(\mathbf{r}) = \sum_i c^i_{p\mathbf{k}\sigma} \varphi_{i\mathbf{k}}(\mathbf{r}) \tag{2.120}$$

2.7 The two-particle Coulomb operator

A matrix element of the Coulomb operator in the Bloch basis introduced in section 2.6 is an eight-index object:

$$V^{i\mathbf{k},j\mathbf{q}}_{k\mathbf{k}',l\mathbf{q}'} = \int d\mathbf{r} \int d\mathbf{r}' \varphi^*_{i\mathbf{k}}(\mathbf{r}) \varphi^*_{j\mathbf{k}'}(\mathbf{r}') \frac{1}{|\mathbf{r}-\mathbf{r}'|} \varphi_{l\mathbf{q}'}(\mathbf{r}') \varphi_{k\mathbf{q}'}(\mathbf{r}). \tag{2.121}$$

Momentum conservation allows reducing the crystal momentum indices from four to three. Direct calculation and storage of this object is generally challenging, which can be addressed by applying a method called resolution of identity or density fitting, as described below.

2.7.1 Auxiliary basis set and resolution of identity

The high computational cost of calculating Coulomb matrix elements can be reduced by using an auxiliary basis set $P_\mu(\mathbf{r}-\mathbf{R}_{at'})$ to expand the products of wavefunctions [38]–[40]. The corresponding Bloch basis functions are constructed similarly to the main basis:

$$P^{\mathbf{k}}_\mu(\mathbf{r}) = \sum_{\mathbf{R}} e^{\mathrm{i}\mathbf{k}\mathbf{R}} P_\mu(\mathbf{r}-\mathbf{R}-\mathbf{R}_{at'}) \tag{2.122}$$

By expanding the products of basis functions needed for the calculation of the Coulomb matrix, we get:

$$\varphi^*_{i\mathbf{k}}(\mathbf{r}) \varphi_{k\mathbf{q}}(\mathbf{r}) = \sum_\mu C^\mu_{i\mathbf{k},k\mathbf{q}} P^{\mathbf{q}-\mathbf{k}}_\mu(\mathbf{r}) \tag{2.123}$$

The product of two single-particle wavefunctions is then:

$$\psi^*_{p\mathbf{k}\sigma}(\mathbf{r}) \psi_{q\mathbf{q}\sigma'}(\mathbf{r}) = \sum_\mu M^\mu_{p\mathbf{k}\sigma,q\mathbf{q}\sigma'} P^{\mathbf{q}-\mathbf{k}}_\mu(\mathbf{r}) \tag{2.124}$$

where $M^\mu_{p\mathbf{k}\sigma,q\mathbf{q}\sigma'} = \sum_{i,j} c^{i*}_{p\mathbf{k}\sigma} c^j_{q\mathbf{q}\sigma'} C^\mu_{i\mathbf{k},j\mathbf{q}}$.
With this, we can expand the Coulomb potential as follows:

$$\begin{aligned} V^{\mathbf{q}-\mathbf{k},\mathbf{q}'-\mathbf{k}'}_{\mu,\mu'} = \int d\mathbf{r} \int d\mathbf{r}' P^{\mathbf{q}-\mathbf{k}}_\mu(\mathbf{r}) \frac{1}{|\mathbf{r}-\mathbf{r}'|} P^{\mathbf{q}'-\mathbf{k}'}_{\mu'}(\mathbf{r}') = \\ \sum_{\mathbf{R},\mathbf{R}'} e^{\mathrm{i}(\mathbf{q}-\mathbf{k})\mathbf{R}} e^{\mathrm{i}(\mathbf{q}'-\mathbf{k}')\mathbf{R}'} \int d\mathbf{r} \int d\mathbf{r}' P_\mu(\mathbf{r}-\mathbf{R}) \frac{1}{|\mathbf{r}-\mathbf{r}'|} P_{\mu'}(\mathbf{r}'-\mathbf{R}') \end{aligned} \tag{2.125}$$

Setting $\mathbf{R}'' = \mathbf{R}' - \mathbf{R}$ yields:

$$\begin{aligned} V_{\mu,\mu'}^{\mathbf{q}-\mathbf{k},\mathbf{q}'-\mathbf{k}'} = \\ \sum_{\mathbf{R},\mathbf{R}''} e^{\mathrm{i}(\mathbf{q}-\mathbf{k})\mathbf{R}} e^{\mathrm{i}(\mathbf{q}'-\mathbf{k}')(\mathbf{R}''+\mathbf{R})} \int d\mathbf{r} \int d\mathbf{r}' P_\mu(\mathbf{r}-\mathbf{R}) \frac{1}{|\mathbf{r}-\mathbf{r}'|} P_{\mu'}(\mathbf{r}'-\mathbf{R}''-\mathbf{R}) = \\ \sum_{\mathbf{R},\mathbf{R}''} e^{\mathrm{i}(\mathbf{q}-\mathbf{k})\mathbf{R}} e^{\mathrm{i}(\mathbf{q}'-\mathbf{k}')(\mathbf{R}''-\mathbf{R})} \int d\mathbf{r} \int d\mathbf{r}' P_\mu(\mathbf{r}) \frac{1}{|\mathbf{r}-\mathbf{r}'|} P_{\mu'}(\mathbf{r}'-\mathbf{R}'') = \\ \sum_{\mathbf{R}} e^{\mathrm{i}(\mathbf{q}'-\mathbf{k}')\mathbf{R}''} \int d\mathbf{r} \int d\mathbf{r}' P_\mu(\mathbf{r}) \frac{1}{|\mathbf{r}-\mathbf{r}'|} P_{\mu'}(\mathbf{r}'-\mathbf{R}'') \sum_{\mathbf{R}} e^{\mathrm{i}[(\mathbf{q}-\mathbf{k})+(\mathbf{q}'-\mathbf{k}')]\mathbf{R}} = \\ N_{\mathbf{R}} \delta_{(\mathbf{q}-\mathbf{k}),-(\mathbf{q}'-\mathbf{k}')+\mathbf{G}} \sum_{\mathbf{R}''} e^{\mathrm{i}(\mathbf{q}'-\mathbf{k}')\mathbf{R}''} \int d\mathbf{r} \int d\mathbf{r}' P_\mu(\mathbf{r}) \frac{1}{|\mathbf{r}-\mathbf{r}'|} P_{\mu'}(\mathbf{r}'-\mathbf{R}'') \end{aligned} \tag{2.126}$$

The δ-function ensures the crystal-momentum conservation. To simplify the formalism, we define the object:

$$V_{\mu,\mu'}^{\mathbf{p}} = \sum_{\mathbf{R}} e^{\mathrm{i}\mathbf{p}\mathbf{R}} \int d\mathbf{r} \int d\mathbf{r}' \frac{P_{\mu'}(\mathbf{r}-\mathbf{R}) P_\mu(\mathbf{r}')}{|\mathbf{r}-\mathbf{r}'|} \tag{2.127}$$

where $\mathbf{p} = \mathbf{q} - \mathbf{k}$ is the momentum transferred by the interaction. Then $V_{\mu,\mu'}^{\mathbf{p},\mathbf{p}'} = N_{\mathbf{R}} \delta_{\mathbf{p},-\mathbf{p}'+\mathbf{G}} V_{\mu,\mu'}^{\mathbf{p}}$ and the Coulomb operator in the basis of the single-particle wavefunctions is:

$$\begin{aligned} V_{p\mathbf{k}\sigma,s\mathbf{q}\sigma}^{q\mathbf{k}'\sigma',r\mathbf{q}'\sigma'} = \int d\mathbf{r} \int d\mathbf{r}' \psi_{p\mathbf{k}\sigma}^*(\mathbf{r}) \psi_{q\mathbf{k}'\sigma'}^*(\mathbf{r}') \frac{1}{|\mathbf{r}-\mathbf{r}'|} \psi_{r\mathbf{q}'\sigma'}(\mathbf{r}') \psi_{s\mathbf{q}\sigma}(\mathbf{r}) = \\ \delta_{\mathbf{q}-\mathbf{k},\mathbf{q}'-\mathbf{k}'} \sum_{\mu\mu'} M_{p\mathbf{k}\sigma,s\mathbf{q}\sigma}^{\mu} M_{q\mathbf{k}'\sigma',r\mathbf{q}'\sigma'}^{\mu'} V_{\mu,\mu'}^{\mathbf{q}-\mathbf{k}} \end{aligned} \tag{2.128}$$

Truncating the basis set and density fitting technique

The incompleteness of the auxiliary basis generates an error when representing products of two functions:

$$\delta\rho_{i,j}(\mathbf{r}) = \phi_i(\mathbf{r})\phi_k(\mathbf{r}) - \sum_{\mu=1}^{N_b} C_{i,k}^{\mu} P_\mu(\mathbf{r}) \tag{2.129}$$

where N_b is the number of auxiliary functions, and $\phi_i(\mathbf{r}), \phi_j(\mathbf{r})$ are the localized atomic orbitals, as described in section 2.6. The coefficients $C_{i,k}^{\mu}$ can be chosen in

different ways. One is to minimize the error directly $\int d\mathbf{r}\|\delta\rho_{i,k}(\mathbf{r})\|$. In this case, the coefficients will be:

$$C_{i,k}^{\nu} = \sum_{\mu=1}^{N_b} S_{\mu,\nu}^{-1}(ik|\mu) = \sum_{\mu=1}^{N_b} S_{\mu,\nu}^{-1} \int d\mathbf{r}\phi_i(\mathbf{r})\phi_k(\mathbf{r})P_\mu(\mathbf{r})$$

where $S_{\mu,\nu} = \int d\mathbf{r}P_\mu(\mathbf{r})P_\nu(\mathbf{r})$. This method is known as RI-SVS (RI stands for resolution of identity) due to the form of the Coulomb integrals:

$$V_{k,l}^{i,j} = \sum_{\mu,\mu',\nu,\nu'} (ik|\mu)S_{\mu,\nu}^{-1}V_{\nu,\nu'}S_{\mu',\nu'}^{-1}(\nu|jl) \tag{2.130}$$

However, we are interested in the accurate evaluation of the Coulomb integrals rather than pair products. In this case, it is better to choose the coefficients that minimize the error in the integrals [44]. The resulting coefficients are:

$$C_{i,k}^{\nu} = \sum_{\mu=1}^{N_b} V_{\mu,\nu}^{-1}(ik|V|\mu) = \sum_{\mu=1}^{N_b} V_{\mu,\nu}^{-1} \int d\mathbf{r}\frac{\phi_i(\mathbf{r})\phi_k(\mathbf{r})P_\mu(\mathbf{r}')}{|\mathbf{r}-\mathbf{r}'|}$$

This method is known as RI-V, because the Coulomb integral becomes:

$$V_{k,l}^{i,j} = \sum_{\mu,\nu} C_{i,k}^{\mu}V_{\mu,\nu}C_{i,k}^{\nu} = \sum_{\mu,\nu}(ik|V|\mu)V_{\mu,\nu}^{-1}(\nu|V|jl) \tag{2.131}$$

While RI-V significantly reduces errors in the Coulomb integrals compared to RI-SVS, it does not reduce the calculation's size scaling [48]. To overcome this problem, as described in the previous reference, a localized version of RI-V, called RI-LVL [40], is employed. In this approach, the coefficients $C_{i,k}^{\mu}$ are set to zero when the auxiliary basis function $P_\mu(\mathbf{r})$ is not centered at one of the two atoms that the functions i or k are centered at:

$$\phi_i(\mathbf{r}-\mathbf{R})\phi_k(\mathbf{r}-\mathbf{R}') \approx \sum_{\mu} \left[C_{i,k}^{\mu}P_\mu(\mathbf{r}-\mathbf{R}) + C_{i,k}^{\mu}P_\mu(\mathbf{r}-\mathbf{R}')\right] \tag{2.132}$$

2.7.2 Calculating Coulomb matrix in real space

One way to evaluate the Coulomb matrix $V_{\mu,\mu'}^{\mathbf{p}}$ defined in equation 2.127 is through a summation in real space as follows:

$$V_{\mu,\mu'}^{\mathbf{p}} = \sum_{\mathbf{R}} e^{-\mathbf{i}\mathbf{p}\mathbf{R}}V_{\mu,\mu'}(\mathbf{R}) \tag{2.133}$$

where $V_{\mu,\mu'}(\mathbf{R})$ represents the Coulomb interaction of two auxiliary basis functions, and $\mathbf{R}$ is a lattice vector:

$$V_{\mu,\mu'}(\mathbf{R}) = \int d\mathbf{r} \int d\mathbf{r}' \frac{P_\mu(\mathbf{r} - \mathbf{R}_{a_\mu}) P_{\mu'}(\mathbf{r}' - \mathbf{R}_{a_{\mu'}} - \mathbf{R})}{|\mathbf{r} - \mathbf{r}'|} \tag{2.134}$$

It is important to remember that each μ is referring to an l, m pair and an atom position $\mathbf{R}_{at}$ where the auxiliary function is centered. When the charge distributions do not overlap, we can use multipole expansion to calculate the interaction [88]. To take advantage of this, the lattice summation is separated into two parts: (i) summation over a set of lattice vectors $\{\mathbf{R}_{ovl}\}$ in which the auxiliary functions $P_\mu(\mathbf{r} - \mathbf{R}_{a_\mu})$ and $P_{\mu'}(\mathbf{r} - \mathbf{R}_{a_{\mu'}} - \mathbf{R})$ overlap, and (ii) summation over the lattice vectors $\{\mathbf{R}_{n-ovl}\}$ in which the functions do not overlap:

$$\begin{aligned} V^{\mathbf{p}}_{\mu,\mu'} = \sum_{\mathbf{R}} e^{-\mathbf{ipR}} V_{\mu,\mu'}(\mathbf{R}) = \sum_{\mathbf{R}\in\{\mathbf{R}_{ovl}\}} e^{-\mathbf{ipR}} V_{\mu,\mu'}(\mathbf{R}) + \\ \sum_{\mathbf{R}\in\{\mathbf{R}_{n-ovl}\}} e^{-\mathbf{ipR}} V_{\mu,\mu'}(\mathbf{R}) \end{aligned} \tag{2.135}$$

For non-overlapping functions we can write [89]:

$$\begin{aligned} V_{\mu,\mu'}(\mathbf{R}) = \sum_{L_A,M_A} \sum_{L_B,M_B} (-1)^{L_B} (-1)^{M_A+M_B} \sqrt{\frac{(2L_A + 2L_B)!}{2L_A!((2L_B))!}} Q_{L_A,M_A} Q_{L_B,M_B} \\ \sqrt{\frac{4\pi}{2L_A + 2L_B + 1}} \langle L_A, M_A; L_B, M_B | L_A + L_B, M_A + M_B \rangle \frac{Y^{-M_A+M_B}_{L_A+L_B}}{R^{L_A+L_B+1}_{AB}} \end{aligned} \tag{2.136}$$

where $R_{AB} = |\mathbf{R}_{a_\mu} - \mathbf{R}_{a_{\mu'}} - \mathbf{R}|$ is the distance between the atoms, Q_{L_1,M_1} are the multipole moments of the charge distribution of each $P_\mu(\mathbf{r})$ around the atom origin:

$$\begin{aligned} Q_{L,M} = \int dr^3 r^L \sqrt{\frac{4\pi}{2L+1}} Y_{LM}(\Omega_{\mathbf{r}}) P_\mu(\mathbf{r}) = \\ \int dr r^L f_\mu(r) \int d\Omega_{\mathbf{r}} Y_{LM}(\Omega_{\mathbf{r}}) Y_{lm}(\Omega_{\mathbf{r}}) = \delta_{L,l}\delta_{M,m} \int dr r^l f_\mu(r) \end{aligned} \tag{2.137}$$

and $\langle L_1, M_1; L_2, M_2 | L_1 + L_2, M_1 + M_2 \rangle$ are the Clebsch-Gordan coefficients.

The summation over infinite space is converging very slowly. Moreover, for $\mathbf{p} = 0$ and $L_A, L_B = 0$, the term is diverging [72]. It is more efficient to transform into the reciprocal space and use the Ewald summation method, as presented in the next sections.

2.7.3 Calculating Coulomb matrix in reciprocal space

To calculate the Coulomb matrix (eq. 2.128) in reciprocal space, we start by defining our space as a Born-von Karmann supercell of N unit cells and a total volume V_N. Then we take the thermodynamic limit $N \to \infty$. The Fourier transform in this volume will be[8]:

$$\tilde{f}(\mathbf{q}) = \frac{1}{V_N} \int_{V_N} d\mathbf{r} e^{-\mathrm{i}\mathbf{q}\mathbf{r}} f(\mathbf{r}) \tag{2.138}$$

Since all functions of interest are periodic in the supercell, there is a discrete set of allowed $\mathbf{q}$ vectors. Therefore, the inverse Fourier transform is a sum:

$$f(\mathbf{r}) = \sum_{\mathbf{q}} e^{\mathrm{i}\mathbf{q}\mathbf{r}} \tilde{f}(\mathbf{q}) \tag{2.139}$$

Furthermore, it holds:

$$\frac{1}{V_N} \int_{V_N} d\mathbf{r} e^{\mathrm{i}\mathbf{r}(\mathbf{q}-\mathbf{q}')} = \delta_{\mathbf{q},\mathbf{q}'} \tag{2.140}$$

For a lattice defined in the system of lattice vectors, $\mathbf{a}_1, \mathbf{a}_2, \mathbf{a}_3$, the lattice points will be $\mathbf{R} = (n_1, n_2, n_3)$. The total volume can be written as $V_N = \Omega N_1 N_2 N_3$, where Ω is the volume of the unit cell, and N_i are the number of unit cells in each direction. Defining the reciprocal vectors as $\mathbf{b}_i \mathbf{a}_j = 2\pi\delta_{i,j}$ with $i, j = 1, 2, 3$, the points of the reciprocal lattice are $\mathbf{G} = (m_1, m_2, m_3)$, with $m_1, m_2, m_3 = 0 \pm 1, \pm 2, ...$ and the allowed crystal momenta are $\mathbf{q} = (\frac{m_1}{N_1}, \frac{m_2}{N_2}, \frac{m_3}{N_3})$. In addition, the following is true:

$$\sum_{\mathbf{R}} e^{\mathrm{i}\mathbf{q}\mathbf{R}} = N\delta_{\mathbf{q}-\mathbf{G},0} \tag{2.141}$$

i.e., the sum is non-zero only for the crystal momentum equal to one of the reciprocal lattice vectors[9]. This also means that functions that have the periodicity of the lattice, e.g., lattice potential, will have non-zero Fourier coefficients only for $\mathbf{q} = \mathbf{G}$.

[8] The normalization of Fourier transform can be different in different definitions

[9] If we confine crystal momentum to first Brillouin zone then only the zero (0,0,0) lattice vector will belong to this zone.

The Fourier transform of the Coulomb potential is:

$$\tilde{V}(\mathbf{q}) = \frac{1}{V_N} \int\limits_{V_N} d\mathbf{r} e^{-\mathrm{i}\mathbf{q}\mathbf{r}} \frac{1}{|\mathbf{r}|} \tag{2.142}$$

This integral can be calculated in the limit of $V_N \to \infty$ using the adiabatic switching method. Let us introduce an exponential factor $e^{-\mu|\mathbf{r}|}$ in the nominator and then take the limit as defined by Fetter and Walecha [86], $\mu \to 0$, under the condition $1/\mu < V^{1/3}$:

$$\tilde{V}(\mathbf{q}) = \frac{1}{V_N} \int\limits_{V_N} d\mathbf{r} e^{-i\mathbf{q}\mathbf{r}} \frac{e^{-\mu|\mathbf{r}|}}{|\mathbf{r}|} = \frac{1}{V_N} \frac{4\pi}{(|\mathbf{q}|^2 + \mu^2)} \tag{2.143}$$

with the inverse:

$$V(\mathbf{r}) = \sum_{\mathbf{q}} e^{\mathrm{i}\mathbf{q}\mathbf{r}} \tilde{V}(\mathbf{q}) \tag{2.144}$$

Inserting the above equation in place of the Coulomb potential in the expression for the Coulomb matrix elements eq. 2.127, we obtain:

$$\begin{aligned} V^{\mathbf{p}}_{\mu,\mu'} = \sum_{\mathbf{R}} e^{\mathrm{i}\mathbf{p}\mathbf{R}} \int d\mathbf{r} \int d\mathbf{r}' P_{\mu'}(\mathbf{r} - \mathbf{R}) P_{\mu}(\mathbf{r}') \sum_{q} e^{\mathrm{i}\mathbf{q}(\mathbf{r}-\mathbf{r}')} \tilde{V}(\mathbf{q}) = \\ V_N \sum_{\mathbf{G}} \tilde{P}^*_{\mu'}(\mathbf{G} - \mathbf{p}) \tilde{P}_{\mu}(\mathbf{G} - \mathbf{p}) \frac{4\pi}{|\mathbf{G} - \mathbf{p}|^2 + \mu^2} \end{aligned} \tag{2.145}$$

where $\tilde{P}_{\mu}(\mathbf{q})$ is the Fourier transform of the basis functions $P_{\mu}(\mathbf{r})$. The above expression is singular for $\mathbf{G} = 0, \mathbf{p} = 0$ for $\mu = 0$.

2.7.4 Ewald summation for Coulomb matrix integrals

The calculation of the Coulomb matrix can be more efficient if it is done partially in real space and partially in reciprocal space. For each localized function $P_{\mu}(\mathbf{r})$ with non-zero multipole moment, we define a charge distribution with zero moment in the far field by introducing $\bar{P}_{\mu}(\mathbf{r}) = P_{\mu}(\mathbf{r}) - Q_{\mu} p_{lm}(\mathbf{r})$, where $p_{lm}(\mathbf{r})$ is a Gaussian charge distribution of the form:

$$p_{lm}(\mathbf{r}) = A_l r^l e^{-\gamma r^2/2} Y_{lm}(\widehat{r})$$

The normalization assures that the Gaussian functions have multipole moments equal to 1 ($A_l = \sqrt{\frac{2}{\pi}}\frac{\gamma^{l+3/2}}{(2l-1)!!}$). The integral in equation 2.134 can then be rewritten as follows:

$$\begin{aligned} V_{\mu,\mu'}(\mathbf{R}) = \int d\mathbf{r} \int d\mathbf{r}' \frac{P_\mu(\mathbf{r}-\mathbf{R}_{a_\mu})P_{\mu'}(\mathbf{r}'-\mathbf{R}_{a_{\mu'}}-\mathbf{R})}{|\mathbf{r}-\mathbf{r}'|} = \\ - \int d\mathbf{r} \int d\mathbf{r}' \frac{\bar{P}_\mu(\mathbf{r}-\mathbf{R}_{a_\mu})\bar{P}_{\mu'}(\mathbf{r}'-\mathbf{R}_{a_{\mu'}}-\mathbf{R})}{|\mathbf{r}-\mathbf{r}'|} + \\ \int d\mathbf{r} \int d\mathbf{r}' \frac{\bar{P}_\mu(\mathbf{r}-\mathbf{R}_{a_\mu})P_{\mu'}(\mathbf{r}'-\mathbf{R}_{a_{\mu'}}-\mathbf{R})}{|\mathbf{r}-\mathbf{r}'|} + \\ \int d\mathbf{r} \int d\mathbf{r}' \frac{P_\mu(\mathbf{r}-\mathbf{R}_{a_\mu}\bar{P}_{\mu'}(\mathbf{r}'-\mathbf{R}_{a_{\mu'}}-\mathbf{R})}{|\mathbf{r}-\mathbf{r}'|} + \\ \int d\mathbf{r} \int d\mathbf{r}' \frac{Q_\mu p_{lm}(\mathbf{r}-\mathbf{R}_{a_\mu})Q_{\mu'}p_{l'm'}(\mathbf{r}'-\mathbf{R}_{a_{\mu'}}-\mathbf{R})}{|\mathbf{r}-\mathbf{r}'|} \end{aligned} \tag{2.146}$$

The first three terms are zero when the orbitals do not overlap, because $\bar{P}_\mu$ and $\bar{P}_{\mu'}$ have zero multipole moments. Therefore, for this part, the summation over lattice vectors for the calculation of the potential $\sum_{\mathbf{R}} e^{\mathrm{i}\mathbf{p}\mathbf{R}} V_{\mu,\mu'}(\mathbf{R})$ can be performed in real space. We focus now on the calculation of the lattice sum for the fourth term, which can be calculated using the Ewald summation method. This term is challenging because the terms proportional to $1/|\mathbf{p}|^2$ that will appear give rise to a singularity for $\mathbf{p} \to 0$.

We start by calculating the Fourier transform of the Gaussian function p_{lm}, as introduced in section 2.7.3:

$$\tilde{p}_{lm}(\mathbf{q}) = \frac{1}{V_N} \int_{V_N} d\mathbf{r} e^{-\mathrm{i}\mathbf{q}\mathbf{r}} p_{lm}(\mathbf{r}) \tag{2.147}$$

To calculate this integral we will use Hankel transform of half-integer order, also known as the spherical Bessel transform. The exponential is expanded in spherical harmonics:

$$e^{\mathrm{i}\mathbf{p}\mathbf{r}} = (2\pi)^{\frac{3}{2}} \sum_{l,m} \mathrm{i}^l \sqrt{\frac{2}{\pi}} j_l(pr) Y_{lm}(\hat{p}) Y^*_{lm}(\hat{r}) \tag{2.148}$$

where the spherical Bessel functions are defined as:

$$j_l(r) = \sqrt{\frac{\pi}{2}} \frac{J_{l+1/2}(r)}{\sqrt{r}}$$

Then we obtain[10]:

$$\tilde{p}_{lm}(\mathbf{q}) = \frac{(2\pi)^{3/2}}{V_N}\mathrm{i}^{-l}\tilde{p}_{lm}(q)Y_{lm}(\Omega_{\mathbf{q}}) \tag{2.149}$$

where:

$$\tilde{p}_{lm}(q) = \int drr^2\sqrt{\frac{2}{\pi}}j_l(pr)[A_l r^l e^{-\gamma r^2/2}] = \tilde{A}_l q^l e^{-q^2/\gamma 2}$$

with $\tilde{A}_l = \frac{A_l}{\gamma^{l+3/2}}$. Then the contribution of the last term in equation 2.146 to the Coulomb matrix elements (eq. 2.145) is:

$$V_{\mu,\mu'}^{\mathbf{p}(Gauss)} = \sum_{\mathbf{R}} e^{\mathrm{i}\mathbf{p}\mathbf{R}} \int d\mathbf{r} \int d\mathbf{r}' \frac{Q_\mu p_{lm}(\mathbf{r}-\mathbf{R}_{a_\mu})Q_{\mu'}p_{lm}(\mathbf{r}'-\mathbf{R}_{a_{\mu'}}-\mathbf{R})}{|\mathbf{r}-\mathbf{r}'|} =$$
$$V_N Q_\mu Q_{\mu'} e^{\mathrm{i}\mathbf{p}\mathbf{D}_{\mu,\mu'}} \sum_{\mathbf{G}} \tilde{p}_{lm}(\mathbf{G}-\mathbf{p})\tilde{p}^*_{l'm'}(\mathbf{G}-\mathbf{p})\frac{4\pi}{|\mathbf{G}-\mathbf{p}|^2+\mu^2} \tag{2.150}$$

where $\mathbf{D}_{\mu,\mu'} = \mathbf{R}_{a_\mu} - \mathbf{R}_{a_{\mu'}}$. Taking into account the form of $\tilde{p}_{lm}(\mathbf{q})$ from equation 2.149, we obtain:

$$V_{\mu,\mu'}^{\mathbf{p}(Gauss)} = V_N Q_\mu Q_{\mu'} e^{\mathrm{i}\mathbf{p}\mathbf{D}_{\mu,\mu'}} \frac{(2\pi)^3}{V_N^2}\mathrm{i}^{-l+l'} \times$$
$$\sum_{\mathbf{G}} \tilde{A}_l \tilde{A}_{l'} |\mathbf{G}-\mathbf{p}|^{l+l'} e^{-(|\mathbf{G}-\mathbf{p}|)^2/\gamma^2} Y_{lm}(\Omega_{\mathbf{G}-\mathbf{p}})Y^*_{l'm'}(\Omega_{\mathbf{G}-\mathbf{p}})\frac{4\pi}{|\mathbf{G}-\mathbf{p}|^2+\mu^2} \tag{2.151}$$

This expression needs special care for $\mathbf{p} \to 0$ since the limit $\mu \to 0$ needs to be taken. In the next section, we are going to explore the behavior of the matrix elements and explore ways to treat them analytically and computationally.

[10]This integral can be found in integral tables, for example see here [90]

Chapter 3

Results

3.1 Singularity of the Coulomb potential

In section 2.7, we showed the expression of the Coulomb matrix elements in terms of a Bloch function basis set, created from atom-centered localized orbitals. We showed that the expression is problematic for small crystal momentum vectors $\mathbf{p}$. This problem is extensively studied for the HF case, but inadequately studied for higher order terms of the many-body perturbation theory, as the second-order corrections. Until now, the main approach is an extrapolation from an assumed law of decay [78]. We begin by analysing the methods used for HF and the reasons why we cannot use them directly for second-order theory. Later, we present the connection between the power of the singularity and the decay law, providing a proper scheme of extrapolation, with no assumptions. Furthermore, we suggest a scheme to generalize the Gygi-Baldereschi method, for the application to second-order theory, which until now was not possible.

3.1.1 Coulomb potential in the limit $\mathbf{p} \to 0$

The singularity problem arises from the non-converging summation over the lattice vectors in the equation 2.127 if $\mathbf{p} = 0$. This demands the integration of a function proportional to $1/|\mathbf{p}|^2$ (see equation 2.151). We now analyze this expres-

sion. The problematic $\mathbf{G} = 0$ term in equation 2.151 is:

$$T^{\mathbf{p}}_{\mu,\mu'} = \frac{(2\pi)^3}{V_N} \mathrm{i}^{-l+l'} \tilde{A}_l \tilde{A}_{l'} Q_\mu Q_{\mu'} e^{\mathrm{i}\mathbf{p}\mathbf{D}_{\mu,\mu'}} |\mathbf{p}|^{l+l'} e^{-(|\mathbf{p}|)^2/\gamma^2} Y_{lm}(\Omega_{\mathbf{p}}) Y^*_{l'm'}(\Omega_{\mathbf{p}}) \frac{4\pi}{|\mathbf{p}|^2 + \mu^2} \tag{3.1}$$

The order of taking limits $\mathbf{p} \to \mathbf{0}$ and $\mu \to 0$ is important. If we first take the limit $\mu \to 0$, then the term will be proportional to $p^{l+l'-2} Y_l m(\Omega_{\mathbf{p}}) Y^*_{l'm'}(\Omega_{\mathbf{p}})$. The behavior of this term for $\mathbf{p} \to 0$ depends on $l + l'$:

- If $l + l' > 2$, the limit is zero.
- When $l + l' = 2$, it will be equal to $\lim_{\mathbf{p}\to 0} Y_l m(\Omega_{\mathbf{p}}) Y^*_{l'm'}(\Omega_{\mathbf{p}})$ which is not well-defined for $l, l' \neq 0$, because it depends on the direction from which $\mathbf{p}$ approaches zero. In any case, it is bound.
- For $l + l' = 1$ the limit diverges. How it diverges depends on the direction of approaching zero.
- For $l + l' = 0$, the limit is diverging to $+\infty$

On the other hand, if we take the limit $\mathbf{p} \to \mathbf{0}$ with finite μ:

- If $l + l' > 0$, the limit is zero.
- For $l + l' = 0$, the limit is diverging to $+\infty$.

Let us examine the dependence on μ and $p = |\mathbf{p}|$ in the equation 3.1. For this, we analyze the dependence of $f(p) = \frac{p^L}{p^2+\mu^2}$ on p for different values of μ in the range between $\mu = 0$ and $\mu = 1/V_0^{1/3}$ in units of $1/V^{1/3}$ for $L = l + l' = 0, 1, 2$.

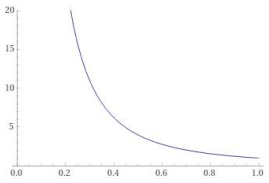

(a) $\mu = 10^{-3} 1/V^{1/3}$

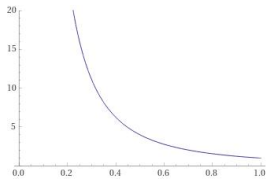

(b) $\mu = 10^{-4} 1/V^{1/3}$

Figure 3.1: $f(p) = \frac{1}{p^2+\mu^2}$

As can be seen in figures 3.1-3.4, for p close to 0, the largest term at $\mu \to 0$ is for $L = 0$, where the function diverges. For $L = 1$, there is a maximum at

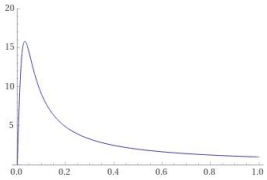

(a) $\mu = 10^{-3}1/V^{1/3}$

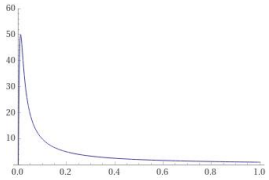

(b) $\mu = 10^{-4}1/V^{1/3}$

Figure 3.2: $f(p) = \frac{p}{p^2+\mu^2}$

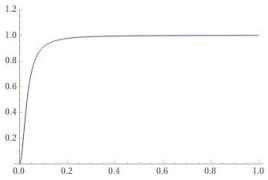

(a) $\mu = 10^{-3}1/V^{1/3}$

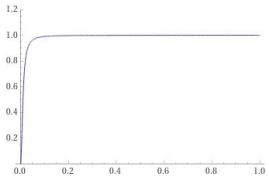

(b) $\mu = 10^{-4}1/V^{1/3}$

Figure 3.3: $f(p) = \frac{p^2}{p^2+\mu^2}$

$p_0 = \frac{\mu}{\sqrt{2}}$ with a magnitude of $\frac{2}{3\sqrt{2}\mu}$ getting larger as $\mu \to 0$. For $L = 2$, the function is bound by 1, increasing from zero as $\frac{1}{\mu}p^2$ for $p << 1$ (in $1/V^{1/3}$ units). For higher L, the term approaches zero as p^L/μ^2 for $p \to 0$. The value of μ affects only the $L = 1$ and $L = 2$ cases.

To address the singularity issue, it is required to take into account that the final expressions we are interested in are always summations over states, meaning that there will be a summation over the first Brillouin zone for the crystal momentum. In the thermodynamic limit, the summation over a crystal momentum $\mathbf{p}$ will become an integral:

$$\sum_{\mathbf{p}} \to \frac{V_N}{(2\pi)^3} \int_{1stBZ} d\mathbf{p}$$

In practical calculations, the integration is performed as a summation over $\mathbf{p}$ on a finite reciprocal-space grid inside the first Brillouin zone. If the chosen grid has N_0 points, the integration step will be $\frac{(2\pi)^3}{N_0}$. The quantities will be calculated per unit-cell volume, since $V_0 = N_0\Omega$. The problem with the Coulomb matrix singularity is that the integrand is very large or even infinite, and the contribution of this singularity to the integral needs to be treated carefully.

As a first step, we must demonstrate that the integral converges. For HF, this

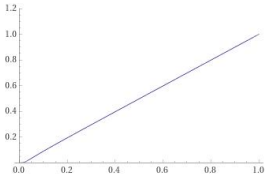

(a) $\mu = 10^{-3}1/V^{1/3}$

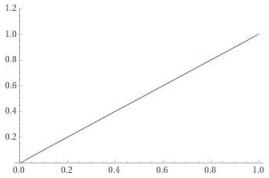

(b) $\mu = 10^{-4}1/V^{1/3}$

Figure 3.4: $f(p) = \frac{p^3}{p^2+\mu^2}$

can be easily demonstrated by writing the integral in spherical coordinates. However, for higher-order corrections of MBPT, it is not so obvious. After showing that the integral converges, a way to continue is by applying a uniform grid and then ignoring the singular point. This method converges very slowly and, for this reason, methods to accelerate it by treating the singularity have been proposed in the case of HF. We review two of the most widely used approaches, the Gygi-Baldereschi and the truncated Coulomb potential, and we show that they cannot be applied directly in the case of second-order MBPT. We then discuss the options we have for second-order correction of MBPT. The main approach until now is to treat the singularity is by fitting the data and extrapolating to the dense k-grid limit.

The Gygi-Baldereschi method

Gygi and Baldereschi suggested a way to treat the singularity when calculating the exchange energy of HF approximation:

$$E_x^{HF} = -\frac{1}{2}\sum_{i,j}^{occ}\sum_{\sigma}\sum_{\mathbf{q}\in BZ}\sum_{\mathbf{k}\in BZ} V_{j\mathbf{k}\sigma,i\mathbf{q}\sigma}^{i\mathbf{q}\sigma,j\mathbf{k}\sigma} \tag{3.2}$$

The main idea is to add and subtract a term that has the same singularity as the Coulomb interaction, but that can be integrated analytically [91].

To explain the method, we will write the quantities that need to be calculated in a similar form as was written originally for HF, which has a linear dependence on Coulomb matrix elements. The method was applied for a plane-wave basis set, so the Coulomb operator is projected in reciprocal space as in equation 2.143, so $\tilde{V}(\mathbf{p}-\mathbf{G}) \propto \frac{1}{|\mathbf{p}-\mathbf{G}|^2}$. Since the integrand in HF has a linear dependence on

the Coulomb matrix, it can be written in the form: $f(\mathbf{p},\mathbf{G})\tilde{V}(\mathbf{p}-\mathbf{G})$, where $\mathbf{p}=\mathbf{q}-\mathbf{k}$ is the momentum transferred from the interaction, so the summation becomes: $\sum_{\mathbf{qk}} \rightarrow \sum_{\mathbf{qp}}$. The function f represents anything that will be a factor of the Coulomb matrix in reciprocal space. Thus, the quantity to be integrated in the thermodynamic limit can be written as:

$$I = \sum_{\mathbf{p}\in BZ}\sum_{\mathbf{G}} \frac{f(\mathbf{p},\mathbf{G})}{|\mathbf{p}-\mathbf{G}|^2} \tag{3.3}$$

To eliminate the singularity, we search for functions that have the same singularity as the above expression. A practical function, suitable for all systems, was suggested by Massidda *et al.* [74]:

$$\sum_{\mathbf{p}\in BZ} F_a(\mathbf{p}) = \sum_{\mathbf{p}\in BZ}\sum_{\mathbf{G}} \frac{e^{-a|\mathbf{p}-\mathbf{G}|^2} f(0,0)}{|\mathbf{p}-\mathbf{G}|^2} \tag{3.4}$$

where a is a parameter whose value is chosen in order to have a Gaussian width comparable to the Brillouin zone linear size. Without the Gaussian, the integral would diverge. The function is integrable and can be taken analytically:

$$\begin{aligned} &\sum_{\mathbf{p}\in BZ}\sum_{\mathbf{G}} \frac{e^{-a|\mathbf{p}-\mathbf{G}|^2} f(0,0)}{|\mathbf{p}-\mathbf{G}|^2} = f(0,0)\sum_{\mathbf{p}} \frac{e^{-a|\mathbf{p}|^2}}{|\mathbf{p}|^2} \rightarrow \\ &f(0,0)\frac{V_N}{(2\pi)^3}\int d\mathbf{p}\frac{e^{-a|\mathbf{p}|^2}}{|\mathbf{p}|^2} = f(0,0)\frac{V_N}{(2\pi)^3}4\pi\sqrt{\frac{\pi}{4a}} \end{aligned} \tag{3.5}$$

Advancing from the first row to the second in the equation 3.5, we consider that the summation over $\mathbf{p}$ on the first Brillouin zone and the summation over all reciprocal lattice points $\mathbf{G}$ results in a summation over the whole space. By rewriting the expression 3.3:

$$\begin{aligned} I = &\sum_{\mathbf{p}\in BZ}\sum_{\mathbf{G}} f(\mathbf{p},\mathbf{G})\tilde{V}(\mathbf{p}-\mathbf{G}) = \\ &\sum_{\mathbf{p}\in BZ}\sum_{\mathbf{G}} \left[\frac{f(\mathbf{p},\mathbf{G})}{|\mathbf{p}-\mathbf{G}|^2} - \frac{e^{-a|\mathbf{p}-\mathbf{G}|^2} f(0,0)}{|\mathbf{p}-\mathbf{G}|^2}\right] \\ &+ \sum_{\mathbf{p}\in BZ}\sum_{\mathbf{G}} \frac{e^{-a|\mathbf{p}-\mathbf{G}|^2} f(0,0)}{|\mathbf{p}-\mathbf{G}|^2} \end{aligned} \tag{3.6}$$

we split it into two parts, one non-singular, and another which is analytically integrable. Therefore, the term for $\mathbf{p} = \mathbf{0}$ can be omitted from the first sum:

$$\frac{\Omega}{N_0}\sum_{\mathbf{p}\in BZ}{}'\sum_{\mathbf{G}}\left[\frac{f(\mathbf{p},\mathbf{G})}{|\mathbf{p}-\mathbf{G}|^2}-\frac{e^{-a|\mathbf{p}-\mathbf{G}|^2}f(0,0)}{|\mathbf{p}-\mathbf{G}|^2}\right] + \frac{\Omega}{(2\pi)^3}\int d\mathbf{p}\frac{e^{-a|\mathbf{p}|^2}f(0,0)}{|\mathbf{p}|^2} \tag{3.7}$$

In practical implementations, the application of the Gygi-Balderesci correction scheme for HF can be applied by excluding the singular point in the calculation of the Coulomb matrix elements and, in its place, include the correction:

$$\left[-\frac{\Omega}{N_0}\sum_{\mathbf{p}}{}'\frac{e^{-a|\mathbf{p}|^2}}{|\mathbf{p}|^2}+\frac{\Omega}{(2\pi)^3}\int d\mathbf{p}\frac{e^{-a|\mathbf{p}|^2}}{|\mathbf{p}|^2}\right]. \tag{3.8}$$

The simple swap of the singular term with a correction is possible because of the linear dependence of the integrand from the Coulomb matrix elements in the case of HF. This is not the case for second-order theory were the integrand is not linearly dependent to the Coulomb matrix elements. Because of this, a simple swap of the singular point with the correction will not work. Instead, we explore possible solutions in the section about the generalization of the Gygi-Balderesci correction scheme 3.1.3.

Moreover, we note that the exact dependence of the integrand on $\mathbf{p}$ depends also on the behavior of $f(\mathbf{p},\mathbf{G})$ around $\mathbf{p} = \mathbf{0}$. Considering a Taylor series expansion around $\mathbf{p} = \mathbf{0}$, one realizes that the above correction takes into account only the contribution from the zero power term of the Taylor expansion, while there might be higher power terms, giving rise to singularities proportional to p^{-1} or p^0. These terms are not corrected by the Gygi-Baldereschi method, but we suggest a scheme to include them in the section about the generalization of the Gygi-Balderesci correction scheme.

The truncated Coulomb potential method

Another approach to address the singularity issue is the truncation of the Coulomb potential, also known as the cut-Coulomb method and it was presented by J. Spencer and A. Alavi [75] in 2008 for the calculation of HF exchange energy, as an

alternative to Gygi-Baldereschi method. They proposed that instead of calculating the Fourier transform of the full Coulomb potential (eq. 2.142), the following potential should be used:

$$V_{cut} = \begin{cases} \frac{1}{|\mathbf{r}-\mathbf{r}'|}, & \text{if } |\mathbf{r}-\mathbf{r}'| \leq R_{cut} \\ 0, & \text{otherwise} \end{cases} \tag{3.9}$$

The radius R_{cut} must be consistent with the volume of the Born-von Karman supercell, V_0, so that when $V_0 \to \infty$ also $R_{cut} \to \infty$. Thus, the correct limit is recovered while increasing the density of the k-point grid. To have an analytical expression of the Fourier transform, the radius can be chosen as the radius of a sphere with the same volume as the Born-von Karman supercell, $\frac{4}{3}\pi R_{cut}^3 = V_0$. The Fourier transform of the modified Coulomb potential becomes:

$$\tilde{V}(\mathbf{q}) = \frac{1}{V_N}\frac{4\pi}{(|\mathbf{q}|^2)}\left(1 - cos(|\mathbf{q}|R_{cut})\right) \tag{3.10}$$

This approach is easier to implement than the Gygi-Baldereschi method and works well for the exchange energy in the case of HF [47].

3.1.2 Singularity in second-order MBPT

To calculate the second-order corrections, eq. 2.53 for the total energy and eq. 2.81 for the single particle energies must be evaluated. As can be concluded from these equations, the Coulomb matrix elements enter the integrals over the reciprocal space in the second power, $|\langle\phi_p\phi_q|\,|\phi_r\phi_s\rangle|^2$. This means that the singularity of the integrand can be $\sim 1/p^4$. This type of singularity will be present in direct terms for $l = l' = 0$. Before proceeding, we prove that the integral in the reciprocal space exists. The proof relies on the cancellation of the $1/p^4$ term due to the orthogonality of the wavefunctions. To the best of our knowledge, such an analysis has not been reported for the second-order MBPT correction formulated in the framework of localized basis sets and Ewald summation.

Convergence of second-order MBPT

From the expression 2.145 for the Coulomb matrix element, we arrive at:

$$V^{\mathbf{p}}_{\mu,\mu'} = V_N \left[\tilde{P}_\mu(\mathbf{p}) \tilde{P}_{\mu'}(\mathbf{p}) \tilde{V}(\mathbf{p}) + {\sum_{\mathbf{G}-\mathbf{p}}}' \tilde{P}^*_{\mu'}(\mathbf{G}-\mathbf{p}) \tilde{P}_\mu(\mathbf{G}-\mathbf{p}) \tilde{V}(\mathbf{G}-\mathbf{p}) \right] \tag{3.11}$$

where we have separated the $\mathbf{G} = 0$ term from the summation. The matrix element of the potential from equation 2.128 for $\mathbf{p} = 0$ can be written as:

$$\begin{aligned} V^{i\mathbf{k}'\sigma',b\mathbf{k}'\sigma'}_{n\mathbf{k}\sigma,a\mathbf{k}\sigma} &= \sum_{\mu\mu'} M^{\mu}_{n\mathbf{k}\sigma,a\mathbf{k}\sigma} M^{\mu'}_{i\mathbf{k}'\sigma',b\mathbf{k}'\sigma'} V^0_{\mu,\mu'} = \\ &\sum_{\mu\mu'} M^{\mu}_{n\mathbf{k}\sigma,a\mathbf{k}\sigma} M^{\mu'}_{i\mathbf{k}'\sigma',b\mathbf{k}'\sigma'} V_N \tilde{P}_\mu(0) \tilde{P}_{\mu'}(0) \tilde{V}(0) + \\ \sum_{\mu\mu'} M^{\mu}_{n\mathbf{k}\sigma,a\mathbf{k}\sigma} M^{\mu'}_{i\mathbf{k}'\sigma',b\mathbf{k}'\sigma'} V_N {\sum_{\mathbf{G}}}' \tilde{P}^*_{\mu'}(\mathbf{G}) \tilde{P}_\mu(\mathbf{G}) \tilde{V}(\mathbf{G}) & \end{aligned} \tag{3.12}$$

The singular terms are the ones proportional to $\tilde{V}(0)$, and to understand their behavior in the above expression, we rewrite the orthogonality relation:

$$\int d\mathbf{r} \psi_{a\sigma\mathbf{k}}(\mathbf{r}) \psi_{i\sigma'\mathbf{k}'}(\mathbf{r}) = N_0 \delta_{\mathbf{k}-\mathbf{k}',\mathbf{G}} \delta_{a,i} \delta_{\sigma\sigma'} \tag{3.13}$$

In the limit of a complete auxiliary basis set, we can express the product of the functions as follows:

$$\psi_{a\sigma\mathbf{k}}(\mathbf{r}) \psi_{i\sigma'\mathbf{k}'}(\mathbf{r}) = \sum_{\mu} M^{\mu}_{a\mathbf{k}\sigma,i\mathbf{k}'\sigma'} P^{\mathbf{k}-\mathbf{k}'}_{\mu}(\mathbf{r}) \tag{3.14}$$

Then we write the orthogonality relation 3.13 as:

$$\begin{aligned} \sum_{\mu} M^{\mu}_{a\mathbf{k}\sigma,i\mathbf{k}'\sigma'} \int d\mathbf{r} P^{\mathbf{k}-\mathbf{k}'}_{\mu}(\mathbf{r}) = N \delta_{\mathbf{k}-\mathbf{k}',\mathbf{G}} \delta_{a,i} \delta_{\sigma\sigma'} \implies \\ \sum_{\mu} M^{\mu}_{a\mathbf{k}\sigma,i\mathbf{k}'\sigma'} \int d\mathbf{r} P_\mu(\mathbf{r}) = \delta_{a,i} \delta_{\sigma\sigma'} \end{aligned} \tag{3.15}$$

Applying the Taylor expansion to the Fourier transformormation of the auxiliary basis functions P_μ, it follows that:

$$\begin{aligned} \tilde{P}_\mu(p) = \frac{1}{V_N} \int d\mathbf{r} e^{-i\mathbf{p}\mathbf{r}} P_\mu(\mathbf{r}) = \\ \frac{1}{V_N} \int d\mathbf{r} e^{-i\mathbf{p}\mathbf{r}} P_\mu(\mathbf{r}) - i\mathbf{p} \frac{1}{V_N} \int d\mathbf{r}\mathbf{r} P_\mu(\mathbf{r}) + ... \end{aligned} \tag{3.16}$$

and:

$$\tilde{P}_\mu(0) = \frac{1}{V_N}\int d\mathbf{r} P_\mu(\mathbf{r}) = \frac{1}{V_N}\delta_{l_\mu,0}\int dr r^2 P_\mu(r) = \frac{1}{V_N}\delta_{l_\mu,0}Q_\mu \tag{3.17}$$

where we take into account that the auxiliary functions $P_\mu(\mathbf{r})$ have a radial part and an angular part: $P_\mu(\mathbf{r}) = P_\mu(r)Y_{l_\mu m_\mu}$. Combining eq. 3.15 with eq. 3.17 yields:

$$\sum_\mu M^\mu_{a\mathbf{k}\sigma,i\mathbf{k}'\sigma'} V_N \tilde{P}_\mu(0) = \sum_\mu M^\mu_{a\mathbf{k}\sigma,i\mathbf{k}'\sigma'}\delta_{l_\mu,0}Q_\mu = \delta_{a,i}\delta_{\sigma\sigma'} \tag{3.18}$$

In second-order correction of MBPT, the two products of wave functions are expanded by P_μ and $P_{\mu'}$ respectively, and at least one of them will be a product of an occupied and an unoccupied function, as demonstrated in equation 2.81. Therefore, the singular part of equation 3.12, resulted from the auxiliary basis functions for $l = l' = 0$ will cancel. The singular part will have a singularity proportional to $1/\mathbf{p}$, which will lead to an integrable singularity proportional to $1/|\mathbf{p}|^2$ in the case of second-order, where we have products of Coulomb matrix elements.

In the Ewald method, the Coulomb matrix is only partially calculated in the reciprocal space (see section 2.7.4), thus only this part will be singular.

3.1.3 Generalized Gygi-Baldereschi method

In this section, we develop a generalization of Gygi-Baldereschi method that includes other contributions to the Coulomb matrix singularity besides the ones proportional to $1/p^2$. The method should improve the convergence of HF further. Moreover, its terms are the only ones relevant for the second-order MBPT singularity.

The Coulomb matrix element in the auxiliary basis from equation 2.128 is:

$$V^{r\mathbf{q}'\sigma',s\mathbf{q}\sigma}_{p\mathbf{k}\sigma,q\mathbf{k}'\sigma'} = \sum_{\mu\mu'} M^\mu_{p\mathbf{k}\sigma,s\mathbf{q}\sigma} M^{\mu'}_{q\mathbf{k}'\sigma',r\mathbf{q}'\sigma'} V^{\mathbf{p}}_{\mu,\mu'} \tag{3.19}$$

where we remind here that $\mathbf{p}$ is the momentum transferred by the interaction $\mathbf{p} = \mathbf{q} - \mathbf{k}$ and it is contained by the momentum conservation $\mathbf{q} - \mathbf{k} = -\mathbf{q}' + \mathbf{k}' + \mathbf{G}$. The analytical form of the long-range singular part of $V^{\mathbf{p}}_{\mu,\mu'}$ is given in equation

2.151. From equation 2.151 we separate the terms that depend on $\mathbf{p}$:

$$F_{lm,l'm'}(\mathbf{p}) = e^{\mathbf{ipD}_{\mu,\mu'}} \sum_{\mathbf{G}} e^{-(|\mathbf{G}-\mathbf{p}|)^2/\gamma^2} Y_{lm}(\Omega_{\mathbf{G}-\mathbf{p}}) Y^*_{l'm'}(\Omega_{\mathbf{G}-\mathbf{p}}) \frac{4\pi|\mathbf{G}-\mathbf{p}|^{l+l'}}{|\mathbf{G}-\mathbf{p}|^2}. \tag{3.20}$$

Expanding the exponential:

$$\begin{aligned} e^{\mathbf{ipD}_{\mu,\mu'}} =& (2\pi)^{\frac{3}{2}} \sum_{l,m} \mathrm{i}^l \sqrt{\frac{2}{\pi}} j_l(pD_{\mu,\mu'}) Y_{lm}(\hat{p}) Y^*_{lm}(\hat{D}_{\mu,\mu'}) = \\ & 1 + \frac{4\pi\mathrm{i}}{3} pD_{\mu,\mu'} \sum_{m=-1}^{1} Y_{1m}(\widehat{p}) Y^*_{1m}(\widehat{D}_{\mu,\mu'}) - \\ & \left(\frac{1}{30} + \frac{1}{15} \sum_{m=-2}^{2} Y_{2m}(\widehat{p}) Y^*_{2m}(\widehat{D}_{\mu,\mu'}) \right) (pD_{\mu,\mu'})^2 + \mathcal{O}(p^3) \end{aligned} \tag{3.21}$$

where $j_l(pr)$ are the spherical Bessel functions:

$$\begin{aligned} j_l(pr) &= \sum_{n=0} a_n^{(l)} (pr)^{2n+l} \\ \text{with } a_{n+1}^{(l)} = -a_n^{(l)} \frac{1}{3(n+1)(2n+2l+3)} &\text{ and } a_0^{(l)} = \frac{1}{(2l+1)!!} \end{aligned} \tag{3.22}$$

and we obtain[1]:

$$\begin{aligned} F_{lm,l'm'}(\mathbf{p}) = \sum_{\mathbf{G}} & e^{-(|\mathbf{G}-\mathbf{p}|)^2/\gamma^2} Y_{lm}(\Omega_{\mathbf{G}-\mathbf{p}}) Y^*_{l'm'}(\Omega_{\mathbf{G}-\mathbf{p}}) \frac{4\pi|\mathbf{G}-\mathbf{p}|^{l+l'}}{|\mathbf{G}-\mathbf{p}|^2} \\ & \left[1 + \left(\frac{4\pi\mathrm{i}}{3} \sum_{m=-1}^{1} Y_{1m}(\widehat{p}) Y^*_{1m}(\widehat{D}_{\mu,\mu'}) \right) pD_{\mu,\mu'} - \right. \\ & \left. \left(\frac{1}{30} + \frac{1}{15} \sum_{m=-2}^{2} Y_{2m}(\widehat{p}) Y^*_{2m}(\widehat{D}_{\mu,\mu'}) \right) (pD_{\mu,\mu'})^2 + \mathcal{O}(p^3) \right] \end{aligned} \tag{3.23}$$

Following the Gygi-Baldereschi method, we introduce a treatment to the singularity that considers that the Coulomb matrix elements dependence on $\mathbf{p}$ has the

[1] In principle, we can also expand the factor $e^{-(|\mathbf{G}-\mathbf{p}|)^2/\gamma^2}$ (coming from Ewald summation) for $\mathbf{G} = \mathbf{0}$ around $\mathbf{p} = \mathbf{0}$. However, in the original Gygi-Baldereschi method, a Gaussian factor must be introduced artificially, so that the integral in equation 3.4 gives a finite result. In the case of Ewald summation, keeping the Gaussian factor $e^{-(|\mathbf{G}-\mathbf{p}|)^2/\gamma^2}$ ensures that the integral is finite. Thus, the already existing Gaussian from the Ewald summation can serve this purpose.

above form, and not the form of equation 3.3. This way, the dependence of the function $f(\mathbf{p}, \mathbf{G})$ on $\mathbf{p}$ is partially treated and, most importantly, it is now possible to treat second-order MBPT in which, as explained in section 3.1.2, the terms proportional to $|\mathbf{p}|^{-2}$ are irrelevant, since they cancel due to the orthogonality.

Generalized Gygi-Baldereschi method for HF

We begin with the application of the generalized Gygi-Baldereschi method to HF. The exchange energy of the HF approximation is:

$$E_x^{HF} = -\frac{1}{2}\sum_{i,j}^{occ}\sum_{\sigma}\frac{1}{N_{\mathbf{k}}}\sum_{\mathbf{k}}\frac{1}{N_{\mathbf{q}}}\sum_{\mathbf{q}}\sum_{\mu\mu'} M^{\mu}_{j\mathbf{k},i\mathbf{q}} M^{\mu'}_{i\mathbf{q},j\mathbf{k}} V^{\mathbf{p}}_{\mu,\mu'} \tag{3.24}$$

where $\mathbf{p} = \mathbf{q} - \mathbf{k}$ is the momentum transferred from the interaction. We can rewrite the summation: $\sum_{\mathbf{qk}} \rightarrow \sum_{\mathbf{qp}}$, as was done also in section 3.1.1.

As demonstrated, we benefit from using Ewald summation to calculate the Coulomb matrix in two parts, each of which converges faster in real or reciprocal space. One part comes from a short-ranged interaction that is non-zero only when the orbitals overlap. The second part is the long-range interaction, described through the interaction of localized Gaussian orbitals with multipole moments equal to the multipole moments of the orbitals they are compensating. The matrix element of the Coulomb potential in equation 3.19 can be written as a sum of the short-range interaction and the long-range interaction:

$$\begin{aligned}\sum_{\mu\mu'} M^{\mu}_{m\mathbf{k},n\mathbf{q}} M^{\mu'}_{n\mathbf{q},m\mathbf{k}} V^{\mathbf{p}}_{\mu,\mu'} = \sum_{\mu\mu'} M^{\mu}_{m\mathbf{k},n\mathbf{q}} M^{\mu'}_{n\mathbf{q},m\mathbf{k}} \sum_{R} e^{i\mathbf{p}\mathbf{R}} V^{sr}_{\mu,\mu'}(\mathbf{R}) + \\ \sum_{\mu\mu'} M^{\mu}_{m\mathbf{k},n\mathbf{q}} M^{\mu'}_{n\mathbf{q},m\mathbf{k}} V^{\mathbf{p}(Gauss)}_{\mu,\mu'}\end{aligned} \tag{3.25}$$

The part that is singular at the point $\mathbf{p} = 0$ is the second term on the right-hand side of the above expression. The singular point needs to be excluded when calculating the summation over $\mathbf{p}$ in the first Brillouin zone, as mentioned in section 3.1.1. Instead, following the Gygi-Baldereschi method analyzed in section 3.1.1, a correction can be added to compensate the exclusion of the singular term at the point $\mathbf{p} = 0$. The correction replaces $V^{\mathbf{p}(Gauss)}_{\mu,\mu'}$ in equation 3.25 for $\mathbf{p} = 0$ and will have the expression:

$$C^{\mu,\mu'} = \frac{(2\pi)^3}{V_N}\mathrm{i}^{-l+l'}Q_\mu Q_{\mu'}\tilde{A}_l\tilde{A}_{l'}\times \left[-\sum_{\mathbf{p}}{}' F^{lm,l'm'}(\mathbf{p}) + \frac{V_0}{(2\pi)^3}\int d\mathbf{p}F^{lm,l'm'}(\mathbf{p})\right] \tag{3.26}$$

where:

$$F^{lm,l'm'}(\mathbf{p}) = |\mathbf{p}|^{l+l'}e^{-(\mathbf{p}|)^2/\gamma^2}Y_{lm}(\Omega_\mathbf{p})Y^*_{l'm'}(\Omega_\mathbf{p})\frac{4\pi}{|\mathbf{p}|^2} \left[1 + \left(\frac{4\pi\mathrm{i}}{3}\sum_{M=-1}^{1} Y_{1M}(\widehat{p})Y^*_{1M}(\widehat{D}_{\mu,\mu'})\right) pD_{\mu,\mu'} - \left(\frac{1}{30} + \frac{1}{15}\sum_{M=-2}^{2} Y_{2M}(\widehat{p})Y^*_{2M}(\widehat{D}_{\mu,\mu'})\right)(pD_{\mu,\mu'})^2 + \mathcal{O}(p^3)\right] \tag{3.27}$$

As mentioned, the l, m and l', m' indices are the indices of the angular part of the auxiliary basis with indices μ and μ', respectively. The summations in equation 3.24 in the thermodynamic limit will be integrals and the angular part of the integral involves the integration of the product of three spherical harmonics. This integral determines the selection rules for the involved orbital momenta via the relation [92]:

$$\int d\widehat{p}Y_{lm}(\Omega_\mathbf{p})Y^*_{l'm'}(\Omega_\mathbf{p})Y_{LM}(\widehat{p}) = \sqrt{\frac{(2l+2)(2l'+2)(2L+2)}{4\pi}}\begin{pmatrix} l & l' & L \\ m & m' & M\end{pmatrix}\begin{pmatrix} l & l' & L \\ 0 & 0 & 0\end{pmatrix} \tag{3.28}$$

The last factor is non-zero for $|l - l'| \leq L \leq |l + l'|$ and $l + l' + L = 2\kappa$, where κ is an integer. For the combinations of l, l', L in which the above integral is zero, the summation of $F^{lm,l'm'}(\mathbf{p})$ over $\mathbf{p}$ converges very fast to zero, so we can keep only the terms with non-zero integrals. For $l + l' = 0$ the integral is:

$$\int d\mathbf{p}F^{(00,00)}(\mathbf{p}) = \int dpp^2e^{-p^2/\gamma^2}\frac{4\pi}{p^2}\left[1 - \frac{1}{30}(pD_{\mu,\mu'})^2 + \mathcal{O}(p^3)\right] \tag{3.29}$$

and the corresponding contribution to the correction is:

$$-\sum_{\mathbf{p}}{}' e^{-p^2/\gamma^2}\frac{4\pi}{p^2}\left[1 - \frac{1}{30}(pD_{\mu,\mu'})^2 + \mathcal{O}(p^3)\right] + \frac{V_0}{(2\pi)^3}\int d\mathbf{p}e^{-p^2/\gamma^2}\frac{4\pi}{p^2}\left[1 - \frac{1}{30}(pD_{\mu,\mu'})^2 + \mathcal{O}(p^3)\right] \tag{3.30}$$

This contribution coincides with Gygi-Baldereschi correction.

As a first approximation, only the terms of the function $F^{lm,l'm'}$ for each pair of $lm, l'm'$ that give terms with p in powers of p^{-2} and up to the power p^0 are kept. In section 3.1.1 we saw that the contribution to the integral close to $p = 0$ will decrease as the power of p increases. For $l = 1, l' = 0$:

$$F^{1m,00}(\mathbf{p}) = \\ p^2 D_{\mu,\mu'} e^{-p^2/\gamma^2} Y_{1m}(\Omega_{\mathbf{p}}) Y^*_{00}(\Omega_{\mathbf{p}}) \frac{4\pi}{p^2} \left(\frac{4\pi \mathrm{i}}{3} \sum_{M=-1}^{1} Y_{1M}(\widehat{p}) Y^*_{1M}(\widehat{D}_{\mu,\mu'}) \right) + \mathcal{O}(p^4) \tag{3.31}$$

where $m = -1, 0, 1$. For $l = 0, l' = 1$, the correction will be the complex conjugate of the $l = 1, l' = 0$ correction.

For $l = 1, l' = 1$:

$$F^{1m,1m'}(\mathbf{p}) = p^2 e^{-p^2/\gamma^2} Y_{1m}(\Omega_{\mathbf{p}}) Y^*_{1m'}(\Omega_{\mathbf{p}}) \frac{4\pi}{p^2} + \mathcal{O}(p^4) \tag{3.32}$$

The remaining temrs involve higher-order corrections.

Generalized Gygi-Baldereschi method for second-order MBPT

As seen in equations 2.53 for total energy and 2.81 for the single-particle excitations, the subject to be corrected is proportional to the product of two Coulomb matrix elements, given in equation 2.128. Even though the integrand is the product of two Coulomb matrix elements, the correction cannot be written as a product of two corrections $C^{\mu_1,\mu'_1} C^{\mu_2,\mu'_2}$. Thus, it depends on four indices $\mu_1, \mu'_1, \mu_2, \mu'_2$. Equation 2.128 shows that if we set $\mathbf{q} - \mathbf{k} = \mathbf{q}' - \mathbf{k}' = 0$, which means $\mathbf{p} = 0$ for the coefficients, it results in integrations over $\mathbf{p}$ of the expression $V^{\mathbf{p}}_{\mu_1,\mu'_1} V^{\mathbf{p}}_{\mu_2,\mu'_2}$ in the thermodynamic limit. The correction will then be expressed as:

$$\begin{aligned} C^{\mu_1,\mu'_1\mu_2,\mu'_2} = & \left[\frac{(2\pi)^3}{V_N} \right]^2 \mathrm{i}^{-l_1+l'_1} \mathrm{i}^{-l_2+l'_2} Q_{\mu_1} Q_{\mu'_1} Q_{\mu_2} Q_{\mu'_2} \tilde{A}_{l_1} \tilde{A}_{l'_1} \tilde{A}_{l_2} \tilde{A}_{l'_2} \times \\ & \left[- {\sum_{\mathbf{p}}}' F^{l_1 m_1, l_1' m_1'}(\mathbf{p}) F^{l_2 m_2, l_2' m_2'}(\mathbf{p}) + \right. \\ & \left. \frac{V_0}{(2\pi)^3} \int d\mathbf{p} F^{l_1 m_1, l_1' m_1'}(\mathbf{p}) F^{l_2 m_2, l_2' m_2'}(\mathbf{p}) \right] \end{aligned} \tag{3.33}$$

where $F^{l_1 m_1, l_1' m_1'}(\mathbf{p})$ and $F^{l_2 m_2, l_2' m_2'}(\mathbf{p})$ are the same as in equation 3.27. From the form of equation 3.27 we conclude that for $l_1 + l_1' + l_2 + l_2' \leq 2$, the product $F^{l_1 m_1, l_1' m_1'}(\mathbf{p}) F^{l_2 m_2, l_2' m_2'}(\mathbf{p})$ is not integrable. However, as it was shown in section 3.1.2, from equation 3.18 the terms cancel if one of the l is zero. Therefore, we consider only $F^{l_1 m_1, l_1' m_1'}(\mathbf{p})$ with $l_1 + l_1' \geq 1$ and $F^{l_2 m_2, l_2' m_2'}(\mathbf{p})$ with $l_2 + l_2' \geq 1$.

As in the case of HF, we can to consider only terms that give non-zero contribution after the integration over $\mathbf{p}$ in the correction $C^{\mu_1, \mu_1' \mu_2, \mu_2'}$. Because the correction contains the products of four spherical harmonics, we can simplify the long-range interaction expression using the identity:

$$Y^*_{lm}(\mathbf{p}) Y_{l'm'}(\mathbf{p}) = \sum_{LM} Y^*_{LM}(\mathbf{p}) \sqrt{\frac{(2l+2)(2l'+2)(2L+2)}{4\pi}} \begin{pmatrix} l & l' & L \\ -m & m' & M \end{pmatrix} \begin{pmatrix} l & l' & L \\ 0 & 0 & 0 \end{pmatrix} \tag{3.34}$$

For the $l + l' = 1$ case, the above expression will be non-zero only for $L = 1$ and $m - m' = M$. The correction function takes the form:

$$C_{l_1 m_1, l_1' m_1', l_2 m_2, l_2' m_2'} = \delta_{l_1 + l_1', 1} \delta_{l_2 + l_2', 1} e^{-2p^2/\gamma^2} \frac{4\pi}{p^2} Y_{1, m_1 - m_1'}(\mathbf{p}) Y^*_{1, m_2 - m_2'}(\mathbf{p}) + \mathcal{O}(1/p) \tag{3.35}$$

Even though powers higher than p^{-2} can be important, this term corrects the very slow k-points convergence that behaves as $\sim 1/(N_{\mathbf{k}})^{1/3}$. The correction to $(V^p_{\mu_1, \mu_1'})^* V^p_{\mu_2, \mu_2'}$ is proportional to:

$$\begin{aligned} &-\delta_{l_1 + l_1', 1} \delta_{l_2 + l_2', 1} {\sum_{\mathbf{p}}}' e^{-2p^2/\gamma^2} \frac{4\pi}{p^2} Y_{1, m_1 - m_1'}(\mathbf{p}) Y^*_{1, m_2 - m_2'}(\mathbf{p}) \\ &+\delta_{l_1 + l_1', 1} \delta_{l_2 + l_2', 1} \frac{V_0}{(2\pi)^3} \int d\mathbf{p} e^{-2p^2/\gamma^2} \frac{4\pi}{p^2} Y_{1, m_1 - m_1'}(\mathbf{p}) Y^*_{1, m_2 - m_2'}(\mathbf{p}) \end{aligned} \tag{3.36}$$

The integral of the above expression is:

$$\int d\mathbf{p} e^{-2p^2/\gamma^2} \frac{4\pi}{p^2} Y_{1, m_1 - m_1'}(\mathbf{p}) Y^*_{1, m_2 - m_2'}(\mathbf{p}) = \delta_{m_1 - m_1', m_2 - m_2'} 4\pi \frac{\gamma}{2} \sqrt{\frac{2}{\pi}} \tag{3.37}$$

In the exchange term $V^p_{\mu_1, \mu_1'} V^{p'}_{\mu_2, \mu_2'}$ is a product of Coulomb matrix elements with different momentum, in contrast to the direct term that has the product: $V^p_{\mu_1, \mu_1'} V^p_{\mu_2, \mu_2'}$

and thus Coulomb matrix elements with the same momentum transfer. The power of p or p' will then be the power of $V^{p}_{\mu_1,\mu'_1}$ or $V^{p'}_{\mu_2,\mu'_2}$ separately, and neglected for now, since the highest power will be lower than the highest power in the direct term. The angular part converges very fast to unity, so the correction can be written as:

$$F^{\mu_1\mu'_1\mu_2\mu'_2} = Q_{\mu_1}Q_{\mu'_1}Q_{\mu_2}Q_{\mu'_2}\left(\frac{(2\pi)^3}{V_N}\right)^2 \mathrm{i}^{-l_1+l'_1}\mathrm{i}^{-l_2+l'_2}\times \\ \tilde{A}_{l_1}\tilde{A}_{l'_1}\tilde{A}_{l_2}\tilde{A}_{l'_2}\delta_{m_1-m'_1,m_2-m'_2}\delta_{l_1+l'_1,1}\delta_{l_2+l'_2,1}\frac{V_0}{(2\pi)^3}F(N_0) \tag{3.38}$$

where $F(N_0)$ is:

$$F(N_0) = 4\pi\frac{\gamma}{2}\sqrt{\frac{2}{\pi}} - \frac{(2\pi)^3}{N_0\Omega}{\sum_{\mathbf{p}}}' e^{-2p^2/\gamma^2}\frac{4\pi}{p^2}\frac{1}{4\pi} \tag{3.39}$$

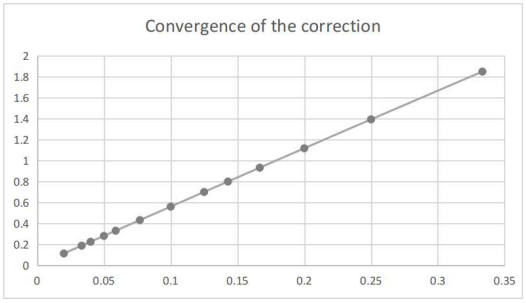

Figure 3.5: $F(N_0)$ from eq. 3.39 as a function of the number of k-points per direction $N = (N_0)^{1/3}$ for $\gamma = 1$ and a cubic lattice with a lattice constant $a = 5.0$

Applying the Gygi-Baldereschi method or its generalization as proposed here is very useful for electronic-structure methods that involve integrals of functions proportional to the first power of the potential matrix elements. This is not the case when the integrand contains higher powers of the Coulomb matrix elements, as in the case of second-order perturbation theory, where the integrand is proportional to the product of the matrix elements. In practice, we need to calculate an object with four indices, $\mu_1, \mu'_1\mu_2, \mu'_2$. This is not as computationally efficient as is in the case of HF.

3.1.4 Integration error and extrapolation

In principle, any integrand, including singular ones, can be expressed as a Laurent series that includes negative powers of the integrand variable **p**. If the series includes powers smaller than -2 the singularity is not integrable for a three-dimensional integration. This is not expected to happen, since MBPT converges to a finite number for all orders, as shown by Jun-Qiang Sun, and Rodney J. Bartlett [72]. The proof provided in their work relies on a real-space lattice summation. In this thesis we proved the finite convergence also when using the Ewald summation in the sp-MP2 and MP2 corrections (see section 3.1.2). This means that Laurent series for the integrand contains a minimum power of -2 around the singularity.

Let us consider the integration of a singular function $f(\mathbf{p}) = f(p, \theta, \phi)$. In general, we can write the function f as a power series of p^n as $\sum_n f_n(\theta, \phi)p^n$. For a singular function, n can be negative. If $n \leq -2$ the singularity is integrable. Then we can write:

$$f(\mathbf{p}) = \frac{f_{-2}((\theta, \phi))}{p^2} + \frac{f_{-1}(\theta, \phi)}{p^1} + \frac{f_0(\theta, \phi)}{p^0} + f_1(\theta, \phi)p + ... \tag{3.40}$$

The integral of tthe function f inside a volume $V \int_V d\mathbf{p} f(\mathbf{p})$ can be problematic if it is not done analytically. Since the value for $\mathbf{p} = 0$ is infinite, we must skip zero in the case of a finite grid summation. The integral can be calculated as $\frac{1}{N^3} \sum_{\mathbf{p}\neq 0} f(\mathbf{p})$ where N are the number of points in the grid per direction, so the total points are N^3. In the limit of an infinitely dense grid, this quantity approaches the calculated analytically integral.

The difference of the summation from the integration shows how close to convergence the summation is:

$$G(N) = \int_V dp f(\mathbf{p}) - \frac{V}{N^3} \sum_{\mathbf{p}\neq 0} f(\mathbf{p}) \tag{3.41}$$

The integral of $f(\mathbf{p})$ can be calculated for each term of the equation 3.40 separately, so we can find the contribution of each of them. We define:

$$G_n(N) = \int d\mathbf{p} f_n((\theta, \phi))p^n - \frac{V}{N^3} \sum_{\mathbf{p}}{}' f_n((\theta, \phi))p^n \tag{3.42}$$

The equation 3.39 found in the generalized Gygi-Baldereschi method for the highest power correction of sp-MP2 singularity, proposed in this thesis, is similar to the contribution for $n = -2$. The difference is the Gaussian factor, which ensures the convergence of the integral when the integration is done in the whole space. Thus, the function defined in equation 3.39 is not only proportional to the correction, but will also show the convergence behavior as a function of N. To model the convergence behavior in any power, we define the function:

$$F_n(N) = \int d\mathbf{p} e^{-a|\mathbf{p}|^2} |\mathbf{p}|^n - \frac{(2\pi)^3}{N^3\Omega} \sum_{\mathbf{p}}{}' e^{-a|\mathbf{p}|^2} |\mathbf{p}|^n \tag{3.43}$$

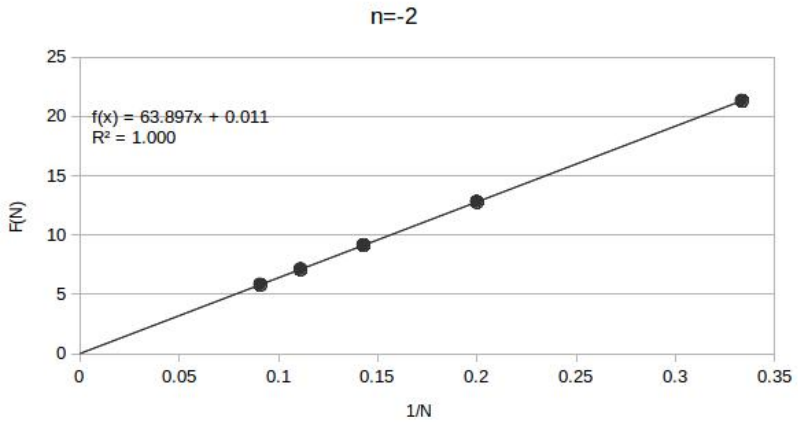

Figure 3.6: The numerical integration error $F_n(N)$ from equation 3.43 for $n = -2$ as a function of $1/N$. The dependence is very close to linear for the considered range of $1/N$.

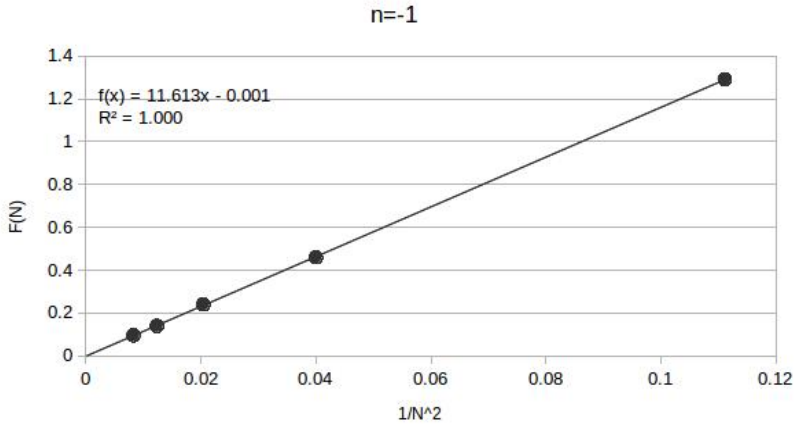

Figure 3.7: The function $F_n(N)$ from equation 3.43 for $n = -1$ as a function of $1/N^2$. The dependence is very close to linear for the considered range of $1/N^2$.

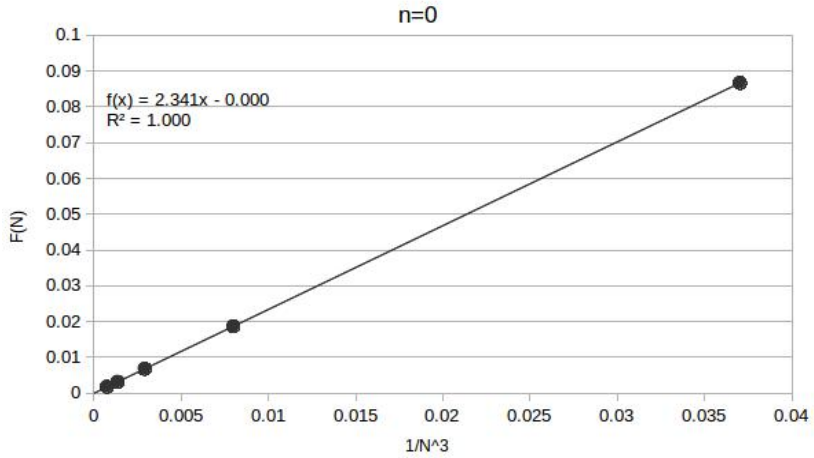

Figure 3.8: The function $F_n(N)$ from equation 3.43 for $n = 0$ as a function of $1/N^3$. The dependence is very close to linear for the considered range of $1/N^2$

From the plots 3.6-3.8 we see that the convergence behavior for $N \to \infty$ is dominated by the minimum power of the inttegrand's expansion. From this schematic analysis, we conclude that the convergence of sp-MP2 band gap, that has a linear behavior when plotted as a function of $1/N$ (as demonstrated for MgO in figure 3.12) is dominated by a $1/p^2$ singularity, in agreement with the analysis done in the section 3.1.2. If the dominant singularity was $1/p$, the convergence

would be linear when plotted with $1/N^2$. If the integrand did not have a singularity, i.e., the power series would start from $n = 0$, and the integration error would behave as $1/N^3$.

It becomes clear that by knowing the behavior of the integration error around the singularity, we can extrapolate properly to the dense grid limit. Moreover, if we know the factors f_n of the singular terms, as, for example, f_{-2} for the singular term p^-2 in equation 3.40, we can analytically calculate that term. This is the core idea behind the generalized Gygi-Baldereschi method.

There are two ways to determine f_{-2}, f_{-1}, and f_0. One is analytically as described in section 3.1.3. Its advantage is that converged results can be obtained with a relatively sparse integration grid. Its drawback is that the **p**-dependence of the coefficients M^μ, present in the integrand of HF, MP2 and sp-MP2 (see equations 3.24, 3.46, and 3.47), is not known. Thus, we can make an expansion as in equation 3.40, but now the factors f_n have a dependency on p, so they can be written as $f_n(p, \theta, \phi)$, and not as $f_n(\theta, \phi)$. This dependence should be smooth and with powers higher or equal to $n = 0$, since the singularity arises from the part that is known analytically. Furthermore, as discussed in section 3.1.3, the construction of the factors f_n is not practical for MP2 and sp-MP2 since they require the calculation of four-index objects.

The alternative way is to fit the numerical integration error as a function of the number of grid points and extrapolate the fitting function to the infinitely dense grid. The factors f_n are determined from the fitting. This is the method adopted in this thesis.

3.2 Bandgaps with second-order MBPT

Having now the tools to calculate the Coulomb operator matrix elements, we focus on second-order correction, with HF wavefunctions as our starting point. This method is advantageous, because HF already includes a part of the interaction, namely, the one described by single excitations as shown in the section 2.3.2. To approach the dense k-grid limit, we use the results of our analysis of the singularity performed in the the section 3.1.

3.2.1 Bandgaps with single-particle MP2

To obtain MP2 single-particle (sp-MP2) energies of a periodic solid, one has to calculate only the first term of eq. 2.81 taking into account the crystal momentum quantum numbers:

$$\begin{aligned}
&\epsilon^{MP2}_{p\mathbf{k}\sigma} = \epsilon^{HF}_{p\mathbf{k}\sigma} + \\
&\frac{1}{2}\sum_{\sigma'}\sum_{i,a,b}\frac{1}{N_{\mathbf{k}'}N_{\mathbf{q}'}N_{\mathbf{q}}}\sum_{\mathbf{k}'\mathbf{q}\mathbf{q}'}\frac{|<\psi_{p\mathbf{k}\sigma},\psi_{i\mathbf{k}'\sigma'}||\psi_{a\mathbf{q}\sigma},\psi_{b\mathbf{q}'\sigma'}>|^2}{\epsilon^{HF}_{p\mathbf{k}\sigma}+\epsilon^{HF}_{i\mathbf{k}'\sigma'}-\epsilon^{HF}_{a\mathbf{q}\sigma}-\epsilon^{HF}_{b\mathbf{q}'\sigma'}} + \\
&\frac{1}{2}\sum_{\sigma'}\sum_{i,j,a}\frac{1}{N_{\mathbf{k}'}N_{\mathbf{q}'}N_{\mathbf{q}}}\sum_{\mathbf{k}'\mathbf{q}\mathbf{q}'}\frac{|<\psi_{p\mathbf{k}\sigma},\psi_{a\mathbf{k}'\sigma'}||\psi_{i\mathbf{q}\sigma},\psi_{j\mathbf{q}'\sigma'}>|^2}{\epsilon^{HF}_{p\mathbf{k}\sigma}+\epsilon^{HF}_{a\mathbf{k}'\sigma'}-\epsilon^{HF}_{i\mathbf{q}\sigma}-\epsilon^{HF}_{i\mathbf{q}'\sigma'}}
\end{aligned} \tag{3.44}$$

where $N_{\mathbf{k}'}$, $N_{\mathbf{q}}$ and $N_{\mathbf{q}'}$ denote the total number of points of the grid for the summation over $\mathbf{k}'$, $\mathbf{q}$, and $\mathbf{q}'$ respectively. This expression is very similar to the total-energy MP2 in periodic boundary conditions, where one has to calculate:

$$\begin{aligned}
&E^{MP2} = E^{HF} + \\
&\frac{1}{4}\sum_{\sigma,\sigma'}\sum_{i,j,a,b}\frac{1}{N_{\mathbf{k}}N_{\mathbf{k}'}N_{\mathbf{q}'}N_{\mathbf{q}}}\sum_{\mathbf{k},\mathbf{k}'\mathbf{q}\mathbf{q}'}\frac{|<\psi_{i\mathbf{k}\sigma},\psi_{j\mathbf{k}'\sigma'}||\psi_{a\mathbf{q}\sigma},\psi_{b\mathbf{q}'\sigma'}>|^2}{\epsilon^{HF}_{i\mathbf{k}\sigma}+\epsilon^{HF}_{j\mathbf{k}'\sigma'}-\epsilon^{HF}_{a\mathbf{q}\sigma}-\epsilon^{HF}_{b\mathbf{q}'\sigma'}}
\end{aligned} \tag{3.45}$$

In the case of sp-MP2 the summation runs over three states instead of four in total-energy MP2.

In the auxiliary basis the Coulomb matrix elements take the form given in eq. 2.128. Then, the total-energy MP2 correction to HF energy can be written as:

$$\begin{aligned}
&E^{MP(2)} = \\
&\frac{1}{4}\sum_{\sigma,\sigma'}\sum_{i,j,a,b}\frac{1}{N_{\mathbf{k}},N_{\mathbf{k}'}N_{\mathbf{q}'}N_{\mathbf{q}}}\sum_{\mathbf{k},\mathbf{k}'\mathbf{q}\mathbf{q}'}\frac{1}{\epsilon^{a\mathbf{q}\sigma,b\mathbf{q}'\sigma'}_{i\mathbf{k}\sigma,j\mathbf{k}'\sigma'}}\Bigg[\Big(\sum_{\mu\mu'}M^{\mu}_{i\mathbf{k}\sigma,a\mathbf{q}\sigma}M^{\mu'}_{j\mathbf{k}'\sigma',b\mathbf{q}'\sigma'}V^{\mathbf{p}}_{\mu,\mu'}\Big)^2 + \\
&\delta_{\sigma,\sigma'}\Big(\sum_{\mu\mu'}M^{\mu}_{i\mathbf{k}\sigma,a\mathbf{q}\sigma}M^{\mu'}_{j\mathbf{k}'\sigma',b\mathbf{q}'\sigma'}V^{\mathbf{p}}_{\mu,\mu'}\Big)\Big(\sum_{\mu\mu'}M^{\mu}_{i\mathbf{k}\sigma,b\mathbf{q}'\sigma'}M^{\mu'}_{j\mathbf{k}'\sigma',a\mathbf{q}\sigma}V^{\mathbf{p}'}_{\mu,\mu'}\Big)\Bigg]
\end{aligned} \tag{3.46}$$

The MP2 single-particle energy corrections to HF energies are expressed as fol-

lows:

$$\epsilon^{MP(2)}_{p\mathbf{k}\sigma} = \frac{1}{2}\sum_{\sigma'}\sum_{i,a,b}\frac{1}{N_{\mathbf{k}'}N_{\mathbf{q}'}N_{\mathbf{q}}}\sum_{\mathbf{k}'\mathbf{q}\mathbf{q}'}\frac{1}{\epsilon^{a\mathbf{q}\sigma,b\mathbf{q}'\sigma'}_{p\mathbf{k}\sigma,i\mathbf{k}'\sigma'}}\Bigg[\Big(\sum_{\mu\mu'}M^{\mu}_{p\mathbf{k}\sigma,a\mathbf{q}\sigma}M^{\mu'}_{i\mathbf{k}'\sigma',b\mathbf{q}'\sigma'}V^{\mathbf{p}}_{\mu,\mu'}\Big)^2 + \delta_{\sigma,\sigma}\Big(\sum_{\mu\mu'}M^{\mu}_{p\mathbf{k}\sigma,a\mathbf{q}\sigma}M^{\mu'}_{i\mathbf{k}'\sigma',b\mathbf{q}'\sigma'}V^{\mathbf{p}}_{\mu,\mu'}\Big)\Big(\sum_{\mu\mu'}M^{\mu}_{p\mathbf{k}\sigma,b\mathbf{q}'\sigma'}M^{\mu'}_{i\mathbf{k}'\sigma',a\mathbf{q}\sigma}V^{\mathbf{p}'}_{\mu,\mu'}\Big)\Bigg] + \frac{1}{2}\sum_{\sigma'}\sum_{i,j,a}\frac{1}{N_{\mathbf{k}'}N_{\mathbf{q}'}N_{\mathbf{q}}}\sum_{\mathbf{k}'\mathbf{q}\mathbf{q}'}\frac{1}{\epsilon^{i\mathbf{q}\sigma,j\mathbf{q}'\sigma'}_{p\mathbf{k}\sigma,a\mathbf{k}'\sigma'}}\Bigg[\Big(\sum_{\mu\mu'}M^{\mu}_{p\mathbf{k}\sigma,i\mathbf{q}\sigma}M^{\mu'}_{a\mathbf{k}'\sigma',j\mathbf{q}'\sigma'}V^{\mathbf{p}}_{\mu,\mu'}\Big)^2 + \delta_{\sigma,\sigma}\Big(\sum_{\mu\mu'}M^{\mu}_{p\mathbf{k}\sigma,i\mathbf{q}\sigma}M^{\mu'}_{a\mathbf{k}'\sigma',j\mathbf{q}'\sigma'}V^{\mathbf{p}}_{\mu,\mu'}\Big)\Big(\sum_{\mu\mu'}M^{\mu}_{p\mathbf{k}\sigma,j\mathbf{q}'\sigma'}M^{\mu'}_{a\mathbf{k}'\sigma',i\mathbf{q}\sigma}V^{\mathbf{p}'}_{\mu,\mu'}\Big)\Bigg] \tag{3.47}$$

Taking into account the crystal momentum conservation as shown in eq. 2.126, $\mathbf{q}-\mathbf{k} = -\mathbf{q}'+\mathbf{k}'+\mathbf{G}$, we can rewrite the summation: $\sum_{\mathbf{k}'\mathbf{q}\mathbf{q}'} \rightarrow \sum_{\mathbf{q}'\mathbf{p}}$, where $\mathbf{p} = \mathbf{q}-\mathbf{k}$ is the momentum transferred by the Coulomb potential. We can now calculate the bandgaps for a test set of solids. Before we present and examine the results, we introduce the details of the implementation carried out in the framework of this thesis.

Implementation of sp-MP2 on the all-electron, full-potential electronic structure code package FHI-aims

We base our implementation of single-particle excitations MP2 (sp-MP2) on the preexisting total-energy MP2 implementation on the all-electron full-potential electronic structure code package FHI-aims electronic-structure package [35]. The MP2 and sp-MP2 implementation challenges emerge mostly from the size of the Coulomb matrix and the singularity, as described in section 3.1.1.

After demonstrating, in section 3.1.2, that the integral converges, we can employ the truncated Coulomb operator, since it must converge to the exact result in the limit of an infinitely dense reciprocal space grid. Applying the truncated Coulomb potential method does not require any special treatment and can be applied as in HF. The Coulomb operator is modified in the same way as in equation 3.9.

We conclude that in the case of second-order single-particle energies, the truncated Coulomb operator does not output a smooth convergence even after increasing the k-grid significantly, as can be seen in figure 3.9. A solution is to use the truncated Coulomb operator only for $\mathbf{p} = 0$. This approach is used for total-energy second-order MBPT [78] and we have also used to obtain our results for the second-order MBPT bandgaps presented in this thesis.

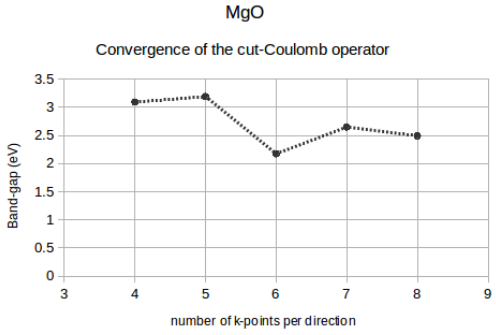

Figure 3.9: Convergence of the sp-MP2 bandgap using truncated Coulomb operator for all momentum transfer values $\mathbf{p}$. The system is MgO with PBE lattice constant (2.1055Å). This figure shows that the truncated Coulomb operator does not give a smooth convergence.

The parallelization of MP2 implementation is done in reciprocal space. From equation 3.46 together with the momentum conservation 2.126, the summation over the k-grid points can be separated to up to $N_{\mathbf{p}} \times N_{\mathbf{k}} \times N_{\mathbf{q}}$ steps[2]. The steps can then be distributed to the available tasks along with the relevant matrices (Coulomb matrix elements, HF eigenfunctions, and eigenvectors) for the calculation of each $\sum_{\mu\mu'} M^{\mu}_{i\mathbf{k}\sigma,a\mathbf{q}\sigma} M^{\mu'}_{j\mathbf{k}'\sigma',b\mathbf{q}'\sigma'} V^{\mathbf{p}}_{\mu,\mu'}$. In practice, it is convenient to create the objects:

$$\begin{aligned} L^{\upsilon}_{i\mathbf{k}\sigma,a\mathbf{q}\sigma} &= \sum_{\mu} M^{\mu}_{i\mathbf{k}\sigma,a\mathbf{q}\sigma} [V^{\mathbf{p}}_{\mu,\upsilon}]^{1/2} \\ R^{\upsilon'}_{j\mathbf{k}'\sigma',b\mathbf{q}'\sigma'} &= \sum_{\mu} [V^{\mathbf{p}}_{\mu,\upsilon}]^{1/2} M^{\mu}_{j\mathbf{k}'\sigma',b\mathbf{q}'\sigma'} \end{aligned} \tag{3.48}$$

[2]In principle the same grid is used for all summations.

Then each summand:

$$E_{sum}(\mathbf{k},\mathbf{q},\mathbf{p}) = \frac{1}{4}\sum_{\sigma,\sigma'}\sum_{i,j,a,b}\frac{1}{\epsilon^{a\mathbf{q}\sigma,b\mathbf{q}'\sigma'}_{i\mathbf{k}\sigma,j\mathbf{k}'\sigma'}}\Bigg[\Big(\sum_{\upsilon}L^{\upsilon}_{i\mathbf{k}\sigma,a\mathbf{q}\sigma}R^{\upsilon}_{j\mathbf{k}'\sigma',b\mathbf{q}'\sigma'}\Big)^2 + \delta_{\sigma,\sigma'}\Big(\sum_{\upsilon}L^{\upsilon}_{i\mathbf{k}\sigma,a\mathbf{q}\sigma}R^{\upsilon}_{j\mathbf{k}'\sigma',b\mathbf{q}'\sigma'}\Big)\Big(\sum_{\upsilon}L^{\upsilon}_{i\mathbf{k}\sigma,b\mathbf{q}'\sigma'}R^{\upsilon}_{j\mathbf{k}'\sigma',a\mathbf{q}\sigma}\Big)\Bigg] \tag{3.49}$$

is calculated. After the calculation of the summand, it is stored in a restart file and then the calculation continues until all steps are done. Next, the summands are added and the MP2 calculation is finished.

Proceeding to sp-MP2 calculation, it can be noticed in equation 3.47 that there is a summation over two instead of three k-point grids. Nonetheless, the index $\mathbf{k}$ still needs to run for the calculation of each $\epsilon^{MP(2)}_{p\mathbf{k}\sigma}$. This process is similar to MP2, but in every step the relevant summand of every $\epsilon^{MP(2)}_{p\mathbf{k}\sigma}$ is calculated. Thus, with the same number of loops as MP2, we can calculate all $\epsilon^{MP(2)}_{p\mathbf{k}\sigma}$ for the relevant k-grid, which can be used for the band structure calculation. In the case that only the bandgap is calculated, the summations over $\mathbf{k}$ and p are not needed, and the calculation is much faster.

Before advancing to the test-set calculations, we compare our periodic sp-MP2 implementation to the respective implementation for molecules on our code FHI-aims. For this purpose, we have considered a water molecule in a large supercell. We found that a supercell of the size 100Åis sufficient. In table 3.1, the only value that has a difference more than 10^{-4} is for the second state. The reason that this value is a result of the breakdown of the nondegenerate perturbation theory. This happens when the denominator of equation 3.47 is zero, so the increased difference between our implementation and the molecular implementation for the second state is due to numerical noise from the diverging denominator. This limitation of sp-MP2 is discussed analytically by Sun and Bartlett [28]. For this reason, the differences between molecular implementation and our implementation are less than $10^{-4}eV$, which is compatible with the accuracy of the calculation. The same finding is true for other molecular systems tested.

To validate of our sp-MP2 implementation, we compare our results with the results reported by Sun and Bartlett[39] for the alternating trans-polyacetylene chain. In their implementation, the lattice summation for the Coulomb potential calculation is done in real space, while FHI-aims uses the Ewald summation, as described

Water molecule ionization energies and electron affinities (eV)		
state	molecular implementation	our implementation
1	-545.1477	-545.1478
2	-43.8191	-43.8198
3	-18.2320	-18.2321
4	-13.8432	-13.8433
5	-12.1483	-12.1484
5	7.4192	7.4191
7	12.7588	12.7587

Table 3.1: Testing the accuracy of our MP2 implementation by calculating the ionization energies and electron affinities of a water molecule in a large supercell (100Å) and comparing with the respective implementation for molecules preexisting on FHI-aims, using minimal basis set.

N of k points	80	100	120
HF (eV)	7.792	7.792	7.792
sp-MP2 (eV)	6.641	6.640	6.640

Table 3.2: MP2 bandgaps calculated with FHI-aims using STO-3G basis set.

in section 2.7.4.

Although different methods are employed for the reciprocal space convergence, from figure 3.10 we can conclude that our results showcase satisfactory agreement.

Bandgap results

We present here the bandgaps for a set of materials, calculated with our implementation of sp-MP2 on the all-electron, full-potential electronic structure code package, FHI-aims. To the best of our knowledge there are no reported data for

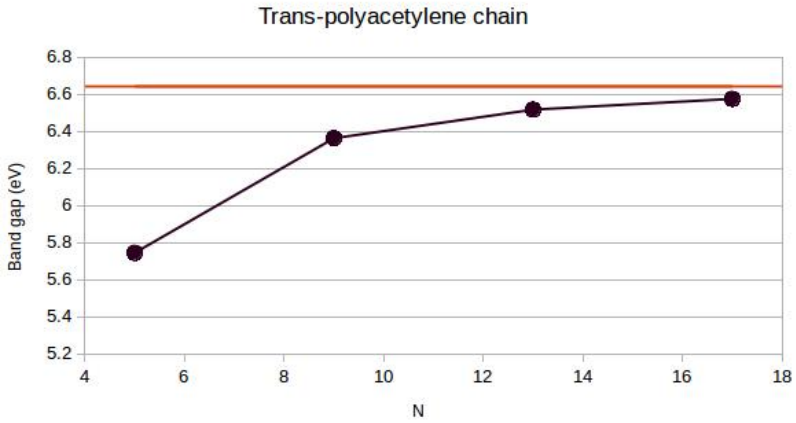

Figure 3.10: The bandgap of alternating trans-polyacetylene (basis set: STO-3G) as reported by Sun and Bartlett. The horizontal axis N is the number of unit cells in the lattice summations. The red line is our result for alternating trans-polyacetylene with the same basis set, obtained from our periodic sp-MP2 implementation. The difference between our value shown in table 3.2 and the last point from Sun and Bartlett calculations for $N = 17$ is 0.066eV, resulting from the fact that their calculation is not converged.

3D semiconductors or insulators to the level of theory of sp-MP2[3]. Our results are in the table 3.3.

Bandgap of solids with sp-MP2		
Material	k points	Bandgap (eV)
MgO	5×5×5	7.12
	6×6×6	6.54
	7×7×7	6.27
	8×8×8	5.96
	9×9×9	5.74
	10×10×10	5.55
	11×11×11	5.38
ZnO	6×6×6	1.95
	7×7×7	1.62
	8×8×8	1.37
ZnS	6×6×6	2.48
	7×7×7	2.03
	8×8×8	1.68
GaAs	6×6×6	-0.76
	7×7×7	-1.35
	8×8×8	-1.99
C (diamond)	6×6×6	1.74
	7×7×7	1.35

Table 3.3: sp-MP2 bandgaps calculated with FHI-aims using tight numerical settings and different k-grids.

Data in table 3.3 show that the convergence is slow in agreement with Sun's and Bartlett[39]'s report. In our code, the Ewald method is used to calculate the lattice summations of the Coulomb potential. This results in the singularity of the

[3]To avoid any confusion, we note here that A. Grüneis [70] reports quasiparticle energies that are of higher level of perturbation theory since the reported values are an approximation of the Dyson(D2), but the name might be confusing, since he calls them MP2 QP. In section 3.2.3 we report the Dyson(D2) bandgaps and there we will present a comparison between Grüneis results and ours.

Coulomb potential which governs the reciprocal space convergence, as was shown in section 3.1.

A slow convergence is also reported in total-energy MP2 calculations [80]. We explore an extrapolation method, as proposed for total-energy MP2 [78]. Zhang et al. proposed that the error in total-energy MP2 due to the finite k-grid follows the relation:

$$\Delta E(N) = E(N) - E(N \to \infty) = \frac{A}{N^{\alpha}}$$

where N is the number of k-grid points per direction ($N = (N_{\mathbf{k}})^{\frac{1}{3}}$). Since the treatment of the singularity is done in the same way in both cases, we will explore a similar law of decay for the bandgap:

$$\Delta G(N) = G(N) - G(N \to \infty) = \frac{A}{N^{\alpha}} \tag{3.50}$$

In contrast to previous research, we have identified the behaviour of the finite-size error analytically and determined the value of α in the case of sp-MP2. Considering the analysis in section 3.1.4, we can find the infinite grid limit $N \to \infty$ by extrapolating to $1/N$ to zero, as in figure 3.1.4.

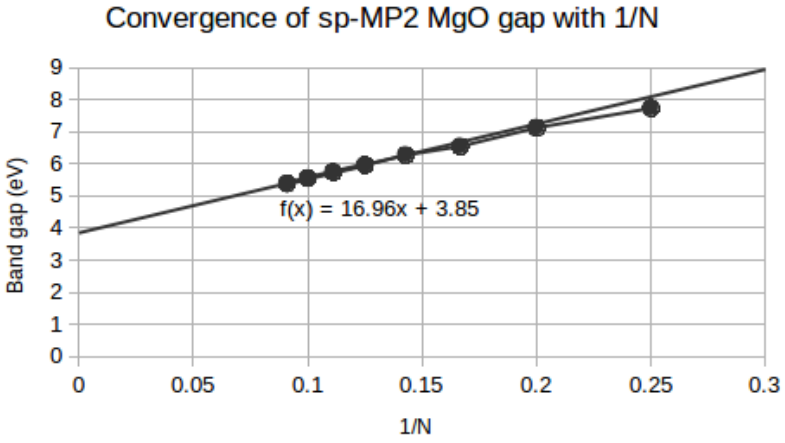

Figure 3.11: Convergence of the sp-MP2 bandgap plotted as a function of $1/N$ where N is the number of points per direction. The equation shows the linear fit of the last four points (8×8×8, 9×9×9, 10×10×10, and 11×11×11). The R^2 value of the linear fit is 0.998.

Material	Extrapolated ($\alpha = 1$) sp-MP2 bandgap (eV)	HF bandgap	Experiment
MgO	3.85	15.70	7.98
ZnO	-0.37	11.33	3.60
ZnS	-0.71	10.43	3.92
GaAs	-5.60	7.16	1.57
C	-0.99	12.71	5.85

Table 3.4: sp-MP2 bandgaps calculated by an extrapolation using eq. 3.50 with $\alpha = 1$ for the grids $N \times N \times N$ with $N = 6, 7, 8$, except C, where the extrapolation was done for $N = 6, 7$. Zero-point renormalization is removed from the experimental points (see: [60] and reference within, and [93]

Table 3.4 demonstrates that sp-MP2 severely underestimate the bandgaps and in many of the cases, sp-MP2 outputs a negative number, thus failing to predict a gap for the material. This was expected, since the same issue of negative gaps is predicted in the quasiparticle energies calculations by Grüneis [70], using a higher level of perturbation theory. For this reason, in section 3.2.2, we go beyond sp-MP2 and employ Dyson(D2), which significantly improves the results.

From figure 3.11, we confirm that the convergence with the number of k-points N is linear when plotted with $1/(N)^{1/3}$. The same behavior is expected and observed for the uncorrected single-particle energies obtained by skipping the singular point, since the correction should, in general, have the same asymptotic behavior. The convergence of sp-MP2 bandgap with the number of k-points obtained with two different approaches is shown in figure 3.12. The first approach is the truncated Coulomb potential method applied to the singular point only, as described previously in section (3.2.1). In the second approach, the singularity is simply omitted from the summation in equation 3.47 while using the bare (unmodified) Coulomb operator. As demonstrated, the convergence behavior is the same in both methods, meaning that the truncated Coulomb approach simply gives a practical way of calculating the singular point, but it does not improve the convergence.

From the results obtained by the linear fit ($\alpha = 1$) in table 3.4, the sp-MP2 bandgaps underestimate the experimental ones. While sp-MP2 is an improve-

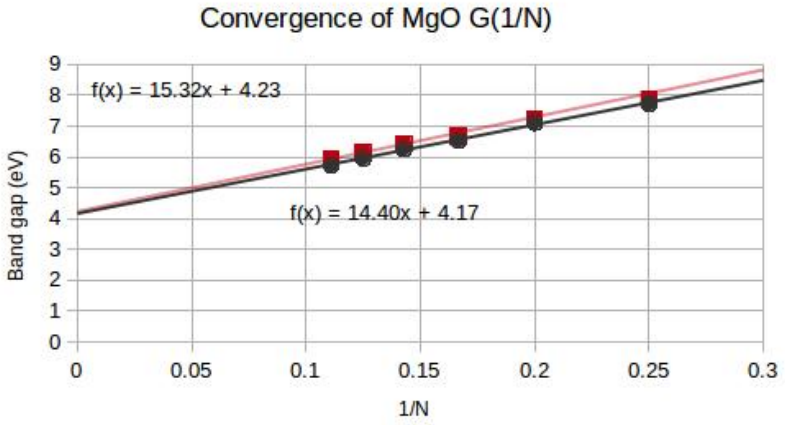

Figure 3.12: The convergence of sp-MP2 bandgap in MgO with k-points per direction N. The black dots are obtained with the truncated Coulomb operator approach applied to the singular point (see section 3.2.1), as was used to obtain the results in figure 3.11. The red dots are obtained by using bare Coulomb operator and excluding the singularity from the summation in eq. 3.47

ment compared to HF bandgaps, which are significantly overestimated, sp-MP2 over-corrects HF. One way to improve the bandgap predictions is to go beyond second-order correction. However, higher orders in truncated MBPT series come with a higher computational cost and complexity. As an alternative, one can turn to methods such as the Dyson equation, described in section 2.5, where the infinite summation is performed for certain classes of diagrams, resulting in a non-perturbative correction to the single-particle energies. In the next section, we present our results by solving the Dyson equation with an approximate second-order self-energy.

3.2.2 Renormalized second-order perturbation theory

Self-consistency in self-energy comes with a high computational cost. For this reason, we implement a non self-consistent second-order self-energy, where the propagators are replaced with the HF propagators as shown in figure 3.13.

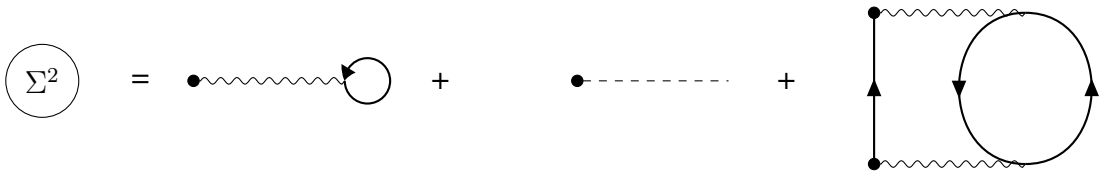

Figure 3.13: Non self-consistent second-order self-energy. The semi-bold propagator lines represent the HF propagator.

The propagator's lines will either be the HF propagator or the propagator of any other approximate single-particle Hamiltonian. While the self-consistent second-order self-energy and the respective propagator from the Dyson equation are independent from the effective potential, in this approximation they are not. Here we calculate the self-energy and single-particle excitation energies using HF as an effective potential. The contribution from the HF potential cancels the contribution from the bubble diagram in self-energy Σ^2 and the only contribution comes from the second-order diagram:

$$\Sigma^2(p,q;\epsilon) = \frac{1}{2}\sum_{iab}\frac{\langle\phi_p\phi_i|\,|\phi_a\phi_b\rangle\,\langle\phi_a\phi_b|\,|\phi_q\phi_i\rangle}{\epsilon+\epsilon_i-\epsilon_a-\epsilon_b+i\eta} + \frac{1}{2}\sum_{ija}\frac{\langle\phi_i\phi_j|\,|\phi_q\phi_a\rangle\,\langle\phi_p\phi_a|\,|\phi_i\phi_j\rangle}{\epsilon+\epsilon_a-\epsilon_i-\epsilon_j-i\eta} \tag{3.51}$$

If we adopt a diagonal approximation for the self-energy the above equation becomes:

$$\Sigma^{D2}(p;\epsilon) = \frac{1}{2}\sum_{iab}\frac{|\,\langle\phi_p\phi_i|\,|\phi_a\phi_b\rangle\,|^2}{\epsilon+\epsilon_i-\epsilon_a-\epsilon_b+i\eta} + \frac{1}{2}\sum_{ija}\frac{|\,\langle\phi_i\phi_j|\,|\phi_p\phi_a\rangle\,|^2}{\epsilon+\epsilon_a-\epsilon_i-\epsilon_j-i\eta} \tag{3.52}$$

We arrive at an expression very similar to the one for second-order correction to the single-particle energies in equation 2.81, obtained in section 2.4.2. In the limit of $\eta \to 0$, if we set $\epsilon = \epsilon_p$ in equation 3.52, we end up with the equation 3.44.

Substituting this self-energy in the Dyson equation, we obtain the poles of the propagator, determining the single-particle excitations as solutions to the equation:

$$\epsilon^{D(D2)} = \epsilon_p + \Sigma^{D2}(p;\epsilon^{D(D2)}) \tag{3.53}$$

This enables going beyond sp-MP2 with a small additional computational effort. In the next section, we present an in-depth analysis of the practical aspects of

solving the Dyson equation with the self-energy in a second-order diagonal approximation (Dyson(D2)).

3.2.3 Bandgaps from Dyson(D2)

We can solve in a practical way the Dyson equation in the second-order diagonal self-energy approximation employing graphical solution by calculating following function:

$$f(\epsilon) = \epsilon - \epsilon_p - \Sigma^{D2}(p;\epsilon) \tag{3.54}$$

for a range of ϵ and then we search for the roots of eq. $f(\epsilon) = 0$. It is helpful to examine the behavior of the above equation. Note that $\pm\eta$ in the denominators in self-energy expression (eq. 3.53) does not affect the position of the roots, as long as they do not coincide with the poles or branch cuts of the self-energy. The self-energy will be a noncontinuous function of ϵ, but in the interval centered in the middle of the gap with a width of $3G$ (where G is the HF bandgap) it will consist of a continuous part [87]. Thus, in the range $\epsilon_{ho} - G < \epsilon < \epsilon_{lu} + G$, self-energy is well-defined without poles, and monotonically decreasing since its nominator is always positive. Then, for each HF eigenstate p, there will be one solution of the Dyson equation in that interval. As a consequence of the many-body nature of the problem, there will be more than one excitation for a state p, but for the bandgap the relevant excitations will lie in this interval.

From the equation 3.54 we can state that if we consider the HF eigenvalue, $\epsilon = \epsilon_p$, then f will be equal to minus the sp-MP2 correction ($\eta = 0$):

$$f(\epsilon_p^{HF}) = -\Sigma^{D2}(p;\epsilon_p^{HF}) \tag{3.55}$$

We know from sp-MP2 that the correction will be negative for the conduction band and positive for the valence band. This can be seen in the form of the correction in equation 3.44. Therefore, the bandgaps predicted by sp-MP2 are smaller than the HF bandgaps, as found also in the section **??**. The solution of eq. 3.54 should be between sp-MP2 and HF energies for the conduction band minimum (CBm), and between HF and sp-MP2 energies for the valence band maximum (VBm).

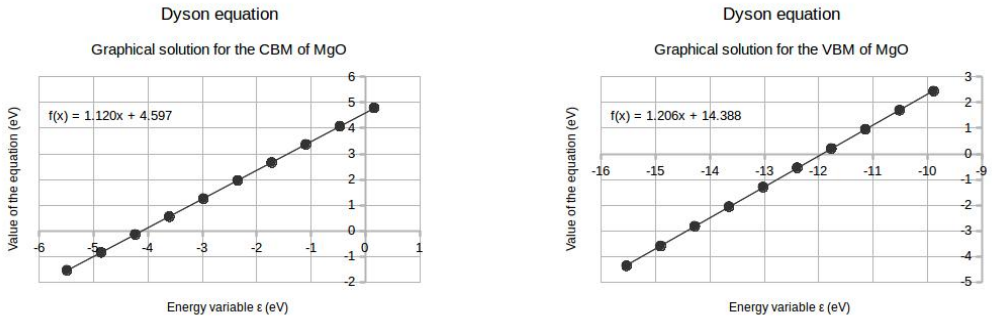

(a) CBm (b) VBm

Figure 3.14: Graphical solution of the Dyson equation for the CBm (a) and VBm (b) of MgO. The calculation is done with tight settings and a 6×6× k-point grid. The values on the y-axis correspond to $f(\epsilon)$ from equation 3.54. The x-value for which y-value is zero is the solution of the Dyson equation.

Figure 3.14 shows the function $f(\epsilon)$ from eq. 3.54 versus ϵ for CBm and VBm in MgO. Clearly, the behavior away from the poles and branch cuts is near-linear. Therefore, we find the solution from the linear fit. The HF value for the CBm is 0.17 eV while sp-MP2-corrected value is -4.29 eV. The solution of the Dyson equation lies in between, with a value of -3.81 eV. For the VBm, the HF value is -15.54 eV and the sp-MP2 value is -11.41 eV. The solution of the Dyson equation gives the value -12.11 eV. The resulting Dyson(D2) bandgap is 8.3 eV, to be compared to sp-MP2 gap 7.12 eV and the HF gap 15.37 eV. This behavior is persistent in all materials and k-point grids calculated. This demonstrates that solving the Dyson equation improves the overcorrection of HF bandgaps by sp-MP2. We identify that the convergence behavior of the bandgap with increasing k-grid density (see figure 3.15) is similar to sp-MP2 (see figure 3.11). Furthermore, in table 3.5 we report the bandgap values obtained by a linear extrapolation to an infinitely dense k-point grid.

In the figure 3.16 we summarize the results of sp-MP2 and Dyson(D2) compared to HF and the experimental values. Dyson(D2) improves significantly HF and sp-MP2 bandgaps. Still, the difference between Dyson(D2) and experimental values is in the order of eV, with the larger difference for diamond and GaAs. We note here that for diamond (C), HF is not converged in the reciprocal space even

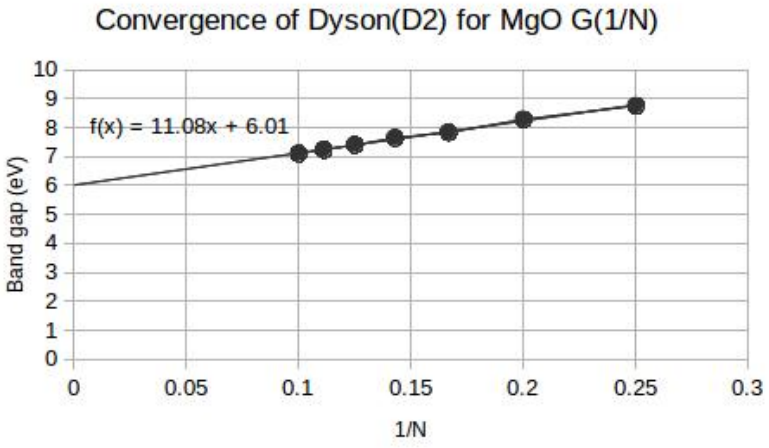

Figure 3.15: Convergence of the Dyson(D2) bandgap with the number of k-points per direction N. The equation shows the linear fit including all points

for the grid of $7 \times 7 \times 7$. There was a difference of $0.06eV$ for the HF values going from $6 \times 6 \times 6$ to $7 \times 7 \times 7$. This is due to the indirect gap of diamond that might affect the extrapolation method, since now the positions of both the CBm and VBm need a denser grid to be accurately calculated for HF.

As mentioned before, Grüneis reports bandgaps for a set of materials using an approximation to Dyson(D2) referring to it as MP2 QP. Although there are many differences between Grüneis calculation and ours, it is worth to discuss them. In Grüneis work a plane-wave basis set is used, while we employ a localized basis set. Due to the pseudopotentials used in the plane-wave case, an accurate numerical comparison is difficult. Moreover, the reciprocal space convergence is not studied in Grüneis work. Moreover, an approximation is done by Grüneis to the solution of the Dyson equation, in which it is assumed a linear behavior of equation 3.54 around the HF energy. As we see from the figures in 3.14 we demonstrate that this is a good approximation for the materials studied, so we do not expect that this approximation results in important discrepancies. The differences seen in the table 3.6 are due to the distinct basis sets and convergence treatment.

Although the numbers have differences, the conclusions from both approaches are similar. In both cases, for semiconductors (GaAs in our case and Si for Greuneis case), Dyson(D2) and the approximate MP2 QP can fail to predict a

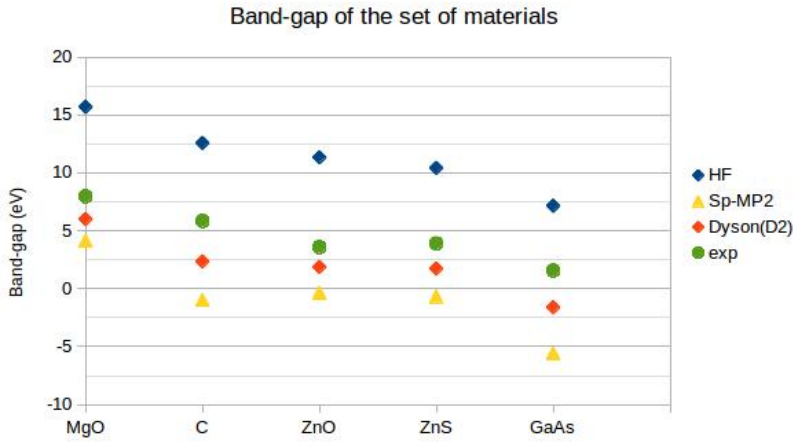

Figure 3.16: Dyson(D2) and MP2 bandgaps for a set of materials. The numbers are obtained using FHI-aims code in tight settings. To converge in reciprocal space, we extrapolate linearly, after plotting the bandgaps obtained from finite grids with N points per direction as a function $1/N$, as described in 3.2.3 for Dyson(D2) and 3.2.1 for sp-MP2. HF (tight settings with an $8 \times 8 \times 8$ reciprocal grid) and the experimental values (also shown in table 3.4) are plotted for reference.

Bandgap of solids with Dyson(D2)			
Material	basis set	k points	Bandgap (eV)
MgO	tight	5×5×5	8.28
		6×6×6	7.83
		7×7×7	7.64
		8×8×8	7.40
		extrapolated	6.01
ZnO	tight	5×5×5	3.88
		6×6×6	3.53
		7×7×7	3.30
		8×8×8	3.11
		extrapolated	1.88
ZnS	tight	5×5×5	4.35
		6×6×6	3.90
		7×7×7	3.59
		8×8×8	3.36
		extrapolated	1.74
GaAs	tight	6×6×6	1.04
		7×7×7	0.70
		8×8×8	0.31
		extrapolated	-1.60
C	tight	6×6×6	3.69
		7×7×7	3.5
		extrapolated	2.36

Table 3.5: Dyson(D2) Bandgaps calculated with FHI-aims, using tight settings for a set of materials with different k-grids.

bandgap. While HF overestimates the bandgaps, Dyson(D2) (and the approximate MP2 QP) overcorrect HF and underestimate the bandgaps. From our work we conclude that sp-MP2 improves HF, and it is improved by Dyson(D2), as expected from the MBPT hierarchy.

material	Dyson(D2)	MP2 QP (Grüneis et al.)
MgO	7.4	7.1
ZnO	3.1	2.1
ZnS	3.36	2.0
C	3.5	1.9
Si	-	-1.2
GaAs	0.31	-

Table 3.6: Comparison between MP2 QP (Andreas Grüneis, Martijn Marsman, and Georg Kresse, J. Chem. Phys. 133, 074107 (2010)) and our Dyson(D2) result for a finite grid ($8 \times 8 \times 8$). The differences are mainly because of the different basis set.

3.2.4 Potential for further development

Figure 3.16 shows that there is still a relatively large difference of 2-3 eV between the Dyson(D2) bandgap and the experimental bandgap in all studied materials. From the analysis of this thesis, we suggest ways to go beyond Dyson(D2) to increase the accuracy of the bandgap prediction.

One of the possible reason for the Dyson(D2) bandgap underestimation is the diagonal approximation to the self-energy, i.e., going from equation 3.51 to equation 3.52. Solving the Dyson equation with the self-energy in a diagonal approximation simplifies significantly its solution, which otherwise would be a relation between matrices [87]. Nonetheless, the non-diagonal part of the self-energy can be significant. Therefore, solving the Dyson equation 2.111 with the approximate self-energy from equation 3.51 is a direct way to surpass Dyson(D2) accuracy.

Another way to possibly improve the bandgap prediction of sp-MP2 and Dyson(D2) (or Dyson(2)) is changing the reference approximation. MBPT depends on the wavefunctions used to construct the ground state $|\Phi\rangle$, as we show in section 2.3.2. The use of a different starting point will give different results. For sp-MP2 this means that now the F_{eff}, as defined in equation 2.56, will not be zero, thus there are more diagrams that need to be taken into account, as shown in equation 2.81. For Dyson(2) and Dyson(D2), the cancellation between the first and second di-

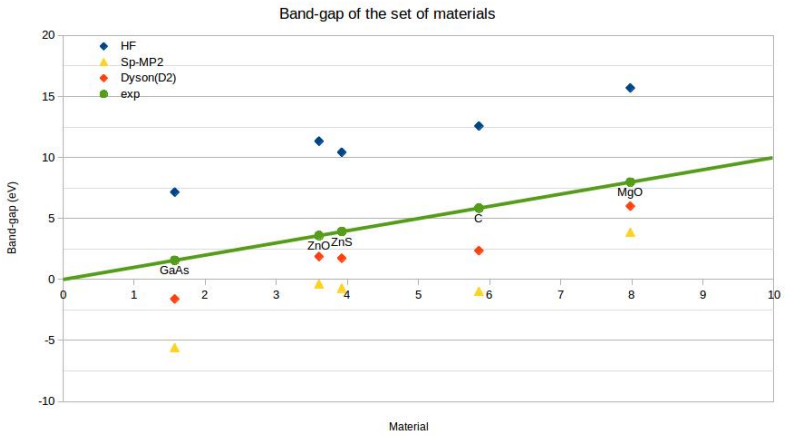

Figure 3.17: Dyson(D2), MP2 and HF bandgaps as a function of the experimental bandgap.

agrams on the right side of figure 3.13 will not happen when a different starting point than HF is used. Hence, these terms have to be included in the self-energy when solving the Dyson equation 2.111. Even though the inclusion of more terms increases the implementation complexity and computational cost, single-particle approximations such as LDA or GGA have proven reliable starting points in the case of G_0W_0 [60]. Since G_0W_0 is based also on the approximation of the self-energy in Dyson equation, it is possible that using LDA and GGA approximations as a reference will improve Dyson(2) and Dyson(D2).

To include more diagrams, the full self-consistent propagator can be used for the calculation of the self-energy. In this case, the Dyson equation needs to be solved self-consistently. When this approximation is applied, the dependence on the starting point is eliminated. We will refer to this approach as sc-Dyson(2), which has not yet been studied for solids to the best of our knowledge.

Another way to go beyond is to combine methods. Analyzing the diagrams that contribute to the G_0W_0 self-energy (fig. 3.18) can help us combine it with diagrams present in Dyson(D2) and Dyson(2) but missing from G_0W_0. To do this, we will not use the antisymmetrized diagrams that we were using until now. Consequently, every interaction line will represent the Coulomb matrix and not the antisymmetrized Coulomb matrix. From the figure 3.18 we see that second-order and higher-order exchange diagrams are missing. We could combine the exchange

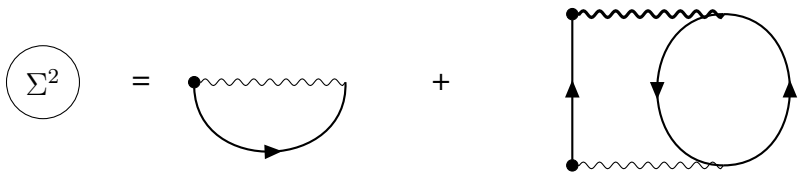

Figure 3.18: G_0W_0 self-energy. The thick line represents the screened Coulomb interaction (see for example Phys. Rev. B92, 081104, 2015).

part of Dyson(2) or Dyson(D2) with G_0W_0 [94]. An alternative approach is to replace the bare interaction with the screened interaction on the exchange diagram. This is known as second-order screened exchange correction (SOSEX) [62]. It can be concluded that there is a variety of approximations that can be explored. The drawback is the computational cost and the slow convergence, caused partially by the low reciprocal convergence, rooted in the Coulomb potential singularity.

In conclusion, MBPT offers a variety of hierarchical approximations that can approach the exact solution of any system. Although second-order is just a first step beyond the single-particle approximations, it paves the way to more accurate methods starting with Dyson(D2) (which is applied here) and going beyond to methods that include more diagrams in their self-energy, as Dyson(2) and sc-Dyson(2). This way, MBPT can provide a systematic approach to ground and excited state properties, by including more and more diagrams. In contrast, approximations as LDA and GGA are limited, since there is no systematical way to improve them. For this reason, it is important to explore the possible ways to go up the hierarchy of MBPT. In this process many issues can occur, such as the singularity of the Coulomb potential present in the application of MBPT to periodic systems, and the computational cost. We hope that this thesis contributes to the application of high-level approximations based on MBPT and the handling of occurring issues, especially in the case of the Coulomb potential singularity.

Chapter 4

Conclusions and outlook

The findings of this thesis contribute to the development of MBPT and wavefunction-based methods applied to condensed matter and materials, which hold a growing interest and investment. Particularly, the results fill a gap in second-order based calculations for solids bandgaps. We have focused on the problem of calculating the bandgap by implementing and applying the second-order MBPT-based methods sp-MP2 and Dyson(D2). In addition, we have studied the long-standing problem of the convergence of MBPT-based theories, and we have contributed by suggesting and applying an extrapolation scheme for the sp-MP2 and Dyson(D2).

The implementation of the all-electron sp-MP2 and Dyson(D2) approaches are based on a canonical formulation of second-order Møller–Plesset PT. It was performed with the periodic version of localized atom-centered orbitals as basis functions and applied to semiconductors and insulators. The method was integrated into the framework of the FHI-aims electronic-structure package, inheriting the advantages of the code, such as the efficiency of its basis set and the robust parallelization potential, both critical for the highly-computationally costly wavefunction-based methods.

Upon reviewing this thesis' results, one can conclude that to achieve adequate accuracy for periodic systems, more diagrams and higher contributions need to be included to sp-MP2. We showed that the quasiparticle problem is even more challenging than the total energy. A qualitative picture can be demonstrated by employing the quasiparticle concept. When we induce a charged excitation, as the single-particle excitations described in this thesis (electrons or holes), a po-

larization cloud is generated, coating the charge and reducing its effective field. Mean-field theories, such as HF, by definition, cannot describe this phenomenon, resulting in overestimated bandgaps. Thus we can rely on correlation methods to account for the polarization, which will reduce the bandgap energy. However, if we consider only the second-order correction to the correlation, we significantly undervalue the bandgap, suggesting an overestimated polarization induction due to the charged excitation.

A simplified approach to help understand this result comes from considering a localized picture for the electrons and the quasiparticles[1]. Adding a localized electron or hole in a solid will repel or attract other electrons in its surroundings, respectively. MP2 overestimates this reaction because it cannot consider that once the polarization cloud is formed, the charge will no longer interact with an effective interaction. Nevertheless, sp-MP2 is the first step beyond mean-field theory and is a highly challenging task. It gives a first estimation of the quasiparticle energies, and a successful application paves the path for more precise theories, such as the Dyson equation and coupled-cluster methods. In this work, we implemented the Dyson(D2), and, as expected, it delivered significant quantitative improvements toward experimental values.

One more substantial contribution of this thesis is the formal analysis of the singularity of the Coulomb operator, addressing the convergence issue of sp-MP2 and Dyson(D2) and the inherent potential for broader applications on MBPT. The singularity of the Coulomb operator, which is present in all orders of MBPT and thus sp-MP2 and Dyson(D2), affects the integration convergence over the first Brillouin zone. The treatment of this singularity has been studied extensively for the case of Hartree-Fock, and it has been addressed with methods that reduce the computational cost, such as Gygi-Baldereschi and truncated Coulomb. However, only extrapolation schemes have been explored for second or higher-order theories such as MP2 and CC. After the exploration and analytical formulation of the finite-size error behaviour, our research enabled the design and application of an extrapolation technique. Our analysis shows that the convergence and the way to treat the singularity depends on the basis functions and how the Coulomb potential

[1] Similar conclusions can be extracted in the reciprocal space, only that in this case, the electrons are localized in reciprocal space.

matrix elements are calculated by integration in k-space. The analysis can be generalized for other MBPT methods, including the Coulomb operator. Furthermore, we explored a generalized Gygi-Baldeschi method that can, in principle, reduce the grid density needed to obtain converged results, although its formulation and computation are more demanding than the Gygi-Baldeschi method itself.

I would like to conclude this thesis with the hope that my study on MBPT for the excitation energies and the analysis of the convergence behaviour will further promote advancement in the application of wavefunction and MBPT methods in materials, a promising path to advance the understanding of the electronic structure of materials and predictive models building.

Bibliography

[1] P. A. M. Dirac and R. H. Fowler, "Quantum mechanics of many-electron systems," *Proceedings of the Royal Society of London. Series A, Containing Papers of a Mathematical and Physical Character*, vol. 123, no. 792, pp. 714–733, 1929. DOI: 10.1098/rspa.1929.0094.

[2] E. Schrödinger, "An undulatory theory of the mechanics of atoms and molecules," *Phys. Rev.*, vol. 28, pp. 1049–1070, 6 Dec. 1926. DOI: 10.1103/PhysRev.28.1049.

[3] P. W. Anderson, "More is different," *Science*, vol. 177, no. 4047, pp. 393–396, 1972. DOI: 10.1126/science.177.4047.393.

[4] P. A. M. Dirac and R. H. Fowler, "The quantum theory of the electron," *Proceedings of the Royal Society of London. Series A, Containing Papers of a Mathematical and Physical Character*, vol. 117, no. 778, pp. 610–624, 1928. DOI: 10.1098/rspa.1928.0023.

[5] J. Autschbach, "Perspective: Relativistic effects," *The Journal of Chemical Physics*, vol. 136, no. 15, p. 150 902, 2012. DOI: 10.1063/1.3702628.

[6] T. Saue, "Relativistic hamiltonians for chemistry: A primer," *ChemPhysChem*, vol. 12, no. 17, pp. 3077–3094, 2011. DOI: https://doi.org/10.1002/cphc.201100682.

[7] M. Born and R. Oppenheimer, "Zur quantentheorie der molekeln," *Annalen der Physik*, vol. 389, no. 20, pp. 457–484, 1927. DOI: https://doi.org/10.1002/andp.19273892002.

[8] A. Szabo and N. Ostlund, *Modern Quantum Chemistry: Introduction to Advanced Electronic Structure Theory*, ser. Dover Books on Chemistry. Dover Publications, 1996, ISBN: 9780486691862. [Online]. Available: https://books.google.de/books?id=6mV9gYzEkgIC.

[9] V. Fock, "Bemerkung zum virialsatz," *Zeitschrift für Physik*, vol. 63, no. 11-12, pp. 855–858, 1930.

[10] J. C. Slater, "A simplification of the hartree-fock method," *Phys. Rev.*, vol. 81, pp. 385–390, 3 Feb. 1951. DOI: 10.1103/PhysRev.81.385.

[11] P. Hohenberg and W. Kohn, "Inhomogeneous electron gas," *Phys. Rev.*, vol. 136, B864–B871, 3B Nov. 1964. DOI: 10.1103/PhysRev.136.B864.

[12] W. Kohn, "Nobel lecture: Electronic structure of matter—wave functions and density functionals," *Rev. Mod. Phys.*, vol. 71, pp. 1253–1266, 5 Oct. 1999. DOI: 10.1103/RevModPhys.71.1253.

[13] W. Kohn and L. J. Sham, "Self-consistent equations including exchange and correlation effects," *Phys. Rev.*, vol. 140, A1133–A1138, 4A Nov. 1965. DOI: 10.1103/PhysRev.140.A1133.

[14] A. D. Becke, "Density-functional exchange-energy approximation with correct asymptotic behavior," *Phys. Rev. A*, vol. 38, pp. 3098–3100, 6 Sep. 1988. DOI: 10.1103/PhysRevA.38.3098.

[15] D. Langreth and J. Perdew, "The gradient approximation to the exchange-correlation energy functional: A generalization that works," *Solid State Communications*, vol. 31, no. 8, pp. 567–571, 1979, ISSN: 0038-1098. DOI: https://doi.org/10.1016/0038-1098(79)90254-0.

[16] J. P. Perdew, K. Burke, and M. Ernzerhof, "Generalized gradient approximation made simple," *Phys. Rev. Lett.*, vol. 77, pp. 3865–3868, 18 Oct. 1996. DOI: 10.1103/PhysRevLett.77.3865.

[17] J. P. Perdew and M. Levy, "Physical content of the exact kohn-sham orbital energies: Band gaps and derivative discontinuities," *Phys. Rev. Lett.*, vol. 51, pp. 1884–1887, 20 Nov. 1983. DOI: 10.1103/PhysRevLett.51.1884.

[18] R. J. Bartlett and M. Musiał, "Coupled-cluster theory in quantum chemistry," *Rev. Mod. Phys.*, vol. 79, pp. 291–352, 1 Feb. 2007. DOI: 10.1103/RevModPhys.79.291.

[19] J. Goldstone and N. F. Mott, "Derivation of the Brueckner many-body theory," *Proceedings of the Royal Society of London. Series A. Mathematical and Physical Sciences*, vol. 239, no. 1217, pp. 267–279, 1957. DOI: 10.1098/rspa.1957.0037.

[20] K. A. Brueckner, "Many-body problem for strongly interacting particles. ii. linked cluster expansion," *Phys. Rev.*, vol. 100, pp. 36–45, 1 Oct. 1955. DOI: 10.1103/PhysRev.100.36.

[21] C. Møller and M. S. Plesset, "Note on an approximation treatment for many-electron systems," *Phys. Rev.*, vol. 46, pp. 618–622, 7 Oct. 1934. DOI: 10.1103/PhysRev.46.618.

[22] I. Shavitt and R. Bartlett, *Many-Body Methods in Chemistry and Physics: MBPT and Coupled-Cluster Theory*, ser. Cambridge Molecular Science. Cambridge University Press, 2009, ISBN: 9780521818322.

[23] C. Sharma and S. Srirankanathan, "A new proof of the brillouin theorem," *Molecular Physics*, vol. 40, no. 4, pp. 1021–1023, 1980. DOI: 10.1080/00268978000102111.

[24] R. J. Bartlett and J. F. Stanton, "Applications of post-hartree—fock methods: A tutorial," in *Reviews in Computational Chemistry*. John Wiley & Sons, Ltd, 1994, pp. 65–169, ISBN: 9780470125823. DOI: https://doi.org/10.1002/9780470125823.ch2.

[25] T. Schäfer, B. Ramberger, and G. Kresse, "Quartic scaling mp2 for solids: A highly parallelized algorithm in the plane wave basis," *The Journal of Chemical Physics*, vol. 146, no. 10, p. 104 101, 2017. DOI: 10.1063/1.4976937.

[26] S. Hirata, X. He, M. R. Hermes, and S. Y. Willow, "Second-order many-body perturbation theory: An eternal frontier," *The Journal of Physical Chemistry A*, vol. 118, no. 4, pp. 655–672, 2014. DOI: https://doi.org/10.1021/jp410587b.

[27] S. Suhai, "Perturbation theoretical investigation of electron correlation effects in infinite metallic and semiconducting polymers," *International Journal of Quantum Chemistry*, vol. 23, no. 4, pp. 1239–1256, 1983. DOI: https://doi.org/10.1002/qua.560230414.

[28] J.-Q. Sun and R. J. Bartlett, "Second-order many-body perturbation-theory calculations in extended systems," *The Journal of Chemical Physics*, vol. 104, no. 21, pp. 8553–8565, 1996. DOI: 10.1063/1.471545.

[29] C. Pisani, M. Busso, G. Capecchi, *et al.*, "Local-mp2 electron correlation method for nonconducting crystals," *The Journal of Chemical Physics*, vol. 122, no. 9, p. 094 113, 2005. DOI: 10.1063/1.1857479.

[30] P. Pulay, "Localizability of dynamic electron correlation," *Chemical physics letters*, vol. 100, no. 2, pp. 151–154, 1983.

[31] P. Y. Ayala, K. N. Kudin, and G. E. Scuseria, "Atomic orbital laplace-transformed second-order møller–plesset theory for periodic systems," *The Journal of Chemical Physics*, vol. 115, no. 21, pp. 9698–9707, 2001. DOI: 10.1063/1.1414369.

[32] M. Marsman, A. Grüneis, J. Paier, and G. Kresse, "Second-order møller–plesset perturbation theory applied to extended systems. i. within the projector-augmented-wave formalism using a plane wave basis set," *The Journal of Chemical Physics*, vol. 130, no. 18, p. 184 103, 2009. DOI: 10.1063/1.3126249.

[33] M. Del Ben, J. Hutter, and J. VandeVondele, "Second-order møller–plesset perturbation theory in the condensed phase: An efficient and massively parallel gaussian and plane waves approach," *Journal of Chemical Theory and Computation*, vol. 8, no. 11, pp. 4177–4188, 2012, PMID: 26605583. DOI: 10.1021/ct300531w.

[34] P. E. Blöchl, "Projector augmented-wave method," *Phys. Rev. B*, vol. 50, pp. 17 953–17 979, 24 Dec. 1994. DOI: 10.1103/PhysRevB.50.17953.

[35] V. Blum, R. Gehrke, F. Hanke, *et al.*, "Ab initio molecular simulations with numeric atom-centered orbitals," *Computer Physics Communications*, vol. 180, no. 11, pp. 2175–2196, 2009, ISSN: 0010-4655. DOI: https://doi.org/10.1016/j.cpc.2009.06.022.

[36] "Efficient o(n) integration for all-electron electronic structure calculation using numeric basis functions," *Journal of Computational Physics*, vol. 228, no. 22, pp. 8367–8379, 2009, ISSN: 0021-9991. DOI: https://doi.org/10.1016/j.jcp.2009.08.008.

[37] I. Y. Zhang, X. Ren, P. Rinke, V. Blum, and M. Scheffler, "Numeric atom-centered-orbital basis sets with valence-correlation consistency from h to ar," *New Journal of Physics*, vol. 15, no. 12, p. 123 033, Dec. 2013. DOI: 10.1088/1367-2630/15/12/123033.

[38] B. Dunlap, "Robust variational fitting: Gáspár's variational exchange can accurately be treated analytically," *Journal of Molecular Structure: THEOCHEM*, vol. 501-502, pp. 221–228, 2000, ISSN: 0166-1280. DOI: https://doi.org/10.1016/S0166-1280(99)00433-9.

[39] K. Eichkorn, O. Treutler, H. Öhm, M. Häser, and R. Ahlrichs, "Auxiliary basis sets to approximate coulomb potentials," *Chemical Physics Letters*, vol. 240, no. 4, pp. 283–290, 1995, ISSN: 0009-2614. DOI: https://doi.org/10.1016/0009-2614(95)00621-A.

[40] J. L. Whitten, "Coulombic potential energy integrals and approximations," *The Journal of Chemical Physics*, vol. 58, no. 10, pp. 4496–4501, 1973. DOI: 10.1063/1.1679012.

[41] C. Pisani, L. Maschio, S. Casassa, M. Halo, M. Schütz, and D. Usvyat, "Periodic local mp2 method for the study of electronic correlation in crystals: Theory and preliminary applications," *Journal of Computational Chemistry*, vol. 8, no. 13, pp. 2113–2124, 2008. DOI: https://doi.org/10.1002/jcc.20975.

[42] C. Pisani, M. Schütz, S. Casassa, *et al.*, "Cryscor: A program for the post-hartree–fock treatment of periodic systems," *Phys. Chem. Chem. Phys.*, vol. 14, pp. 7615–7628, 21 2012. DOI: 10.1039/C2CP23927B.

[43] F. Weigend, M. Häser, H. Patzelt, and R. Ahlrichs, "Ri-mp2: Optimized auxiliary basis sets and demonstration of efficiency," *Chemical Physics Letters*, vol. 294, no. 1, pp. 143–152, 1998, ISSN: 0009-2614. DOI: https://doi.org/10.1016/S0009-2614(98)00862-8.

[44] X. Ren, P. Rinke, V. Blum, *et al.*, "Resolution-of-identity approach to hartree–fock, hybrid density functionals, RPA, MP2 and GW with numeric atom-centered orbital basis functions," *New Journal of Physics*, vol. 14, no. 5, p. 053 020, May 2012. DOI: 10.1088/1367-2630/14/5/053020.

[45] P. Merlot, T. Kjærgaard, T. Helgaker, *et al.*, "Attractive electron–electron interactions within robust local fitting approximations," *Journal of Computational Chemistry*, vol. 34, no. 17, pp. 1486–1496, 2013. DOI: https://doi.org/10.1002/jcc.23284.

[46] F. P. Billingsley and J. E. Bloor, "Limited expansion of diatomic overlap (ledo): A near-accurate approximate ab initio lcao mo method. i. theory and preliminary investigations," *The Journal of Chemical Physics*, vol. 55, no. 11, pp. 5178–5190, 1971. DOI: 10.1063/1.1675655.

[47] S. V. Levchenko, X. Ren, J. Wieferink, *et al.*, "Hybrid functionals for large periodic systems in an all-electron, numeric atom-centered basis framework," *Computer Physics Communications*, vol. 192, pp. 60–69, 2015, ISSN: 0010-4655. DOI: https://doi.org/10.1016/j.cpc.2015.02.021.

[48] A. C. Ihrig, J. Wieferink, I. Y. Zhang, *et al.*, "Accurate localized resolution of identity approach for linear-scaling hybrid density functionals and for many-body perturbation theory," *New Journal of Physics*, vol. 17, no. 9, p. 093 020, Sep. 2015. DOI: 10.1088/1367-2630/17/9/093020.

[49] R. D. Mattuck, *A guide to Feynman diagrams in the many-body problem*. Courier Corporation, 1992.

[50] P. Fulde, *Electron correlations in molecules and solids*. Springer Science & Business Media, 1995, vol. 100.

[51] D. Pines, *Theory of Quantum Liquids: Normal Fermi Liquids*. CRC Press, 2018.

[52] F. Bechstedt, *Many-body approach to electronic excitations*. Springer, 2016.

[53] P. C. Martin and J. Schwinger, "Theory of many-particle systems I," *Phys. Rev.*, vol. 115, pp. 1342–1373, 6 Sep. 1959. DOI: 10.1103/PhysRev.115.1342.

[54] H. Lehmann, "Über eigenschaften von ausbreitungsfunktionen und renormierungskonstanten quantisierter felder," *Il Nuovo Cimento (1943-1954)*, vol. 11, no. 4, pp. 342–357, 1954.

[55] F. J. Dyson, "The radiation theories of Tomonaga, Schwinger, and Feynman," *Phys. Rev.*, vol. 75, pp. 486–502, 3 Feb. 1949. DOI: 10.1103/PhysRev.75.486.

[56] F. J. Dyson, "The S matrix in quantum electrodynamics," *Phys. Rev.*, vol. 75, pp. 1736–1755, 11 Jun. 1949. DOI: 10.1103/PhysRev.75.1736.

[57] L. Hedin, "New method for calculating the one-particle green's function with application to the electron-gas problem," *Phys. Rev.*, vol. 139, A796–A823, 3A Aug. 1965. DOI: 10.1103/PhysRev.139.A796.

[58] L. Hedin and A. Johansson, "Polarization corrections to core levels," *Journal of Physics B: Atomic and Molecular Physics*, vol. 2, no. 12, pp. 1336–1346, Dec. 1969. DOI: 10.1088/0022-3700/2/12/313.

[59] D. Golze, M. Dvorak, and P. Rinke, "The gw compendium: A practical guide to theoretical photoemission spectroscopy," *Frontiers in Chemistry*, vol. 7, 2019, ISSN: 2296-2646. DOI: 10.3389/fchem.2019.00377.

[60] X. Ren, F. Merz, H. Jiang, *et al.*, "All-electron periodic G_0W_0 implementation with numerical atomic orbital basis functions: Algorithm and benchmarks," *Phys. Rev. Materials*, vol. 5, p. 013 807, 1 Jan. 2021. DOI: 10.1103/PhysRevMaterials.5.013807.

[61] M. Shishkin and G. Kresse, "Self-consistent GW calculations for semiconductors and insulators," *Phys. Rev. B*, vol. 75, p. 235 102, 23 Jun. 2007. DOI: 10.1103/PhysRevB.75.235102.

[62] X. Ren, N. Marom, F. Caruso, M. Scheffler, and P. Rinke, "Beyond the GW approximation: A second-order screened exchange correction," *Phys. Rev. B*, vol. 92, p. 081 104, 8 Aug. 2015. DOI: 10.1103/PhysRevB.92.081104.

[63] M. Nooijen and J. G. Snijders, "Coupled cluster approach to the single-particle Green's function," *International Journal of Quantum Chemistry*, vol. 44, no. S26, pp. 55–83, 1992. DOI: https://doi.org/10.1002/qua.560440808.

[64] M. Nooijen and J. G. Snijders, "Coupled cluster Green's function method: Working equations and applications," *International Journal of Quantum Chemistry*, vol. 48, no. 1, pp. 15–48, 1993. DOI: https://doi.org/10.1002/qua.560480103.

[65] J. McClain, Q. Sun, G. K.-L. Chan, and T. C. Berkelbach, "Gaussian-based coupled-cluster theory for the ground-state and band structure of solids," *Journal of chemical theory and computation*, vol. 13, no. 3, pp. 1209–1218, 2017. DOI: 10.1021/acs.jctc.7b00049.

[66] H. Katagiri, "Equation-of-motion coupled-cluster study on exciton states of polyethylene with periodic boundary condition," *The Journal of Chemical Physics*, vol. 122, no. 22, p. 224 901, 2005. DOI: 10.1063/1.1929731.

[67] J.-Q. Sun and R. J. Bartlett, "Many-body perturbation theory for quasiparticle energies," *The Journal of Chemical Physics*, vol. 107, no. 13, pp. 5058–5071, 1997. DOI: 10.1063/1.474869.

[68] H. Shang and J. Yang, "Implementation of laplace transformed mp2 for periodic systems with numerical atomic orbitals," *Frontiers in chemistry*, vol. 27, p. 589 992, Oct. 2020. DOI: 10.3389/fchem.2020.589992.

[69] S. Suhai, "Quasiparticle energy-band structures in semiconducting polymers: Correlation effects on the band gap in polyacetylene," *Phys. Rev. B*, vol. 27, pp. 3506–3518, 6 Mar. 1983. DOI: 10.1103/PhysRevB.27.3506.

[70] A. Grüneis, M. Marsman, and G. Kresse, "Second-order møller–plesset perturbation theory applied to extended systems. ii. structural and energetic properties," *The Journal of Chemical Physics*, vol. 133, no. 7, p. 074 107, 2010. DOI: 10.1063/1.3466765.

[71] S. W. de Leeuw, J. W. Perram, E. R. Smith, and J. S. Rowlinson, "Simulation of electrostatic systems in periodic boundary conditions. i. lattice sums and dielectric constants," *Proceedings of the Royal Society of London. A. Mathematical and Physical Sciences*, vol. 373, no. 1752, pp. 27–56, 1980. DOI: 10.1098/rspa.1980.0135.

[72] J.-Q. Sun and R. J. Bartlett, "Convergence of many-body perturbation methods with lattice summations in extended systems," *The Journal of Chemical Physics*, vol. 106, no. 13, pp. 5554–5563, 1997. DOI: 10.1063/1.473577.

[73] F. Gygi and A. Baldereschi, "Self-consistent hartree-fock and screened-exchange calculations in solids: Application to silicon," *Phys. Rev. B*, vol. 34, pp. 4405–4408, 6 Sep. 1986. DOI: 10.1103/PhysRevB.34.4405.

[74] S. Massidda, M. Posternak, and A. Baldereschi, "Hartree-fock lapw approach to the electronic properties of periodic systems," *Phys. Rev. B*, vol. 48, pp. 5058–5068, 8 Aug. 1993. DOI: 10.1103/PhysRevB.48.5058.

[75] J. Spencer and A. Alavi, "Efficient calculation of the exact exchange energy in periodic systems using a truncated coulomb potential," *Phys. Rev. B*, vol. 77, p. 193 110, 19 May 2008. DOI: 10.1103/PhysRevB.77.193110.

[76] M. Betzinger, C. Friedrich, and S. Blügel, "Hybrid functionals within the all-electron flapw method: Implementation and applications of pbe0," *Phys. Rev. B*, vol. 81, p. 195 117, 19 May 2010. DOI: 10.1103/PhysRevB.81.195117.

[77] J. J. Shepherd, A. Grüneis, G. H. Booth, G. Kresse, and A. Alavi, "Convergence of many-body wave-function expansions using a plane-wave basis: From homogeneous electron gas to solid state systems," *Phys. Rev. B*, vol. 86, p. 035 111, 3 Jul. 2012. DOI: 10.1103/PhysRevB.86.035111.

[78] I. Y. Zhang, A. J. Logsdail, X. Ren, S. V. Levchenko, L. Ghiringhelli, and M. Scheffler, "Main-group test set for materials science and engineering with user-friendly graphical tools for error analysis: Systematic benchmark of the numerical and intrinsic errors in state-of-the-art electronic-structure

approximations," *New Journal of Physics*, vol. 21, no. 1, p. 013 025, Jan. 2019. DOI: 10.1088/1367-2630/aaf751.

[79] K. Liao and A. Grüneis, "Communication: Finite size correction in periodic coupled cluster theory calculations of solids," *The Journal of Chemical Physics*, vol. 145, no. 14, p. 141 102, 2016. DOI: 10.1063/1.4964307.

[80] G. H. Booth, A. Grüneis, G. Kresse, and A. Alavi, "Towards an exact description of electronic wavefunctions in real solids," *Nature*, vol. 493, pp. 365–370, 7432 2013. DOI: 10.1038/nature11770.

[81] J.-Q. Sun and R. J. Bartlett, "Convergence behavior of many-body perturbation theory with lattice summations in polymers," *Phys. Rev. Lett.*, vol. 80, pp. 349–352, 2 Jan. 1998. DOI: 10.1103/PhysRevLett.80.349.

[82] J. Sólyom, *Fundamentals of the Physics of Solids: Volume II: Electronic Properties*. Springer Science & Business Media, 2008, vol. 2.

[83] ——, *Fundamentals of the Physics of Solids: Volume 3-Normal, Broken-Symmetry, and Correlated Systems*. Springer Science & Business Media, 2010, vol. 3.

[84] R. M. Martin, *Electronic structure: basic theory and practical methods*. Cambridge university press, 2020.

[85] N. W. Ashcroft, N. D. Mermin, *et al.*, *Solid state physics*, 1976.

[86] A. L. Fetter and J. D. Walecka, *Quantum theory of many-particle systems*. Courier Corporation, 2012.

[87] W. H. Dickhoff and D. V. Van Neck, *Many-body theory exposed! Propagator description of quantum mechanics in many-body systems*. World Scientific Publishing Company, 2008.

[88] J. D. Jackson, *Classical electrodynamics*, 1999.

[89] C. Friedrich, A. Schindlmayr, and S. Blügel, "Efficient calculation of the coulomb matrix and its expansion around k=0 within the flapw method," *Computer Physics Communications*, vol. 180, no. 3, pp. 347–359, 2009, ISSN: 0010-4655. DOI: https://doi.org/10.1016/j.cpc.2008.10.009.

[90] H. Bateman, *Tables of integral transforms [volumes I & II]*. McGraw-Hill Book Company, 1954, vol. 1.

[91] F. Gygi and A. Baldereschi, "Quasiparticle energies in semiconductors: Self-energy correction to the local-density approximation," *Phys. Rev. Lett.*, vol. 62, pp. 2160–2163, 18 May 1989. DOI: 10.1103/PhysRevLett.62.2160.

[92] J. D. Talman, "Numerical methods for multicenter integrals for numerically defined basis functions applied in molecular calculations," *International Journal of Quantum Chemistry*, vol. 93, no. 2, pp. 72–90, 2003. DOI: https://doi.org/10.1002/qua.10538.

[93] M. Cardona and M. L. W. Thewalt, "Isotope effects on the optical spectra of semiconductors," *Rev. Mod. Phys.*, vol. 77, pp. 1173–1224, 4 Nov. 2005. DOI: 10.1103/RevModPhys.77.1173.

[94] N. Marom, F. Caruso, X. Ren, *et al.*, "Benchmark of GW methods for azabenzenes," *Phys. Rev. B*, vol. 86, p. 245 127, 24 Dec. 2012. DOI: 10.1103/PhysRevB.86.245127.